CHARACTERIZATION OF COLD PLASMA RETICULATED SHAPE MEMORY POLYMER FOAM

A Thesis

by

NICOLE C. RIVERA

Submitted to the Office of Graduate and Professional Studies of
Texas A&M University
in partial fulfillment of the requirements for the degree of

MASTER OF SCIENCE

Chair of Committee,	Duncan J. Maitland
Committee Members,	John C. Criscione
	Daniel L. Alge
Head of Department,	Gerard L. Coté

May 2015

Major Subject: Biomedical Engineering

ABSTRACT

Reticulation, the process of opening and removing cell membranes from shape memory polymer (SMP) foam, is an important processing technique to improve the permeability of SMP foam for utilization in several biomedical applications. Embolization biomedical applications, such as in the prevention of type II endoleaks (EII) associated with abdominal aortic aneurysms (AAAs), require specific reticulation levels for enhanced cell infiltration and thrombosis upon foam implantation. While several techniques have been employed to reticulate polyurethane SMP foam, reticulation of ultra-low density polyurethane SMP foam ($\rho_{app} < 0.02$ g/cm^3) using these techniques has been mostly ineffective. The focus of this work was to investigate the use of cold plasma treatment as a technique for controlled reticulation of ultra-low density polyurethane SMP foam for EII prevention.

Four plasma processes were developed to accomplish moderate (60-80%) and complete (>95%) reticulation of two SMP foam geometries, blocks and sheets. After the plasma processes were developed, the percent reticulation (P_{ret}) achieved by each plasma process was quantified to show that the processes satisfied the moderate and complete P_{ret} requirements. The P_{ret} homogeneity throughout the foam blocks was measured by calculating the percent sample volume with complete membrane removal. These results suggested that the moderate reticulation process for the foam blocks was inhomogeneous while the completely reticulated blocks exhibited complete membrane removal

throughout >98% of the sample volume.

Material characterization was performed on as-made and plasma reticulated SMP foam to evaluate the effect of plasma reticulation on the material properties. Overall, plasma reticulation decreased foam apparent density, increased permeability, decreased form factor, had mixed effects on volume expansion, and did not change wet T_g. The as-made and plasma-reticulated sheet samples exhibited reduced mechanical integrity after cleaning. The results of this thesis indicate that cold plasma reticulation is a viable technique for achieving controlled reticulation of ultra-low density polyurethane SMP foam. However, further studies must be conducted to optimize the control over P_{ret} achieved via plasma reticulation and expand the utility of plasma reticulation to different foam geometries.

DEDICATION

To my Granddad and Grandpa, my inspiration for utilizing my interests in science for improving medicine and healthcare through biomedical engineering.

Mom and Dad, I will never be able to thank you enough for all of the love, support, and sacrifices you have made for me. I am so blessed to have two parents in my life who love me as much as you do. It is through both of your example that I have learned that with hard work, dedication, and God I can accomplish anything. Mom, you are my best friend and my biggest role model. You give yourself completely as a wife, mother, and career woman without sacrificing any of those three roles, and I can only hope to become half of the woman you are. Dad, you are my ray of sunshine in the darkness that always helps me get through. You have always taught me to keep my head up and to turn to God in times of struggle.

Steven, you have always been my greatest motivator. Everything I have accomplished I did so because I wanted to make you proud. Since we were little you have always taken care of me and tried to help me learn from your experiences. From teaching me the days of the week when we were supposed to be going to bed to reviewing my resume to help me get a job, you have always been the best big brother.

Ted, since the day we met you have always supported me and my dreams. You have never questioned my decisions or made me choose between you and my desire to become a biomedical engineer. Your never-ending love and support has been the light at the end of the tunnel and I can't wait to spend the rest of my life with you.

ACKNOWLEDGEMENTS

First and foremost, I would like to thank God for blessing me with the people to whom this thesis is dedicated, for the opportunity to pursue my dreams, and the strength to overcome any challenge that has come my way.

I want to thank my committee chair and mentor, Dr. Maitland for his guidance and support throughout my time at Texas A&M University. He was instrumental in my decision to attend Texas A&M for my master's degree and provided me the opportunity to have a master's experience that was challenging and rewarding far beyond that of the average master's program. He guided my work on this thesis but also encouraged me to work on a number of other projects that exposed me to several components of the medical device industry. Dr. Maitland challenged me as student, engineer, and a person. While at the times I felt I was faced with insurmountable challenges and tasks, Dr. Maitland's encouragement of "what doesn't kill you only makes you stronger," proved true in the end. I can honestly say I have become a much stronger and more confident student, engineer, and person from this experience, thank you Dr. Maitland.

I want to thank Dr. Criscione and Dr. Alge for their support and guidance throughout the completion of my thesis. Your genuine interest and insight into the material and clinical problems surrounding this project helped me to design this project in way that was relevant and to take a well thought-out approach to evaluating plasma reticulation.

I would also like to thank Plasma Technology Systems, specifically Khoren Sahagian and Frank De Francesco, for all of their help in familiarizing me with the AURORA 0350 Plasma Surface Treatment System and answering any questions I had regarding plasma.

I want to thank Dr. Keller for teaching me about GLP and GMP systems throughout the implementation of the quality system in the Biomedical Device Laboratory (BDL). Also, I want to thank Dr. Keller for assisting me in my research and keeping the lab operating smoothly so all of us in the BDL could do our research efficiently and effectively.

My lab mates in the BDL deserve a great deal of thanks for the support, encouragement, and distractions from research. This lab is full of hard working graduate students who support one another in and outside of the lab. You all have helped me work through the trivial, and not so trivial, challenges of research and graduate school. Working with people who wanted to see me succeed and are fun to be around made going to work easy and my experience in the BDL one that I will never forget.

Anthony Wingate, who was my manager for two summers at Sandia National Laboratories, is one of the most influential mentors I have ever had the pleasure of working with. Anthony was the person who ignited my interest in Quality Engineering and showed me that I could merge my desire to work in the medical device industry with my interest and experience in Quality Engineering. Beyond my internship experience, Anthony taught me that I could hold firm to my faith and personal values without compromise in the work place as long as I was respectful of the faiths and values of

others. Anthony, thank you for your guidance, support of my goals, and seeing my potential as a young engineer.

I would also like to thank my family. Each one of them has shown me their love and support in their own way, which has helped me to become the unique person I am today. I especially want to thank my Uncle Jim and Uncle Robb for their advice and insight to help me make the best academic and career decisions to become a successful biomedical engineer.

Finally, I want to thank all of the teachers who molded me into the engineer I am today. Each of my teachers and professors at Holy Ghost, St. Pius X High School, the University of Notre Dame and Texas A&M University guided me to this point in my academic and professional careers. Without these educators, I do not know if I would have made it this far and for that I am forever grateful.

NOMENCLATURE

AAA	Abdominal aortic aneurysm
C	Form Factor (m^{-1})
C^*	Radical site on polymer chain
C-C	Carbon-Carbon bond
CF_4	Tetrafluoromethane
CNT	Carbon nanotubes
$\frac{\partial P}{\partial x}$	Pressure gradient (Pa/m)
D_c	Compressed diameter (mm)
DI	Deionized
D_r	Recovered diameter (mm)
DSC	Differential Scanning Calorimetry
e^-	Electrons
EII	Type II endoleaks
EVAR	Endovascular aneurysm repair
F	Fluorine
F^*	Fluorine radical
FHDD	Forchehheimer-Hazen-Dupity-Darcy
H	Hydrogen
H_{ij}	Sample height in *ij* plane (mm)
HMI	Human Machine Interface

HPED	N,N,N'N'-Tetrakis(2-hydroxypropyl) ethylenediamine
K	Permeability (m^2)
m	mass (g)
N_{open}	Number of ruptured or fully removed cell membranes
N_{total}	Total number of cell membranes
NCO	Isocynate
OF^-	Oxyfluoride ion
OH	Hydroxyl
O_2	Oxygen
ρ	Density (g/cm^3)
ρ_{app}	Apparent density (g/cm^3)
PLC	Programmable Logic Controller
PMMA	Poly(methyl methacrylate)
P_{ret}	Percent reticulation
Q	Flow rate (mL/min)
RF	Radio frequency
RO	Alkoxy radicals
RO	Reverse osmosis
sccm	Standard cubic centimeters
SEM	Scanning Electron Microscope
SMA	Shape memory alloy
SME	Shape memory effect

SMP	Shape memory polymer
TEA	2,2',2'-Nitrilotriethanol
T_g	Glass transition temperature (°C)
TMHDI	2,4,4-trimethyl-1,6-hexamethyene diisocyanate
μ	Dynamic viscosity (Pa•s)
UV	Ultraviolet light
v_0	Darcy velocity (m/s)
V	Geometrical volume (cm^3)
V_E	Volume expansion
V_S	Sample Volume (cm^3)
V_{wMBR}	Sample volume with cell membranes (cm^3)
W_{ij}	Sample width in *ij* plane (mm)
$2O^+$	Oxygen ion

TABLE OF CONTENTS

Page

ABSTRACT ii

DEDICATION iv

ACKNOWLEDGEMENTS v

NOMENCLATURE viii

TABLE OF CONTENTS xi

LIST OF FIGURES xiv

LIST OF TABLES xxi

CHAPTER I INTRODUCTION AND LITERATURE REVIEW 1

I.1 Shape Memory Polymer Foam 3
I.2 Biomedical Applications of Shape Memory Polymer Foam 5
I.2.1 Considerations for Biomedical Applications of Shape Memory Polymer Foam 5
I.2.2 Specific Biomedical Applications of Ultra-Low Density Polyurethane Shape Memory Polymer Foam 7
I.2.3 Embolization of Abdominal Aortic Aneurysms for Prevention of Type II Endoleaks Associated with Endovascular Aneurysm Repair 10
I.3. Reticulation of Polyurethane Shape Memory Polymer Foam 13
I.3.1 Fabrication of Polyurethane Shape Memory Polymer Foam 13
I.3.2 Reticulation Techniques 14
I.3.3 Plasma Reticulation 14
I.4 Summary of the Thesis 18

CHAPTER II DEVELOPMENT OF COLD PLASMA RETICULATION PROCESSES AND EVALUATION OF RETICULATION RESULTS 21

II.1 Materials and Methods 22
II.1.1 Synthesis of Ultra-Low Density Polyurethane Shape Memory Polymer Foam 22

Page

II.1.2 Fabrication of Ultra-Low Density Polyurethane Shape Memory Polymer Foam Samples....22
II.1.3 Development and Selection of Final Plasma Process Parameters....23
II.1.4 Plasma Reticulation....26
II.1.5 Quantifying Reticulation....28
II.1.6 Shape Memory Polymer Foam Block Sample Volume With Complete Membrane Removal....30
II.2 Results and Discussion....31
II.2.1 Quantifying Reticulation....31
II.2.2 Shape Memory Polymer Foam Block Sample Volume With Complete Membrane Removal....35
II.3. Conclusions....36

CHAPTER III MATERIAL CHARACTERIZATION OF PLASMA-RETICULATED ULTRA LOW-DENSTIY POLYURETHANE SMP FOAM....39

III.1 Materials and Methods....39
III.1.1 Measuring Apparent Density....39
III.1.2 Shape Memory Polymer Foam Cleaning....40
III.1.3 Permeability Measurements....41
III.1.4 Volume Expansion in Water....45
III.1.5 Differential Scanning Calorimetry (DSC)....46
III.2 Results and Discussion....46
III.2.1 Measuring Apparent Density....46
III.2.2 Permeability Measurements....47
III.2.3 Volume Expansion in Water....50
III.2.4 DSC....53
III.3 Conclusions....54

CHAPTER IV CONCLUSIONS AND FUTURE WORK....56

REFERENCES....62

APPENDIX A PLASMA PROCESS DEVELOPMENT....70

APPENDIX B SEM IMAGES FOR QUANTIFYING PERCENT RETICULATION....92

Page

APPENDIX C MACRO-IMAGES FOR MEASURING PERCENT VOLUME WITH COMPLETE MEMBRANE REMOVAL 117

LIST OF FIGURES

Page

Figure 1: Shape memory effect of shape memory polymer foam. Shape memory polymer foam can be fixed in a secondary shape by heating it above its T_g and applying a mechanical force to deform the foam into the desired secondary shape. Cooling the foam below its T_g, while constraining it in the secondary shape will fix the foam in the secondary shape until it is heated above its T_g. Increasing the temperature will act as a stimulus to actuate the foam to the primary shape. 5

Figure 2: (A) Procedure for implanting modular endovascular stent graft for abdominal aortic aneurysm repair begins with surgeon gaining bilateral access to the common femoral artery via a femoral artery cut down. A guide wire is inserted into the femoral artery and advanced to the aneurysm. Once in the aneurysm sac, a catheter is inserted over the guide wire. The compressed bifurcated body component of the graft is inserted through a sheath and advanced along the guide wire to the aneurysm. At the aneurysm, the sheath is withdrawn, allowing the bifurcated body graft to expand into the artery wall. The contralateral limb gate of the bifurcated body graft, where the iliac limb component of the graft attaches, is cannulated via a guide wire and catheter that are inserted through the contralateral femoral artery. After cannulation of the contralateral limb gate, the contralateral iliac limb graft is inserted through a sheath, advanced along the guide wire, and deployed at the contralateral limb gate. Angiogram confirms patency of both renal arteries and lack of a proximal endoleak. The introducer sheaths and guide wires are removed, and the femoral arteries are closed. (B) Types of endoleaks that occur after endovascular aneurysm repair of abdominal aortic aneurysms. (C) Prevention of Type II endoleaks by deploying shape memory polymer foam into aneurysm sac during endovascular aneurysm repair. 11

Figure 3: Coordinate system used to define the foam axes; Z is defined as the direction of foaming. Sample dimensions for plasma-reticulated shape memory polymer foam are not drawn to scale. 26

Figure 4: (A) A top-view schematic of the reaction chamber of the plasma machine. The green dots represent the reactive gas species (i.e. atoms, molecules, ions, electrons, free radicals, and metastables) present in the reaction chamber during plasma treatment. The reactive species chemically modify and reticulate the sample within the chamber. (B) Foam block loaded into the chamber on the 127 mm tall mesh aluminum stage.

(C) Foam sheet loaded into the chamber on a 127 mm tall mesh aluminum stage. 27

Figure 5: SEM image of as-made reticulated ultra-low density polyurethane shape memory polymer foam. Cell membranes circles in blue are closed and cell membranes circled in red are open. 30

Figure 6: SEM images of plasma-reticulated and as-made ultra-low density polyurethane shape memory polymer foam taken in the XY and ZY planes. All SEM images were taken at 15 kV and 27X magnification. 32

Figure 7: Macro-images of the slices taken in the XY and ZY planes of shape memory polymer foam block samples plasma-reticulated with Block Moderate and Block Complete processes. 35

Figure 8: Diagram of permeability measurement system [62]. 44

Figure 9: Average pressure gradient versus Darcy velocity measurements and Forchheimer-Hazen-Dupid-Darcy equation second order fitted curves for Control foam samples, Block Moderate, and Block Complete plasma-reticulated samples. 48

Figure 10: Average pressure gradient versus Darcy velocity measurements and Forchheimer-Hazen-Dupid-Darcy equation second order fitted curve for Block Complete plasma-reticulated samples. 48

Figure A-1: Foam block geometry of sample evaluated with plasma reticulation Processes 1-3. 70

Figure A-2: Placement of block samples on 38.1 mm Delrin cylinder supports for Processes 4-13. 73

Figure A-3: Image used to measure length of completely reticulated region within plasma-reticulated sample treated with Process 8. The length of Line 1 is 2.96 mm, Line 2 is 3.09 mm, and length of Line 3 is 3.93 mm. 76

Figure A-4: First two stages evaluated using Process 12 to improve reticulation homogeneity throughout ultra-low density shape memory polymer foam block samples. (A) Stage 1 consisted of two 1 mm diameter aluminum rods press fit into a 25.4 mm tall PMMA block, and the foam sample was gently pressed onto the aluminum rods. Image not drawn to scale. (B) Stage 2 consisted of one 1 mm diameter aluminum rod press fit into a 25.4 mm tall PMMA block, and the foam sample was gently pressed

onto the aluminum rod. Both stages were placed in the center of the reaction chamber and elevated the sample 127 mm above the glass shelf. 79

Figure A-5: Third stage, S3, evaluated using Process 12 to improve reticulation homogeneity throughout ultra-low density shape memory polymer foam block samples without piercing foam with sample stage. S3 consisted of two 1 mm diameter aluminum rods press fit into a 25.4 mm tall PMMA block, and a 76.2 x 76.2 mm (L x W) mesh polypropylene sheet epoxied to the tops of the aluminum rods, allowing the sample to be elevated 139.7 mm above the glass shelf in the reaction chamber. After S3 was placed in center of the reaction chamber, the foam sample was gently placed at the center of the mesh polymer sheet for plasma reticulation. Image not drawn to scale. 80

Figure A-6: Fourth stage, S4, evaluated using Process 12 to improve reticulation homogeneity throughout ultra-low density shape memory polymer foam block samples without piercing foam with sample stage. S4 consisted of a 50.8 x 50.8 x 25.4 mm (L x W x H) aluminum mesh cage, allowing the sample to be elevated 25.4 mm above the glass shelf in the reaction chamber. After S4 was placed in center of the reaction chamber, the foam sample was gently placed on the center of the stage for plasma reticulation. 81

Figure A-7: Fifth stage, S5, evaluated using Process 12 to improve reticulation homogeneity throughout ultra-low density shape memory polymer foam block sample. S5 consisted of a 50.8 x 50.8 x 127 mm (L x W x H) aluminum mesh stage, allowing the sample to be elevated 127 mm above the glass shelf in the reaction chamber. S5 was utilized while orienting the foam with such that the foaming direction was perpendicular to the electrode. 82

Figure A-8: First sample stage for plasma reticulating ultra-low density shape memory polymer foam sheet samples, S6. The sample stage was made of two stainless steel L-brackets screwed into a PMMA base, and a 0.2 mm diameter nitinol wire suspended between the L-brackets. The sheet samples were threaded onto the wire along the 101.6 mm edge, allowing the sample to be elevated 114.3 mm above the glass shelf. The samples were oriented such that the foaming direction was perpendicular to the electrode. 84

Figure A-9: (A) S7, the second sample stage evaluated to plasma reticulate ultra-low density shape memory polymer foam sheet samples. This sample

stage was constructed of mesh aluminum and utilized pieces of the mesh to hold the sample upright. (B) S8, the third sample stage evaluated for plasma reticulating the sheet samples. The sample stage was constructed of mesh aluminum and one 10 x 10 mm (W x H) piece of mesh aluminum on each side of the sample to hold it upright. (C) S9, the fourth sample stage evaluated for plasma reticulating sheet samples. The sample stage was constructed of mesh aluminum and three 10 x 10 mm (L x H) pieces of mesh aluminum on each side of the sample to hold it upright. All three of these sample stages were 152.4 x 76.2 x 127 mm (L x W x H), and elevated the sample 127 mm above the glass shelf within the reaction chamber. All samples were oriented such that the foaming direction was perpendicular to the electrode. 88

Figure A-10: Fifth sample stage for plasma reticulating ultra-low density shape memory polymer foam sheet samples, S10. The sample stage was made of mesh aluminum with dimensions: 152.4 x 76.2 x 127 mm (L x W x H), and elevated the sample 127 mm above the glass shelf within the reaction chamber. All samples were oriented such that the foaming direction was parallel to the electrode. 89

Figure B-1: SEM images in XY and ZY plan for quantifying percent reticulation of Block Moderate n1. 92

Figure B-2: SEM images in XY and ZY plan for quantifying percent reticulation of Block Moderate n2. 93

Figure B-3: SEM images in XY and ZY plan for quantifying percent reticulation of Block Moderate n3. 94

Figure B-4: SEM images in XY and ZY plan for quantifying percent reticulation of Block Moderate n4. 95

Figure B-5: SEM images in XY and ZY plan for quantifying percent reticulation of Block Moderate n5. 96

Figure B-6: SEM images in XY and ZY plan for quantifying percent reticulation of Block Complete n1. 97

Figure B-7: SEM images in XY and ZY plan for quantifying percent reticulation of Block Complete n2. 98

Figure B-8: SEM images in XY and ZY plan for quantifying percent reticulation of Block Complete n3. 99

Page

Figure B-9: SEM images in XY and ZY plan for quantifying percent reticulation of Block Complete n4. 100

Figure B-10: SEM images in XY and ZY plan for quantifying percent reticulation of Block Complete n5. 101

Figure B-11: SEM images in XY and ZY plan for quantifying percent reticulation of Sheet Moderate n1. 102

Figure B-12: SEM images in XY and ZY plan for quantifying percent reticulation of Sheet Moderate n2. 103

Figure B-13: SEM images in XY and ZY plan for quantifying percent reticulation of Sheet Moderate n3. 104

Figure B-14: SEM images in XY and ZY plan for quantifying percent reticulation of Sheet Moderate n4. 105

Figure B-15: SEM images in XY and ZY plan for quantifying percent reticulation of Sheet Moderate n5. 106

Figure B-16: SEM images in XY and ZY plan for quantifying percent reticulation of Sheet Complete n1 107

Figure B-17: SEM images in XY and ZY plan for quantifying percent reticulation of Sheet Complete n2 108

Figure B-18: SEM images in XY and ZY plan for quantifying percent reticulation of Sheet Complete n3 109

Figure B-19: SEM images in XY and ZY plan for quantifying percent reticulation of Sheet Complete n4 110

Figure B-20: SEM images in XY and ZY plan for quantifying percent reticulation of Sheet Complete n5 111

Figure B-21: SEM images in XY and ZY plan for quantifying percent reticulation of Control n1. 112

Figure B-22: SEM images in XY and ZY plan for quantifying percent reticulation of Control n2. 113

Figure B-23: SEM images in XY and ZY plan for quantifying percent reticulation of Control n3. 114

Page

Figure B-24: SEM images in XY and ZY plan for quantifying percent reticulation of Control n4. 115

Figure B-25: SEM images in XY and ZY plan for quantifying percent reticulation of Control n5. 116

Figure C-1: Macro-images of the slices taken in the XY and ZY planes for measuring percent volume with complete membrane removal within Block Moderate n1. 117

Figure C-2: Macro-images of the slices taken in the XY and ZY planes for measuring percent volume with complete membrane removal within Block Moderate n2. 117

Figure C-3: Macro-images of the slices taken in the XY and ZY planes for measuring percent volume with complete membrane removal within Block Moderate n3. 118

Figure C-4: Macro-images of the slices taken in the XY and ZY planes for measuring percent volume with complete membrane removal within Block Moderate n4. 118

Figure C-5: Macro-images of the slices taken in the XY and ZY planes for measuring percent volume with complete membrane removal within Block Moderate n5. 118

Figure C-6: Macro-images of the slices taken in the XY and ZY planes for measuring percent volume with complete membrane removal within Block Complete n1. 119

Figure C-7: Macro-images of the slices taken in the XY and ZY planes for measuring percent volume with complete membrane removal within Block Complete n2. 119

Figure C-8: Macro-images of the slices taken in the XY and ZY planes for measuring percent volume with complete membrane removal within Block Complete n3. 119

Figure C-9: Macro-images of the slices taken in the XY and ZY planes for measuring percent volume with complete membrane removal within Block Complete n4. 120

Page

Figure C-10: Macro-images of the slices taken in the XY and ZY planes for measuring percent volume with complete membrane removal within Block Complete n5. 120

LIST OF TABLES

Page

Table 1: Potential biomedical applications of ultra-low density polyurethane shape memory polymer foam, percent reticulation and biodegradability requirement for optimal design performance. 7

Table 2: Plasma process parameters provided by Plasma Technology Systems (Belmont, CA). These process parameters were used by Singhal to cold plasma reticulate ultra-low density polyurethane shape memory polymer foam [16]. 24

Table 3: Plasma process parameters selected for achieving moderate and complete reticulation of ultra-low density polyurethane shape memory polymer foam. The 'Plasma Process' defines the sample geometry and desired amount of reticulation. 28

Table 4: Percent reticulation in each plane and for the overall foam sample achieved by each plasma process selected for full evaluation and of as-made foam. 33

Table 5: Percent sample volume with complete membrane removal achieved by the plasma processes performed on the foam block samples. 36

Table 6: The apparent density before and after plasma treatment and the change in apparent density achieved by each plasma process. 46

Table 7: Permeability and form factor parameters calculated for as-made samples, Block Moderate, and Block Complete plasma-reticulated samples by applying second-order least squares fit to pressure gradient versus Darcy velocity data. 49

Table 8: Crimped diameter, recovered diameter, and volume expansion of as-made foam and of foam plasma-reticulated with one of the four plasma processes evaluated in this thesis. 51

Table 9: Wet T_g results of as-made foam and of foam plasma-reticulated with one of the four plasma processes evaluated in this thesis. 53

Table A-1: Plasma process parameters provided by Plasma Technology Systems (Belmont, CA). These parameters were the first process parameters utilized to plasma reticulate ultra-low density shape memory polymer foam with the block geometry. 70

Page

Table A-2: Percent reticulation results in the XY and ZY planes and for the overall foam samples achieved by the first three plasma processes. 71

Table A-3: Plasma process parameters utilized to plasma reticulate ultra-low density shape memory polymer foam with the block geometry via Processes 4-11. 74

Table A-4: Percent reticulation and depth of complete reticulation boundary layer for ultra-low density shape memory polymer foam block samples treated with Processes 4-9. 77

Table A-5: Plasma process parameters utilized to plasma reticulate ultra-low density shape memory polymer foam via Processes 12 and 13..... 78

Table A-6: Plasma process parameters utilized to plasma reticulate ultra-low density shape memory polymer foam with the block geometry via Processes 14-18. 83

Table A-7: Percent reticulation results in the XY and ZY planes and for the overall foam samples achieved by the Processes 16-18. 83

Table A-8: Plasma process parameters utilized to plasma reticulate ultra-low density shape memory polymer foam with the sheet geometry via Processes 19-22. 85

Table A-9: Percent reticulation results in the XY and ZY planes and for the overall foam samples achieved by the Processes 19-22. 86

Table A-10: Plasma process parameters utilized to plasma reticulate ultra-low density shape memory polymer foam with the sheet geometry via Processes 19-27. 86

Table A-11: Plasma process parameters utilized to plasma reticulate ultra-low density shape memory polymer foam with the sheet geometry via Processes 27-31. 89

Table A-12: Percent reticulation results in the XY and ZY planes and for the overall foam samples achieved by the Processes 27-31. 90

CHAPTER I

INTRODUCTION AND LITERATURE REVIEW

Shape memory polymer (SMP) foam is an active material with several properties that give it the potential to be utilized in a variety of industries. These properties include low densities, easy processability, low cost, high recovery ratios, tunable glass transition temperature (T_g), and excellent biocompatibility and shape memory behavior [1-7]. SMP foams have proposed applications in biomedical, aerospace, structural, textile, and oil and gas industries [5]. However, utilization of SMP foams for this breadth of industries has not yet been fully accomplished because SMP foams are continuously being developed and analyzed. Furthermore, each specific application has explicit thermal and mechanical requirements that must be met in order to exploit the full potential of SMP foam. Satisfying the explicit requirements for a specific application requires research and development of each factor that influences overall SMP foam performance, as well as complete characterization of the fabricated SMP foam. Factors in the foam synthesis process that must be tailored for specific applications include the fabrication method, the constituent blowing agents, catalysts and surfactants, fillers that may be physically or chemically loaded into the SMP foam, and post-synthesis processing techniques.

Biomedical applications of SMP foam take advantage of its volume recovery, characteristic large surface area to volume ratio, and its ability to self-actuate upon exposure to an external stimulus. Biomedical applications include embolic vascular devices, scaffolds for filling bone defects, hemostatic sponges, soft tissue scaffolds, and

drug-delivery systems [5]. Each of these applications has specific requirements regarding average pore size, porosity, pore shape, pore interconnectivity, surface characteristics, mechanical properties, and biodegradability. These parameters are important because each influences specific cell infiltration, proliferation and differentiation within the foam, the rate of diffusion of nutrients and wastes, the inflammatory response, and what types of tissue scaffolds can be supported by the foam [1].

The leading focus of biomedical application research of SMP foam has been for embolic vascular devices [5]. Prevention of endoleaks associated with endovascular aneurysm repair (EVAR) of abdominal aortic aneurysms (AAAs) is an application in which SMP foam can be utilized as an embolic vascular device. An AAA is a weakened, ballooned region of the abdominal aorta that has expanded to greater than 50% of the normal vessel diameter [8]. Large, fast-growing or leaking aneurysms are treated via EVAR, and endoleak complications occur in up to 40% of EVAR patients [8-10]. Endoleaks occur when blood flows outside the stent-graft lumen and into the aneurysm sac, increasing sac pressure and risk of rupture. The goal of SMP foam in this application is to prevent type II endoleaks (EII) by implanting foam during EVAR into the aneurysm sac to promote rapid clot formation and allow components of the healing pathway to migrate throughout the foam for enhanced embolization within the aneurysm sac.

The influence of pore interconnectivity on physiological responses to SMP foam has led investigators to research methods for increasing and controlling pore

interconnectivity of SMP foam and was the focus of this thesis. In this thesis, the amount of pore interconnectivity was analogous to the amount of reticulation. The motivation for increasing and controlling reticulation of SMP foam for EII prevention are the factors that influence thrombosis: the blood coagulation cascade and changes in blood flow. Increasing and controlling the amount of reticulation will: 1) optimize the foam surface to volume ratio to enhance contact activation of the clotting cascade, 2) create flow stagnation and abnormal thrombogenic fluid shear rates within the foam, and 3) promote the mobility of cellular components required for the deposition of connective tissue throughout the foam [11-15].

Several methods for reticulating polyurethane SMP foam have been proposed, including hydrolysis, oxidation, heat or mechanical treatment, quenching, and zapping. However, reticulation of ultra-low density foam ($\rho_{app} < 0.02$ g/cm^3) using these techniques has been mostly ineffective. The SMP foam analyzed in this project was an ultra-low density polyurethane SMP foam that has been effectively reticulated via cold plasma treatment [16]. This thesis focused on the utilization of cold plasma treatment to effectively reticulate ultra-low density SMP polyurethane foam for EII prevention.

I.1 Shape Memory Polymer Foam

SMPs are smart materials with the ability to be deformed and fixed in a temporary shape and upon exposure to an external stimulus (i.e. heat, UV light) return to their primary shape [6, 7]. Compared to other materials that exhibit the shape memory effect (SME), such as shape memory alloys (SMAs), SMPs are lightweight, easy to process, low cost to manufacture, have high recovery ratios, tunable T_g, excellent

biocompatibility and shape memory behavior [1-7]. The unique properties of SMPs give them major advantages over other biomaterials and allow them to have numerous biomedical applications. Fabricating SMPs into foam further advances the advantages of SMPs by resulting in lower mass, faster deployment rates, and greater expanded to compressed volume ratio [2].

The SME of SMPs is based upon molecular structure and molecular movements of the polymer chains within the foam. SMPs are made up of elastic polymer networks, which contain stimuli-sensitive switches that induce macroscopic shape modification when activated by temperature variations, chemical gradients, or electromagnetic fields [1]. Most SMPs are thermally activated; the SMP changes from a temporary shape to its original, permanent shape when exposed to heat [7]. The polymer network of SMPs is made of two types of segments, "netpoints" and "switching segments". Chemical or physical crosslinks are the "netpoints" which determine the permanent shape, while the "switching segments" soften when heated above T_g to allow the SMP to maintain a temporary shape and recover the permanent shape [17]. To observe the SME, a SMP is heated above T_g, which causes it to enter a rubbery elastic state in which it is easily deformed into a temporary shape. When the SMP is cooled below its T_g and fixed in the temporary shape, the temporary shape is retained as the SMP returns to its rigid state and loses its rubbery elasticity. The SMP recovers its original shape when it is heated above T_g [2]. The SME of SMP foam is illustrated in Figure 1 [18].

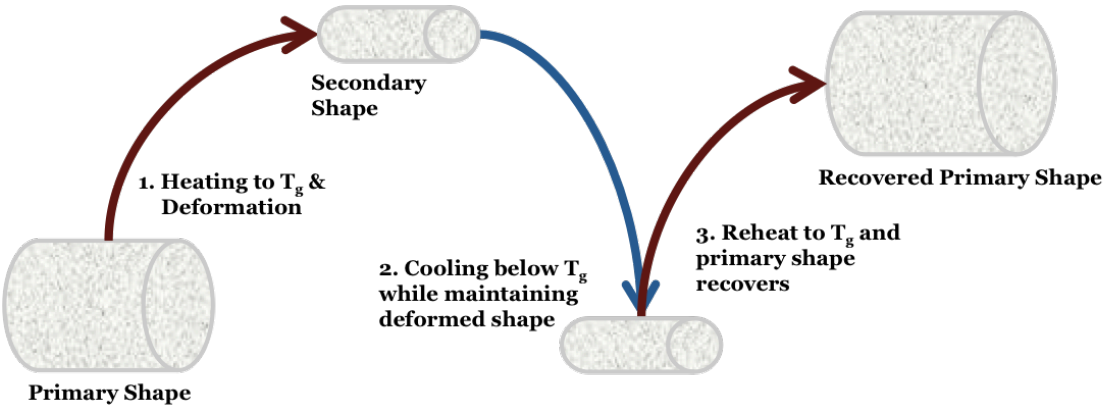

Figure 1: Shape memory effect of shape memory polymer foam. Shape memory polymer foam can be fixed in a secondary shape by heating it above its T_g and applying a mechanical force to deform the foam into the desired secondary shape. Cooling the foam below its T_g, while constraining it in the secondary shape will fix the foam in the secondary shape until it is heated above its T_g. Increasing the temperature will act as a stimulus to actuate the foam to the primary shape.

The SMP chemistry used in this thesis was 100% TMHDI polyurethane SMP foam, which is an advantageous and popular material for biomedical applications for several reasons in addition to the SME it exhibits. Polyurethane foams are highly biocompatible and thrombogenic [3, 4, 6, 7, 19, 20]. The T_g can range from -100°C to +80°C for thermal actuation, thus T_g can be tuned such that the foam actuates at body temperature when deployed into the body [3, 4, 6, 7].

I.2 Biomedical Applications of Shape Memory Polymer Foam

I.2.1 Considerations for Biomedical Applications of Shape Memory Polymer Foam

SMP foam has the potential to be utilized in several biomedical applications, and each potential application has specific requirements for average pore size, porosity, pore shape, amount of reticulation, surface characteristics, mechanical properties, and biodegradability. Each of these parameters influences the physiological response to SMP foam. Specific pore sizes can enhance cellular activity of specific cell types; the optimal

pore size for neovascularization is 5 μm, 5-15 μm for fibroblast ingrowth, 75-250 μm for bone growth, and 200-300 μm for fibro-cartilaginous tissue [1, 21, 22]. While the specific magnitudes of porosity and reticulation are undefined, several experiments have shown that porosity and reticulation influence tissue regeneration. Larger pores enhance mass transport and neo-vascularization within SMP foam, while smaller pores provide larger surface to volume ratio for optimal cell attachment and proliferation [21, 22]. Furthermore, reticulation is critical for ensuring that all cells are within 200 μm of the blood supply in order to allow for sufficient mass transfer of nutrients and waste [21].

Biocompatibility of SMP foam is affected by the surface characteristics: surface wettability, hydrophilicity/hydrophobicity ratio, bulk chemistry, surface charge and charge distribution, surface roughness, and rigidity [21]. Each of these characteristics affects adsorption, desorption, and proliferation of different types of mammalian cells. Different formulations of SMP foam and surface treatments can be utilized to favorably induce adhesion of specific cells or deliver drugs at the implant site. When implanted into the body, the foam must have sufficient mechanical properties to prevent it from fracturing and dislodging from its implantation site. Furthermore, the foam must have high strength and rigidity if it is to be implanted into load bearing tissue or low strength and rigidity if it is to be implanted into soft tissue. For tissue engineering applications, SMP foam must be able to support loads and stresses that the tissue it is generating will ultimately bear, while also degrading at a specific rate that optimally transfers loads to the growing tissue [21].

I.2.2 Specific Biomedical Applications of Ultra-Low Density Polyurethane Shape Memory Polymer Foam

Considering the requirements for each potential biomedical application of SMP foam, the low strength and rigidity of the ultra-low density polyurethane SMP foam used in this thesis focuses its biomedical applications to three major categories: embolization, soft tissue engineering, and thrombectomy, as shown in Table 1. While Table 1 is not an exhaustive list of potential biomedical applications of ultra-low density polyurethane SMP foam, it shows how much potential this material has in the biomedical field. The importance of reticulation in influencing the physiological response to SMP foam is the motivation for emphasizing the optimal reticulation level for biomedical applications of ultra-low density polyurethane SMP foam.

Table 1: Potential biomedical applications of ultra-low density polyurethane shape memory polymer foam, percent reticulation and biodegradability requirement for optimal design performance.

	Purpose of SMP Foam	Specific Applications	Amount of Reticulation	Biodegradable
Embolization [2, 23, 24]	- Rapid, Stable Clot Formation - Scar Tissue Formation	- AAA Endoleak Prevention - Aneurysm Embolization - Ateriovenous Fistula - Ateriovenous Malformation - Chronic Venous Insufficiency - Tumors - Upper and Lower Gastrointestinal Bleeding - Uterine Fibroid	60-80% - Cell Membranes Present, Ruptured Open	Application specific
Thrombectomy [25]	- Immediate Clot Formation - Remove Embolus - Fill Blood Vessel to Prevent Embolus Fragments from Traveling Past Device	Thrombectomy	100% - Cell Membranes Present, Ruptured Open	No

Table 1 Continued.

	Purpose of SMP Foam	Specific Applications	Amount of Reticulation	Biodegradable
Soft Tissue Engineering [1, 2, 21, 26-30]	- Promote Ingrowth of Cells and Tissue - Mechanical Integrity to Support Regenerating Tissue	- Artificial Blood Vessels - Coronary Graft - Intervertebral Disk Regeneration - Vascular Graft - Peripheral Nerve Growth - Skin Graft - Smooth Muscle Growth	100% - Cell Membranes Completely Removed	Yes

Embolization applications require the foam to achieve rapid, stable clot formation and promote cell movement throughout the foam. Temporary embolization will require the foam to be biodegradable and the morphology to allow cells for recanalization and vessel healing to migrate throughout the foam [2, 23, 24]. Permanent embolization does not require the foam to be biodegradable, but the morphology must allow cell migration throughout the foam to deposit connective tissue for fibrous tissue formation [14]. The application of ultra-low density polyurethane SMP foam in a thrombectomy procedure requires the foam to expand to fill the occluded vessel and stop embolus fragments from traveling past the device and causing downstream complications [25]. Furthermore, the foam should induce immediate thrombosis in an effort to allow the foam-induced thrombus to form as a continuation of the embolus that is being removed. This approach will allow complete thrombus extraction, while current mechanical thrombus removal techniques fragment the thrombus and either allow the

fragments to enter into pulmonary circulation or pull the fragments into the device for removal [31].

Embolization applications require the foam to be 60-80% reticulated while the thrombectomy application requires 100% reticulation. Both applications desire high reticulation levels with cell membranes still intact. These reticulation percentage requirements are motivated by the factors that influence thrombosis: the blood coagulation cascade and changes in blood flow. The blood coagulation cascade is traditionally broken into three pathways: the intrinsic, extrinsic, and common pathways [32]. The intrinsic pathway, also known as the contact pathway, has been recognized as the pathway that initiates the coagulation cascade [13]. Reticulation of SMP foam increases the surface to volume ratio for enhanced contact activation of the clotting cascade. Reduced and elevated blood shear rates have been identified as contributors to thrombus formation. Reduced shear rates correspond to low blood velocities and stagnation, while elevated shear rates correspond to tortuous blood flow and high blood velocities [32, 33]. High reticulation, with cell membranes still present, is desired for embolization applications because high pore interconnectivity will allow blood to flow throughout the foam implant for enhanced activation of the contact pathway, while the membranes will create recirculation zones with regions of reduced and elevated shear rates. However, complete reticulation is desired for the thrombectomy application because it will result in maximum surface to volume ratio for optimal activation of the contact pathway, in an effort to achieve immediate thrombosis.

The use of ultra-low density polyurethane SMP foam for soft tissue engineering is highly application specific and may require the foam to be mixed with other materials, such as carbon nanotubes (CNT), to improve the mechanical properties and tissue regeneration capabilities [27]. In general, the foam must maintain its mechanical properties and morphology while supporting the attachment, proliferation, and differentiation of cells [1, 2, 21, 26-30]. Furthermore, the foam should degrade at the same rate that the tissue is regenerated [22]. The percent reticulation requirement for soft tissue engineering applications is 100%, and the membranes must be completely removed. The requirement for full reticulation is driven by the need to provide the cells with a large surface area for cell adhesion, while removing the membranes allows cells to move freely throughout the foam volume as they proliferate and differentiate [21]. A fully reticulated morphology will also promote diffusion of nutrients and waste products required for cell survival [30].

I.2.3 Embolization of Abdominal Aortic Aneurysms for Prevention of Type II Endoleaks Associated with Endovascular Aneurysm Repair

The focus of this thesis was the embolization application of ultra-low density polyurethane SMP foam for prevention of EII associated with EVAR of AAAs. Ruptured AAA is the 13th leading cause of death in the U.S. [34]. Annually, 35,000-40,000 AAAs are repaired by open or endovascular surgery in the U.S., costing approximately $18,000 and $20,700, respectively [9]. Open repair requires an incision to be made in the abdomen to remove the damaged section of the aorta and suturing a graft in its place [8, 35]. EVAR is minimally invasive, requiring the surgeon to only make a

small incision in each groin for bilateral access [8, 35]. Most endovascular stent graft designs are modular, consisting of a bifurcated body and an iliac limb component. During the procedure, a catheter is guided through one femoral artery to deploy the bifurcated body component of the stent, then another catheter guides the iliac limb component through the contralateral femoral artery to attach it to the bifurcated body component, as shown in Figure 2 (A) [36-38]. This modular design ensures proper proximal and distal fixation of the stent graft to minimize migration and endoleaks [39].

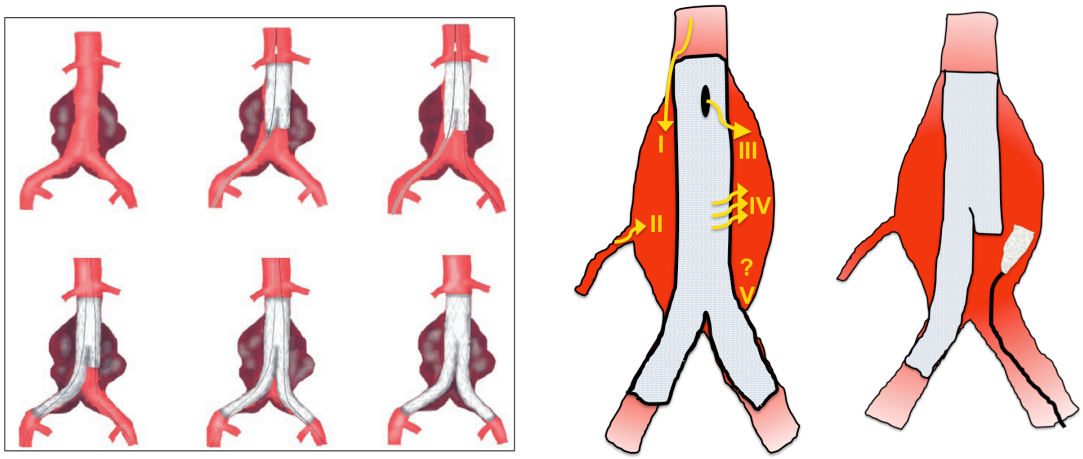

Figure 2: (A) Procedure for implanting modular endovascular stent graft for abdominal aortic aneurysm repair begins with surgeon gaining bilateral access to the common femoral artery via a femoral artery cut down. A guide wire is inserted into the femoral artery and advanced to the aneurysm. Once in the aneurysm sac, a catheter is inserted over the guide wire. The compressed bifurcated body component of the graft is inserted through a sheath and advanced along the guide wire to the aneurysm. At the aneurysm, the sheath is withdrawn, allowing the bifurcated body graft to expand into the artery wall. The contralateral limb gate of the bifurcated body graft, where the iliac limb component of the graft attaches, is cannulated via a guide wire and catheter that are inserted through the contralateral femoral artery. After cannulation of the contralateral limb gate, the contralateral iliac limb graft is inserted through a sheath, advanced along the guide wire, and deployed at the contralateral limb gate. Angiogram confirms patency of both renal arteries and lack of a proximal endoleak. The introducer sheaths and guide wires are removed, and the femoral arteries are closed. (B) Types of endoleaks that occur after endovascular aneurysm repair of abdominal aortic aneurysms. (C) Prevention of Type II endoleaks by deploying shape memory polymer foam into aneurysm sac during endovascular aneurysm repair.

Endoleak complications have been reported to occur in up to 40% of EVAR patients; EII is the most common, with occurrence rates as high as 10-30% [9, 40]. Endoleaks are classified according to the leak source, as shown in Figure 2 (B). Type I endoleaks are leaks that develop at the proximal or distal attachment sites of the stent graft. EII occur when collateral flow causes retrograde blood from visceral arteries to leak into the aneurysm sac. Type III endoleaks are attributed to holes, defects, or separations within the stent-graft material itself, while Type IV endoleaks are due to porosity of the stent-graft material. Type V endoleaks are not associated with a leak into the aneurysm sac; instead the aneurysm sac continues to expand without evidence of a leak [40]. The development of EII has a high incidence of required secondary intervention, graft explantation, or observations of continued aneurysm sac growth. Secondary intervention methods for treating EII include transarterial embolization, translumbar embolization, ligation of the back bleeding arteries, and sac plication. Successful EII prevention would decrease additional costs for secondary procedures, as well as patient exposure to radiation and contrast agents associated with the additional procedures [9, 41]. Inducing thrombosis within the aneurysm sac during EVAR by injecting liquid embolics, fibrin glue, microcoils, a thrombogenic absorbable gelatin sponge, or polyurethane foam has been proposed for EII prevention [19, 41, 42]. However, no specific dose of material for EII prevention has been standardized [9].

Ultra-low density polyurethane SMP foam is a potential material for EII prevention because it can be fixed in a temporary compressed geometry and expanded to its original geometry, via passive actuation due to water plasticization, when exposed to

body temperature during deployment into the aneurysm sac [19, 20]. Figure 2 (C) shows the deployment of SMP foam into the aneurysm sac during EVAR.

I.3. Reticulation of Polyurethane Shape Memory Polymer Foam

I.3.1 Fabrication of Polyurethane Shape Memory Polymer Foam

SMP foam morphology is a significant component of its successful utilization in biomedical applications. The inherit morphology of polyurethane SMP foam is an anisotropic cellular structure with thin residual membranes between cells [7]. Whether SMP foam morphology is open-celled, closed-celled, or mixed open- and closed-cell is mostly determined by the fabrication technique and process parameters used to synthesize the SMP foam [5]. Fabrication techniques include particulate leaching, fiber bonding, saturation with supercritical gases, high internal phase emulsion polymerization, thermally induced phase separation, stereolithography, selective laser sintering, fused deposition modeling and gas foaming [7]. For the fabrication of ultra-low density polyurethane SMP foam, gas foaming is utilized because it can produce foam that has ultra-low density, is compatible with highly cross-linked materials, and multiple additives are commercially available to modulate the physical properties of the SMP foams [7]. Polyurethane SMP foam synthesized via gas foaming is generally anisotropic and can be open-, closed-, or mixed-celled, with pore sizes ranging from sub-micron to mm [5]. The ultra-low density polyurethane SMP foam used in this thesis was mixed-celled, the foam was 27.51 ± 8.24% (average ± standard deviation, n = 5) reticulated; percent reticulation (P_{ret}) corresponds to the percent of membranes that are open or completely removed.

I.3.2 Reticulation Techniques

Reticulation is a secondary physical process in which residual cell membranes are opened and removed from SMP foam to improve permeability. Polyurethane foam may be reticulated via hydrolysis, oxidation, heat, or mechanical treatment [16]. Standard industry methods include quenching and zapping. Quenching requires submerging as-made foam in a bath of warm sodium hydroxide while beating the bath to break the residual membranes. In zapping, as-made foam is placed into a pressure chamber where the foam is exposed to flammable gases for controlled burning of the membranes [43].

I.3.3 Plasma Reticulation

Plasma treatment of materials has been used throughout industry for etching, sterilization and functionalization of material surfaces [44-47]. The etching capability of plasma treatment has been shown to be a viable method for reticulating polymer foam. Hild and Biering applied for a US patent in which plasma was cited as a mechanism for reticulating polyimide foams used for insulation [48]. Reticulation of polyurethane foam via plasma has been observed for other purposes, such as sterilization and surface modifications [1, 49, 50]. Singhal successfully used cold plasma treatment to fully reticulate ultra-low density polyurethane SMP foam [16]. This thesis further investigated the use of cold plasma treatment to control reticulation levels of ultra-low density polyurethane SMP foam.

The plasma treatments in this thesis were performed using a cold plasma treatment system (Aurora 0350 Plasma Surface Treatment System, Plasma Technology

Systems, Belmont, CA). Plasma systems can operate at atmospheric pressure (760 Torr) or under vacuum at low pressures (0.005-0.5 Torr). Atmospheric pressure plasma processes have high collision rates between electrons and gas molecules within the plasma [51]. The high collision rates cause the electrons, ions and gas molecules within the plasma to reach thermal equilibrium and the plasma process to occur at temperatures as great as 1,000,000°C [52]. Low-pressure plasma processes have lower collision rates between electrons and gas molecules, preventing the electrons, ions and gas molecules from reaching thermal equilibrium [51, 52]. The non-thermal equilibrium condition in low-pressure plasma processes allows them to operate at approximately 23-30°C. Utilization of atmospheric plasma processes would not be feasible for reticulating ultra-low density polyurethane SMP foam because the material would not be able to withstand the extreme temperatures observed in these plasma processes. Therefore, the use of a cold plasma treatment system that operates under vacuum, as the Aurora 0350 Plasma Surface Treatment System does, is optimal for plasma reticulation of ultra-low density polyurethane SMP foam.

Plasma is defined as an ionized gas; neutral mixture of positive ions and negative electrons formed by stripping electrons from atoms [53, 54]. The processes that accomplish plasma etching are analogous to those that accomplish plasma reticulation. Polymer etching employs a mixture of gases, usually oxygen (O_2) and tetrafluoromethane (CF_4). The high electronegativities of oxygen and fluorine (F) atoms cause them to form reactive species that most readily accomplish hydrogen (H) abstraction and polymer chain cleavage [55]. Mixing O_2/CF_4 during the plasma process

creates the oxyfluoride ion (OF^-). Oxyfluoride is proficient at cleaving the carbon-carbon (C-C) bonds that make up the polymer backbone. Thus, O_2/CF_4 is the gas mixture that is used for optimizing plasma etching/reticulation rates and homogeneity [56].

Plasma reticulation using O_2/CF_4 process gases can be broken down into five steps: 1) Radio frequency (RF) power ionizes the process gases, releasing ions ($2O^+$), electrons (e^-) and radicals (F^*), as show in Equation 1A and 1B.

$$O_2 \rightarrow 2O^+ + 2e^- \quad (1A)$$

$$CF_4 + e^- \rightarrow CF_3 + F^* + e^- \quad (1B)$$

2) Ionized O_2/CF_4 gases react to form the OF^- reactive species, as shown in Equation 2 [56].

$$3e^- + 2O^+ + CF_3 \rightarrow COF_2 + OF^- \quad (2)$$

3) Fluorine radicals (F^*), made in step 1, and O_2 molecules abstract H from the polymer chain to create radical sites (C^*) on the polymer chain [57], shown in Equation 3A and 3B.

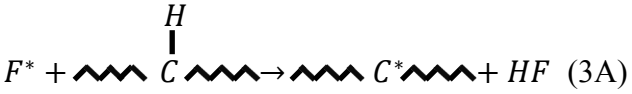

(3A)

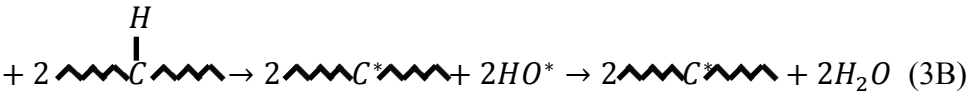

(3B)

4) O_2 is incorporated at radical sites to form unstable alkoxy radicals (RO).

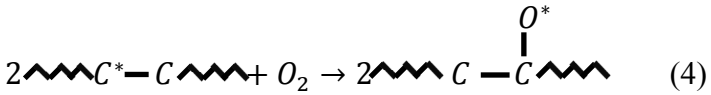

(4)

5) The OF^- reactive species cleave the polymer chains at C-C bonds into successively smaller fragments until the chains are lost as volatile species, shown in Equation 5 [55].

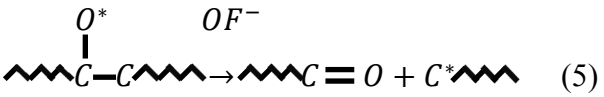

(5)

In polyurethane SMP foam, the membranes have a high surface area and low thickness compared to the cell struts, allowing the membranes to be volatized while the struts remain intact during plasma treatment.

The molar ratio of O_2/CF_4, gas flow rate, process pressure, duration, and RF power are plasma process parameters that determine the depth, rate, and homogeneity of plasma reticulation [46, 47, 56]. Once the processes gases have been ionized, reticulation is initiated when H is abstracted from the polymer chains. Ionized O_2 readily abstracts H at nominal reticulation rates, but the addition of F atoms in plasma increases oxygen dissociation and enhances reticulation rates [58]. Adding CF_4 as a source of F to the plasma process increases electron densities within the plasma and allows $2O^+$ ions to react with F^* radicals to form OF^-, which acts as a reactive species to enhance C-C cleavage beyond that accomplished only by O_2 [58]. Thus, mixing O_2 and CF_4 in a plasma process increases reticulation rates, but the molar ratio of O_2/CF_4 is critical in determining optimal reticulation rates. Maximum reticulation rates occur at 20-30% CF_4. At CF_4 concentrations < 20%, small amounts of F contribute to the reticulation process. Conversely, at CF_4 concentrations > 30% the reticulation reactions that utilize CF_4 compete with fluorine passivation of the surface and polymerization of CF_4 [58].

The flow rate of the process gases, measured in standard cubic centimeters (sccm), is analogous to the process pressure; greater flow rates correspond to greater process pressures. Plasma processes that operate at low pressures (< 200 mTorr) yield anisotropic reticulation. At low pressures, sheath collisions of ions and electrons are

minimized, allowing ions ($2O^+$) to cleave the majority of C-C bonds in the normal direction, and fewer reactive species (OF^-) to cleave C-C bonds in the perpendicular direction via chemical etching [58]. Thus, at low process pressures, higher etch rates are observed in the normal direction, yielding anisotropic reticulation amounts. At higher pressures the ions ($2O^+$) reach lower energies, and react with more free electrons (e^-) and radicals (F^*) which allows an equivalent number of C-C bonds to be cleaved via ion bombardment in the normal direction and via chemical etching in the perpendicular direction [58]. Thus, higher pressures yield isotropic reticulation throughout the material. Process pressure of 400 mTorr has been reported to produce fast and isotropic reticulation [59].

Selecting the RF power and process duration is a balancing exercise because reticulation rates should be maximized without over reticulating or damaging the material. RF power governs the reticulation rate because it dictates the fraction of original neutral gases that are ionized and the ion energies achieved during the plasma process [58, 60]. Furthermore, higher RF power corresponds to greater overall process temperature, which may damage heat sensitive materials.

I.4 Summary of the Thesis

Controlling the P_{ret} of SMP foam is desired for furthering its potential in biomedical applications. This thesis specifically aimed to achieve moderate and complete reticulation of ultra-low density polyurethane SMP foam to enhance thrombosis and embolization of the aneurysm sac during treatment of AAA to prevent EII. The goal of this thesis was to develop a new method for controlled reticulation of

ultra-low density polyurethane SMP foam and to characterize the effects of cold plasma reticulation on the foam. The thesis is organized as follows:

Chapter II discusses the approach taken to develop the plasma processes used to achieve moderate (60-80%) and complete (>95%) reticulation via cold plasma treatment, of two different geometries of ultra-low density polyurethane SMP foam. The two geometries of SMP foam investigated were foam blocks and foam sheets. The final plasma process parameters selected for achieving each reticulation level for each foam geometry are presented. The method for quantifying the reticulation level achieved by each of the final plasma processes is described. Concern regarding the development of a percent reticulation gradient from the surface of the foam block samples to the center motivated the sample volume with complete membrane removal to be measured for the foam block samples. The results from quantifying the reticulation levels achieved by each plasma process for both geometries are presented, along with the percent volume with complete membrane removal achieved within the block samples.

Chapter III presents the methods and results of the characterization techniques performed on the plasma-reticulated SMP foam samples identified in Chapter II. The density of the plasma-reticulated SMP foam was measured before and after treatment to calculate the change in apparent density achieved by each reticulation process. The major motivation for controlling reticulation was optimizing permeability of the foam, thus characterization of the plasma-reticulated foam's permeability was important for evaluating the effectiveness of the plasma processes. The small geometry of the foam sheets limited permeability characterization to the foam block samples. A porous media

approach was employed to calculate the geometrical parameters permeability (K) and form factor (C) from the Forchehheimer-Hazen-Dupity-Darcy (FHDD) equation. To evaluate the effects of plasma reticulation on shape recovery of SMP foam via thermal actuation in an aqueous environment, volume expansion (V_E) studies were performed in water at a temperature above the wet T_g of the SMP foam. Finally, the wet T_g of the plasma-reticulated foams was measured using Differential Scanning Calorimetry (DSC) to determine whether increasing reticulation levels had an effect on the actuation temperature of the foam. The results of the material characterization techniques are presented and discussed to evaluate the overall effects of plasma reticulation on ultra-low density polyurethane SMP foam.

CHAPTER II

DEVELOPMENT OF COLD PLASMA RETICULATION PROCESSES AND EVALUATION OF RETICULATION RESULTS

A literature review of the mechanisms of plasma reticulation and the plasma process parameters that influence the rate, depth, and homogeneity of plasma reticulation are discussed in Chapter I. This chapter briefly describes the foaming process used for synthesizing the ultra-low density polyurethane SMP and the sample preparation technique for fabricating the specific foam geometries used in this thesis. The approach used to identify the combination of plasma process parameters that achieve moderate (60-80%) and complete (>95%) reticulation of two SMP foam geometries is also discussed. The method and results are presented for quantifying the reticulation level achieved by each selected plasma process. Plasma reticulation occurs from the material surface inward; the reactive species reticulate the cell membranes at the surface first, which allows the reactive species to progressively access membranes deeper within the foam. Reticulation from the surface to the center may be observed as a gradient, with complete membrane removal at the surface and moderate reticulation at the center. The development of a reticulation gradient was only a concern for the block samples due to the large sample depth. To evaluate the development of a reticulation gradient from the surface to the center of the block samples, the percent volume of the block samples with complete membrane removal was measured.

II.1 Materials and Methods

II.1.1 Synthesis of Ultra-Low Density Polyurethane Shape Memory Polymer Foam

The foam utilized in this thesis was synthesized in a three-step method reported previously [7, 16, 61]. First, an isocynate (NCO) premix was made from N,N,N'N'-Tetrakis(2-hydroxypropyl) ethylenediamine (HPED, 99% Sigma Aldrich, St. Louis MO), 2,2',2'-Nitrilotriethanol (TEA, Sigma Aldrich, St. Louis, MO), and 2,4,4-trimethyl-1,6-hexamethyene diisocyanate (TMHDI, TCI America Inc.); the NCO premix was allowed to react at ambient temperature for 2 days. In the second step, HPED, TEA, deionized (DI) water (Millipore water purifier system, Millipore, Inc.), and catalysts (BL-22 and T-131 (Huntsman Corporation)) were mixed together to make a hydroxyl (OH) premix. Lastly, the NCO premix was combined with surfactants (DC 198 and DC 5943 (Air Products and Chemical Inc.)), the OH premix, and a physical blowing agent, Enovate (Honeywell, College Station, TX), to ensure the foam rose correctly as it cured in an oven for 20 minutes at 90°C. The foam was brought out of the oven and cooled to room temperature before further processing.

II.1.2 Fabrication of Ultra-Low Density Polyurethane Shape Memory Polymer Foam Samples

The use of cold plasma treatment to control the reticulation level of ultra-low density polyurethane SMP foam was evaluated using two SMP foam geometries. The sample geometries were selected based on the procedure for deploying SMP foam into the aneurysm sac during EVAR for EII prevention. The two foam geometries were: 1)

foam block with 50.8 x 50.8 x 25.4 mm dimensions, and 2) foam sheet with 50.8 x 101.6 x 5 mm dimensions. The block geometry was selected to allow a single piece of SMP foam to be plasma reticulated and smaller devices to be cut out of the block post plasma processing. The sheet geometry was selected as a preliminary device geometry for EII prevention. It was proposed that post plasma reticulation, the sheet would be heated above its T_g, then compressed and rolled into a small temporary geometry that would fit into a catheter for delivery into the aneurysm sac. Upon exposure to blood at body temperature, the foam sheet would actuate and recover its original sheet geometry and fill the aneurysm sac for optimal embolization for EII prevention.

It has been observed that pore size influences plasma penetration depth [47]. Within bulk foam, pore size increases and density decreases along the height of the foam. Thus, inhomogeneity of pore size and density throughout the height of the bulk foam could be sources of inconsistencies in P_{ret} achieved by a single plasma process. To minimize the effects of pore size and density inconsistencies on the reticulation results, a resistive wire cutter was used to cut all samples from the middle of bulk foam.

II.1.3 Development and Selection of Final Plasma Process Parameters

The plasma processes performed in this thesis were conducted in the Aurora 0350 Plasma Surface Treatment System, manufactured by Plasma Technology Systems (Belmont, CA). The process parameters that can be set at the Human Machine Interface (HMI) of the Aurora 0350 Plasma Surface Treatment System are the process gases, flow rate of each gas, RF power, and process duration. At the initiation of this project, Plasma Technology Systems provided the plasma process parameters previously investigated by

Pooja Singhal to show cold plasma treatment is a viable technique for reticulating ultra-low density polyurethane SMP foam [16]. The plasma process parameters provided by Plasma Technology Systems are presented in Table 2.

Table 2: Plasma process parameters provided by Plasma Technology Systems (Belmont, CA). These process parameters were used by Singhal to cold plasma reticulate ultra-low density polyurethane shape memory polymer foam [16].

Gas Flow Rate O_2 | CF_4 (sccm)	RF Power (W)	Process Duration (min)	Target Pressure (mTorr)
200 | 200	150	10	185

After receiving the plasma process parameters from Plasma Technology Systems, and conducting several experimental combinations of plasma processes, an extensive literature search was conducted to identify the optimal parameters for achieving fast, homogenous reticulation of SMP foam samples without sample degradation. The findings of the literature review are presented in Chapter I. Taking advantage of the parameters identified in the literature search that would produce fast and homogenous reticulation, the plasma processes analyzed in this thesis were developed.

A mixture of O_2/CF_4 was the process gas selected for all reticulation studies. The molar ratio of O_2/CF_4 correlated to the ratio of the gas flow rates; the ratio of the gas flow rates was equal to the molar ratio of the process gases. From the literature review, the optimal O_2/CF_4 molar ratio of 80:20 O_2/CF_4 was selected to be constant for the trial reticulation processes. The literature review also motivated the trial reticulation

processes to be conducted at a target pressure of 400 mTorr. The programmed gas flow rates were selected in an effort to run each process at 400 mTorr. Calibration studies were conducted to identify which gas flow rates preserved the 80:20 O_2/CF_4 ratio and completed plasma processes at 400 mTorr. This calibration showed that the gas flow rates of 800|200 sccm for O_2/CF_4 allowed the plasma processes to be conducted at 400 mTorr. As a result, the trial reticulation processes were conducted at 400 mTorr by setting the gas flow rates to 800|200 sccm of O_2/CF_4.

In a system of trial and error, over 30 plasma processes were tested to identify the sample placement within the reaction chamber, RF power, and process duration parameters that achieved moderate and complete reticulation of the two sample geometries. Sample placement within the reaction chamber was important because different configurations resulted in inhomogeneous reticulation or a shielding effect. From the tested configurations, it was determined that the optimal configuration was to place the sample at the center of the reaction chamber on a mesh aluminum stage that elevated the sample 127 mm above the glass shelf within the reaction chamber.

The RF power was increased from 150 W in the provided plasma process up to 600 W, in an effort to increase the reticulation rate by increasing the amount of ionized gas. Also, the process duration was evaluated at 2-50 minutes. Setting the RF power to 300 W successfully reticulated the foam samples without degradation and the process duration for each foam geometry was selected specifically for each geometry and the amount of reticulation desired.

II.1.4 Plasma Reticulation

After selecting the final process parameters for achieving moderate and complete reticulation within the foam block and sheet samples, all of the samples analyzed in this thesis were plasma treated using the procedure detailed here. The samples were cut from bulk foam, as described in section II.1.2, and placed on a mesh aluminum stage within the plasma reaction chamber to expose all surfaces to plasma. The block samples were oriented within the reaction chamber such that the direction of foaming (Z direction) was perpendicular to the electrode and the sheet samples were oriented such that the foaming direction was parallel to the electrode. Figure 3 demonstrates the coordinate system used to define the foam axes and the sample dimensions. Figure 4 shows a schematic of the plasma reaction chamber and each of the foam geometries loaded in the chamber on its stage.

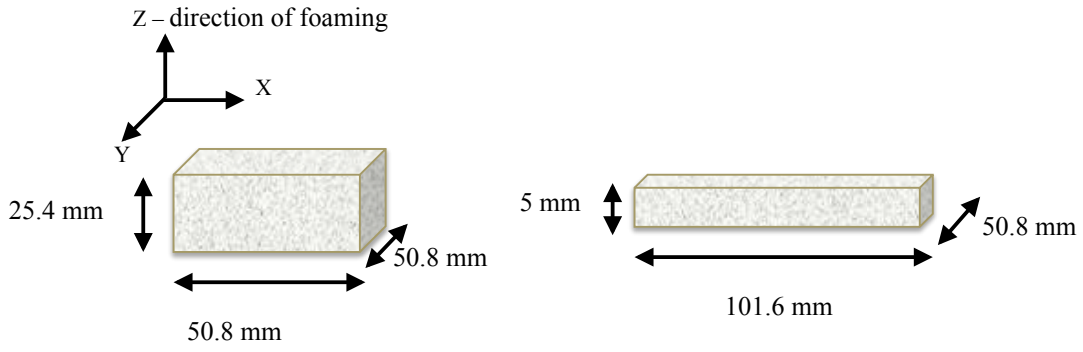

Figure 3: Coordinate system used to define the foam axes; Z is defined as the direction of foaming. Sample dimensions for plasma-reticulated shape memory polymer foam are not drawn to scale.

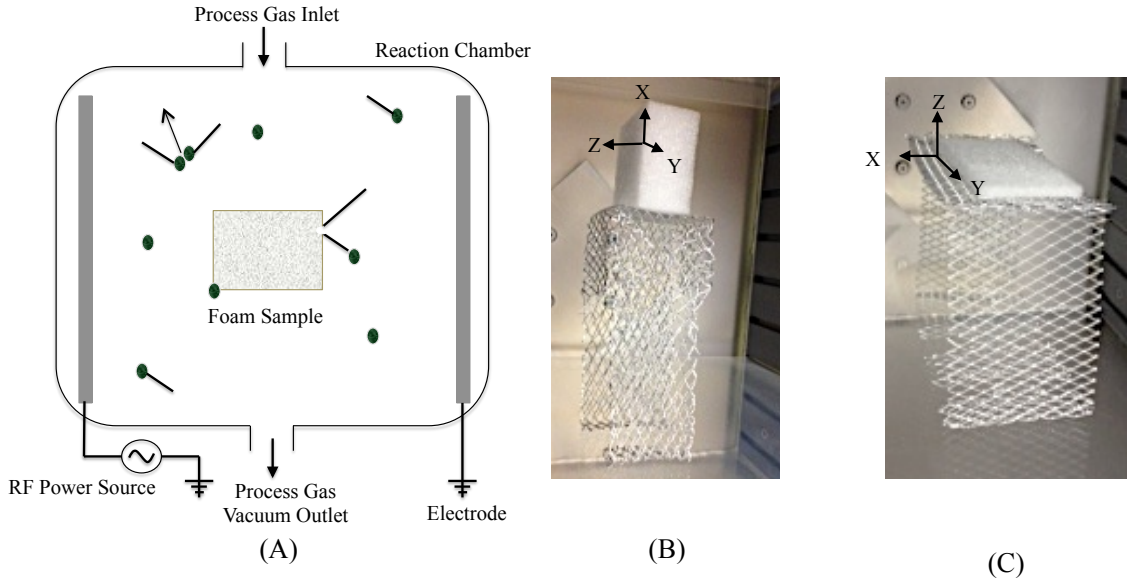

Figure 4: (A) A top-view schematic of the reaction chamber of the plasma machine. The green dots represent the reactive gas species (i.e. atoms, molecules, ions, electrons, free radicals, and metastables) present in the reaction chamber during plasma treatment. The reactive species chemically modify and reticulate the sample within the chamber. (B) Foam block loaded into the chamber on the 127 mm tall mesh aluminum stage. (C) Foam sheet loaded into the chamber on a 127 mm tall mesh aluminum stage.

The plasma process parameters for achieving moderate and complete reticulation of the block and sheet samples were selected based on the trial plasma processes described in section II.1.3. The plasma process parameters that were selected are presented in Table 3.

Table 3: Plasma process parameters selected for achieving moderate and complete reticulation of ultra-low density polyurethane shape memory polymer foam. The 'Plasma Process' defines the sample geometry and desired amount of reticulation.

Plasma Process	Gas Flow Rate O_2 | CF_4 (sccm)	RF Power (W)	Process Duration (min)	Target Pressure (mTorr)
Block Moderate	800 | 200	300	8	400
Block Complete	800 | 200	300	15	400
Sheet Moderate	800 | 200	300	3	400
Sheet Complete	800 | 200	300	8	400

The 'Plasma Process' column identifies the type of sample and desired level of reticulation. The four final plasma processes were programmed into the Aurora 0350 Plasma Surface Treatment System and saved with the file name corresponding to the 'Plasma Process' shown in Table 3. To moderately or completely plasma-reticulate a sample, the sample was loaded in the chamber as described above and the appropriate file was loaded into the Aurora 0350 Plasma Surface Treatment System Programmable Logic Controller (PLC). Once loaded into the PLC, the Aurora 0350 Plasma Surface Treatment System automatically ran the plasma process. Upon completion of the plasma process, the sample was removed from the reaction chamber and stored in a dry container with desiccant for subsequent evaluation.

II.1.5 Quantifying Reticulation

After selecting the four plasma processes for achieving moderate and complete reticulation for the two sample geometries evaluated in this thesis, the P_{ret} achieved by each process was verified by quantifying the reticulation level of the samples after

plasma treatment. A resistive wire cutter was used to cut < 1 mm thick slices from each plasma-reticulated sample. Each plasma-reticulated sample was first cut in half along the ZY plane. Next, one < 1 mm slice was cut along the ZY plane from one half of the sample and one < 1 mm slice was cut along the XY plane from the other half of the sample. Both slices were cut from the middle of the sample in the specific plane. Each slice was mounted on a stage with carbon black tape and sputter coated with gold for 90 seconds at 20 mA using a Cressington Sputter Coater (Ted Pella, Inc., Redding, CA). Each slice was then visualized using Joel NeoScope JCM-5000 Scanning Electron Microscope (SEM) (Nikon Instruments, Inc., Melville, NY). Three high-resolution SEM images were collected from the center region of each slice under high vacuum at 15 kV and 27x magnification. The number of ruptured and fully removed cell membranes (N_{open}) and total number of cell membranes (N_{total}) were counted for each SEM image. Figure 5 shows a SEM image of as-made ultra-low density polyurethane SMP foam to demonstrate open and closed membranes. The N_{open} and N_{total} for each slice were calculated by summing N_{open} and N_{total} of the three SEM images take of that slice. The P_{ret} of the slice was calculated using the following equation,

$$P_{ret} = 100 * \frac{N_{open}}{N_{total}} \quad (6)$$

and corresponded to the P_{ret} of the plane (ZY or XY) the slice was taken from. The P_{ret} for the entire sample was calculated by the averaging the P_{ret} of the ZY and XY planes. The P_{ret} for as-made reticulated bulk foam, 'Control,' was calculated using the same method described here.

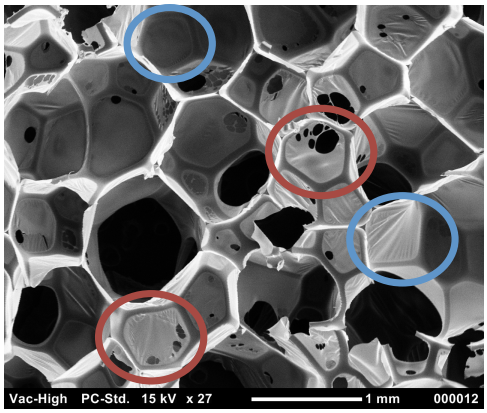

Figure 5: SEM image of as-made reticulated ultra-low density polyurethane shape memory polymer foam. Cell membranes circles in blue are closed and cell membranes circled in red are open.

II.1.6 Shape Memory Polymer Foam Block Sample Volume With Complete Membrane Removal

The slices from the plasma-reticulated block samples that were utilized for quantifying P_{ret} were also used for collecting microscope images of the slices. Each slice was mounted on a stage with carbon black tape and placed under a microscope (Leica MZ16, Meyer Instruments, Houston, TX) with a cold light for enhanced illumination (Leica KL2500 LCD, Meyer Instruments, Houston, TX). The microscope was zoomed in to allow visualization of the cell membranes. The first image was taken at the upper left corner of the slice, and then the slice was moved sequentially laterally and downward, with an image taken at each position, to allow the entire slice to be photographed. All of the images taken of a single slice were stitched together using Gimp software to create a macro-image of the whole slice. The macro-image was loaded into ImageJ software, which was used to measure the height and width of each slice, as well as the height and

width of the region with cell membranes. The slice from the XY plane was half of the full XY plane of the block sample, therefore calculating the volume of the sample, and the volume with cell membranes, required doubling the height of the XY slice. The volume of the sample was calculated using the following equation,

$$V_S = 2 \times H_{XY} \times W_{XY} \times H_{ZY} \quad (7)$$

where, V_S, was the sample volume, H_{ij} was the slice height, W_{ij} was the slice width, and the subscript identifies the plane the dimension corresponds to. The volume of the sample with membranes was calculated using the following equation,

$$V_{wMBR} = 2 \times H_{XYwMBR} \times W_{XYwMBR} \times H_{ZYwMBR} \quad (8)$$

where, V_{wMBR} was the volume of the sample with membranes, H_{ij} was the slice height, W_{ij} was the slice width, and the subscript identifies the plane the dimension corresponds to and that the region had membranes present. The percent of the sample volume without any membranes was calculated as,

$$Percent\ Volume\ {}^{w}/_{o}\ Membanes = 100 \times \left(\frac{V_S - V_{wMBR}}{V_S}\right) \quad (9)$$

II.2 Results and Discussion

II.2.1 Quantifying Reticulation

SEM images collected in the XY and ZY planes for each plasma-reticulated foam sample geometry and as-made SMP foam are presented in Figure 6. The P_{ret} in each plane and for the whole sample are reported in Table 4 for each plasma-reticulated foam geometry and for as-made ultra-low density polyurethane SMP foam.

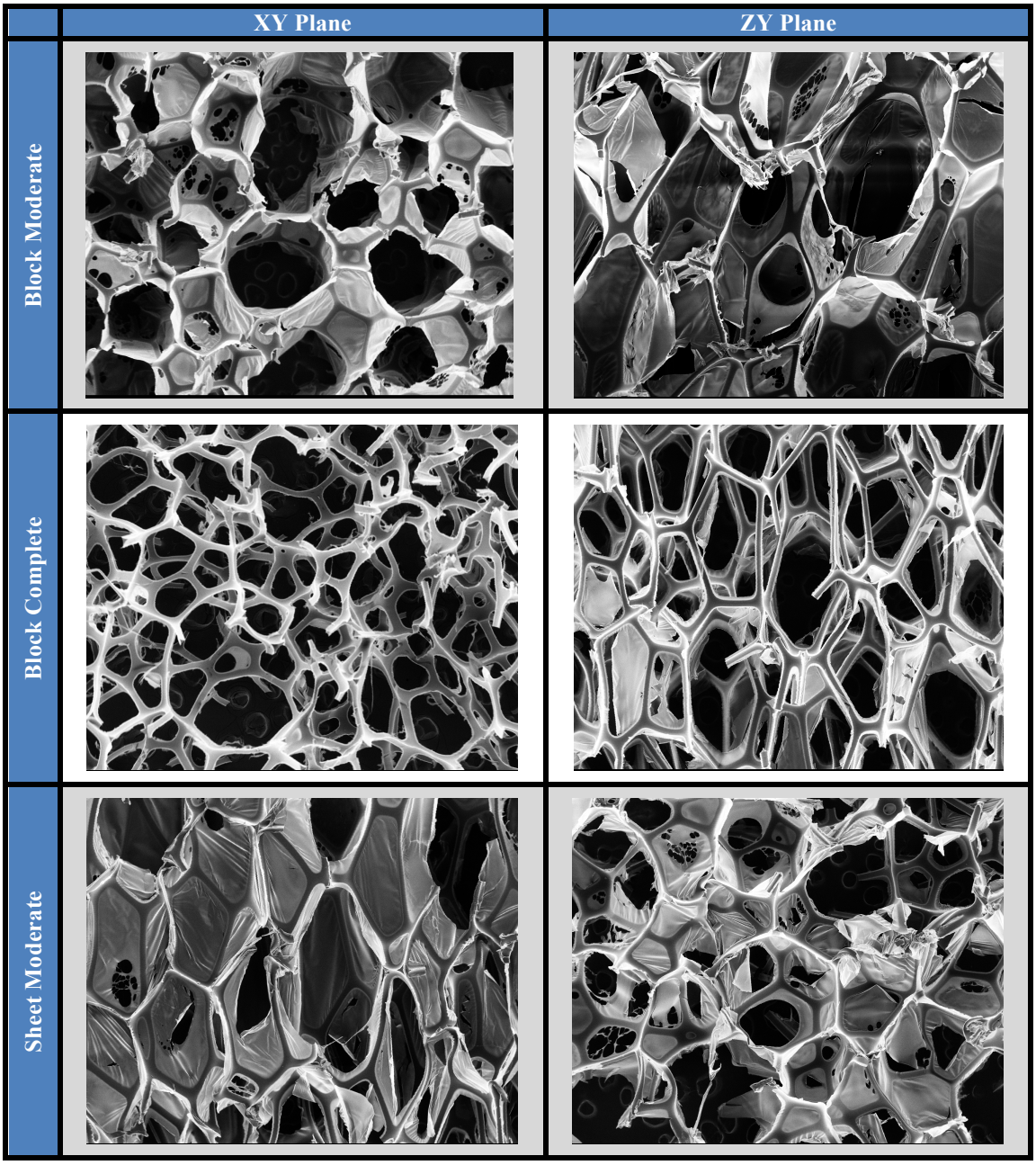

Figure 6: SEM images of plasma-reticulated and as-made ultra-low density polyurethane shape memory polymer foam taken in the XY and ZY planes. All SEM images were taken at 15 kV and 27X magnification.

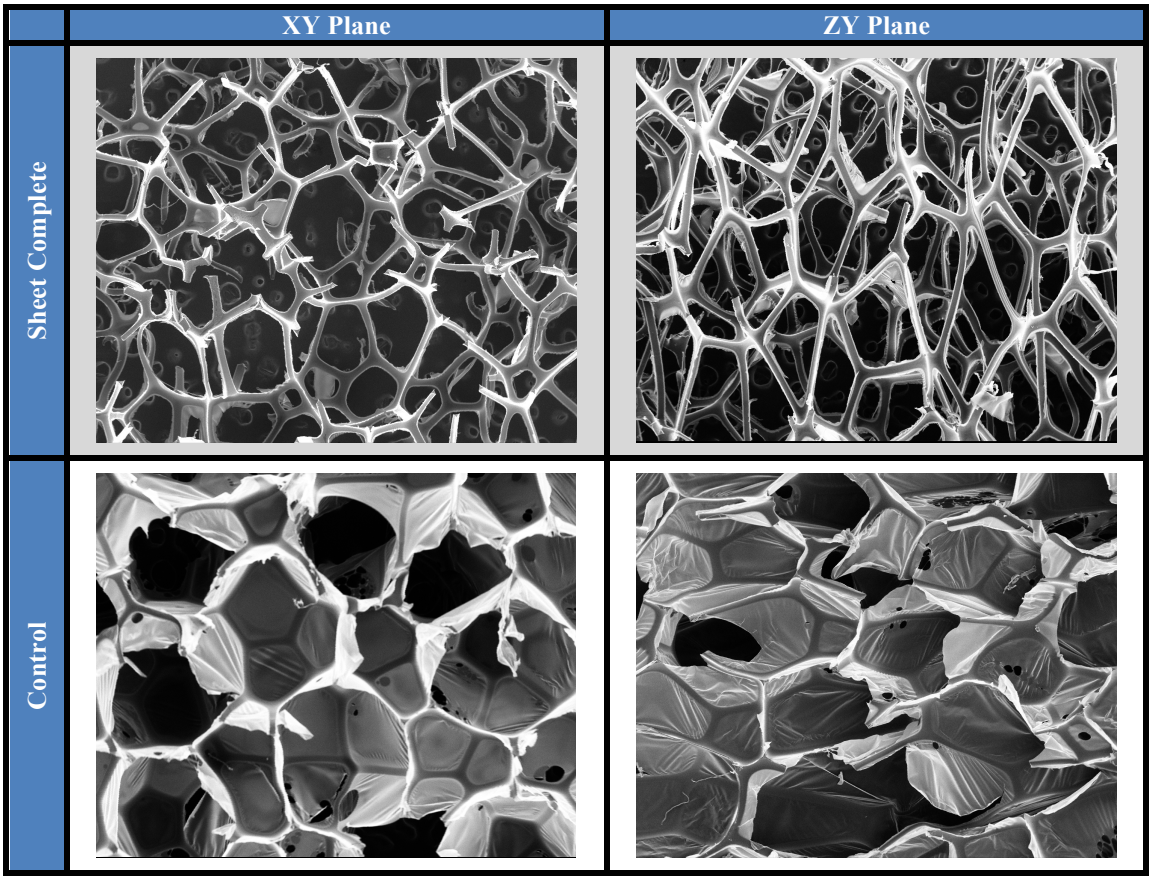

Figure 6 Continued.

Table 4: Percent reticulation in each plane and for the overall foam sample achieved by each plasma process selected for full evaluation and of as-made foam.

Plasma Process	Whole Sample Percent Reticulation (%)*	XY Plane Percent Reticulation (%)*	ZY Plane Percent Reticulation (%)*
Block Moderate	71.5 ± 8.3	74.3 ± 5.6	67.6 ± 2.9
Block Complete	97.2 ± 2.9	97.7 ± 2.9	96.6 ± 3.1
Sheet Moderate	68.1 ± 3.6	70.4 ± 5.3	66.64 ± 5.6
Sheet Complete	98.2 ± 0.9	98.3 ± 1.1	98.1 ± 1.1
Control	27.5 ± 8.2	28.3 ± 6.9	25.0 ± 10.6

* Average ± Standard Deviation, n = 5

Block Moderate and Sheet Moderate reticulated the foam samples within the prescribed P_{ret} range of 60-80% and Block Complete and Sheet Complete achieved P_{ret} >95%. The evaluated plasma processes significantly increased the P_{ret} of the Control, as-made ultra-low density polyurethane SMP foam. These results indicate that cold plasma is a viable reticulation technique for controlling reticulation levels within ultra-low density polyurethane SMP foam. The P_{ret} in the XY plane was > P_{ret} in the ZY plane for all foam samples, including as-made foam. However differences between the planar P_{ret} were not statistically significant (One-Way ANOVA, $p > 0.05$), therefore the P_{ret} of as-made foam and P_{ret} accomplished by the plasma processes evaluated in this thesis are isotropic. The P_{ret} of as-made foam and of the plasma processes for moderate P_{ret} had greater variability than the plasma processes for complete reticulation. The variability of as-made foam may be attributed to inconsistency within the foam and between bulk foam batches. The variability within bulk foam is carried through to the moderate reticulation plasma processes because only a limited amount of membranes are volatized and ruptured open. To decrease variability in P_{ret} for the moderate plasma processes, the bulk foams need to have more consistent P_{ret} or the plasma process duration should be increased. However, increasing the process time would increase the P_{ret}. Increasing the process time from 8 min to 15 min for the block samples, and from 3 min to 8 min for the sheet samples, allowed the reactive species to penetrate and reticulate the full sample volume. While a few membranes remained at the end of the longer processes, even longer process durations would allow the reactive species to begin volatizing the cell struts and degrading the foam structure.

II.2.2 Shape Memory Polymer Foam Block Sample Volume With Complete Membrane Removal

The XY and ZY plane macro-images for one of the Block Moderate and Block Complete samples used to calculate the percent sample volume without membranes are presented in Figure 7. The percent sample volume with complete membrane removal corresponding to each plasma process is reported in Table 5.

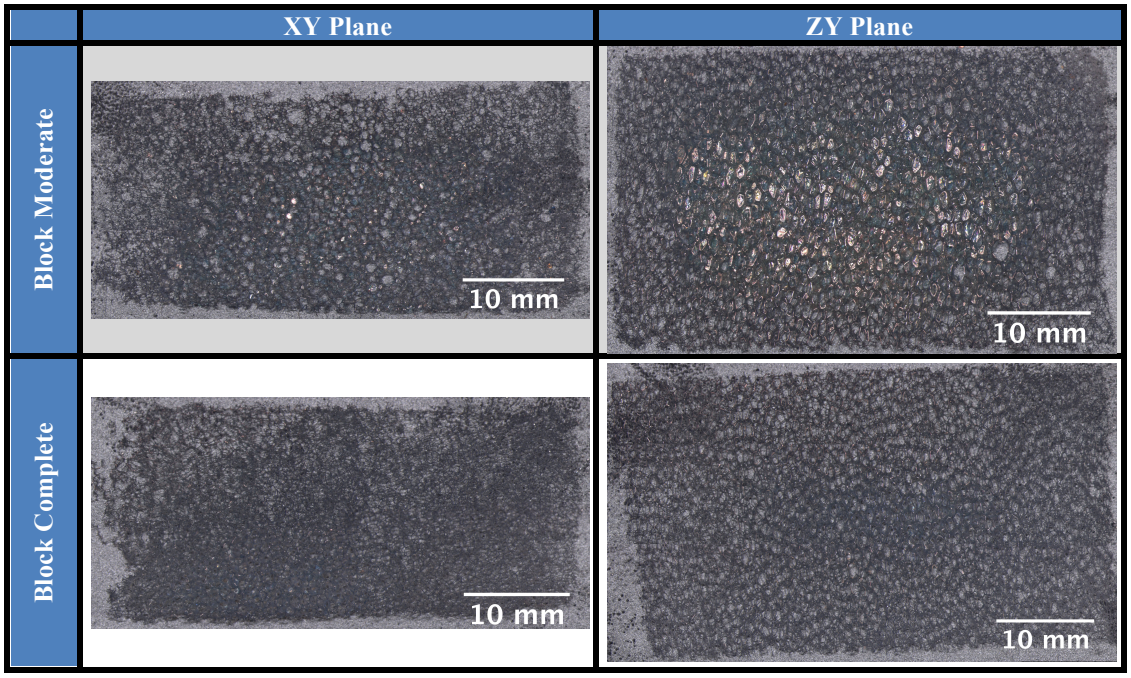

Figure 7: Macro-images of the slices taken in the XY and ZY planes of shape memory polymer foam block samples plasma-reticulated with Block Moderate and Block Complete processes.

Table 5: Percent sample volume with complete membrane removal achieved by the plasma processes performed on the foam block samples.

Plasma Process	Percent Volume Without Cell Membranes (%)*
Block Moderate	56.7 ± 8.6
Block Complete	98.9 ± 2.5

* Average ± Standard Deviation, n = 5

Measuring the volume with complete membrane removal showed that Block Moderate completely reticulated 56.65 ± 8.57% of the foam block. Thus, approximately 43.35% of the foam block volume was 71.46 ± 8.33% reticulated, as reported in Table 4. Block Complete completely removed the cell membranes from 98.88 ± 2.50% of the sample volume. This indicates that while the reticulation level achieved by Block Complete is 97.18 ± 2.86%, the process duration of this process was long enough to allow the reactive species to go beyond rupturing the cell membranes open and to volatize most of the cell membranes. The observations made by measuring the percent volume with complete membrane removal indicate that the Block Moderate achieved 71.46 ± 8.33% reticulation with most of the cell membranes intact but ruptured open in the central region of the samples. In contrast, Block Complete achieved 97.18 ± 2.86% reticulation with most of the cell membranes completely removed throughout the entire sample.

II.3. Conclusions

Cold plasma treatment is a viable technique for controlling the reticulation level of different sample geometries of ultra-low density polyurethane SMP foam. The four

plasma processes selected for full evaluation in this thesis successfully achieved the required levels of moderate and complete reticulation of foam blocks and sheets. Furthermore, the P_{ret} of all the samples was isotropic, indicating that gas foaming and plasma reticulation non-directionally reticulate SMP foam.

Measuring the volume of foam block samples with complete membrane removal indicated that the method used for quantifying P_{ret} at the sample center was not a comprehensive measure of reticulation for the whole sample. The P_{ret} of the moderate reticulation process predominantly reported the number open cell membranes while the complete reticulation process predominantly reported the number of volatized membranes. A P_{ret} of 75% that is predominantly open cell membranes and a P_{ret} of 75% that is predominantly volatized membranes will have different material properties, such as permeability and form factor. Thus, P_{ret} may need to be quantified with a technique that utilizes weighted values for open and partially open cell membranes that reduces their effect on P_{ret}. The remaining characterization techniques, such as measuring the apparent density, permeability, and form factor will provide more insight into the levels of reticulation achieved by each plasma process. Furthermore these results support the concern of plasma reticulation being a diffusive process. The reactive species first rupture open then volatize the cell membranes at the surface, which provides further access to membranes located deeper within the foam for continued reticulation. Shorter process durations prevent the reactive species from having sufficient time to penetrate the entire sample, thus the outer region of the sample exhibits complete membrane removal, while the inner region only exhibits the opening of cell membranes.

Conversely, longer process durations allow the reactive species to volatize nearly all of the cell membranes. To achieve 100% reticulation throughout the entire sample, the process would have to proceed longer than the times evaluated in this thesis and the cell struts would begin to be degraded and volatized by the reactive species.

CHAPTER III

MATERIAL CHARACTERIZATION OF PLASMA-RETICULATED ULTRA LOW-DENSTIY POLYURETHANE SMP FOAM

Ultra-low density polyurethane SMP foam that was plasma-reticulated with the plasma processes identified in Chapter II were further characterized to evaluate the effect of plasma reticulation on the material properties that are important for successful performance of SMP foam in biomedical device applications. The method and results for measuring the apparent density (ρ_{app}) of each sample before and after plasma reticulation are presented in this chapter. The porous media approach utilized in this thesis to calculate the permeability (K) and form factor (C) of each of the block samples and the measured K and C for each of the samples are reported. Finally, to evaluate the effect of plasma reticulation on the SME and activation temperature of ultra-low density polyurethane SMP foam, the volume expansion (V_E) and wet T_g of the samples were measured using techniques described in this chapter.

III.1 Materials and Methods

All foam characterizations, except measuring the change in ρ_{app}, were performed on foam that was cleaned per the protocol described below and stored in a dry container with desiccant until testing.

III.1.1 Measuring Apparent Density

The ρ_{app} of each sample was measured twice: first after the sample was cut from the bulk foam using a resistive wire cutter, as described in section II.1.2, and again after

the sample was plasma-reticulated. To measure the ρ_{app}, the length, width, and height of the sample was measured three times using a dial caliper, and the average of each dimension was used to calculate the geometrical volume. The sample mass was recorded and the apparent sample density was calculated using the following equation,

$$\rho_{app} = \frac{m}{V} \quad (10)$$

where, ρ_{app} is the apparent sample density (g/cm^3), m is the mass (g), and V (cm^3) is the geometrical volume [61].

III.1.2 Shape Memory Polymer Foam Cleaning

All samples evaluated in the permeability, V_E, and wet T_g studies in this thesis were cleaned after plasma treatment, the as-made Control, samples were cleaned after foam synthesis, to remove any residual surfactants and catalysts from the foam. The samples were cleaned using reverse osmosis (RO) water and a detergent, Contrad® 70 solution (Decon Laboratories, King of Prussia, PA). The devices were initially submerged in RO water in glass jars, and placed in a sonication bath for 2 hrs. This step was followed by changing the RO water in the vial to an 80:20 volume %, RO water-Contrad® 70 solution. The glass jars were placed back into the sonication bath for 15 min, after which the RO water-Contrad® 70 solution was changed for fresh RO water-Contrad® 70 solution and sonication for 15 min was repeated. The glass jars were sonicated in fresh RO water-Contrad® 70 solution for 15 min a total of 4 times. The samples were then washed multiple times in RO water to removal residual detergent, which was verified by the absence of bubble generation upon shaking [20]. Once the detergent was completely rinsed out of the samples, the samples were submerged in

glass jars with RO water and placed back into the sonication bath for 15 min. The RO water was then changed out for fresh RO water and the glass jars were placed into the sonication bath for a final 15 min. After the final sonication step, the samples were removed from the glass jars, placed in aluminum trays filled with RO water. The aluminum trays containing the samples were placed in a -80°C freezer overnight and subsequently lyophilized for 3 days to ensure the block samples were completely dehydrated for material characterization.

III.1.3 Permeability Measurements

The porous media properties, *K* and *C*, of the plasma-reticulated block samples and as-made ultra-low density polyurethane SMP foam were calculated using the Forchheimer-Hazen-Dupid-Darcy (FHDD) equation,

$$-\frac{\partial P}{\partial x} = \frac{\mu}{K} v_0 + \rho C v_0^2 \quad (11)$$

where, $\frac{\partial P}{\partial x}$ is the pressure gradient along the sample in the direction of flow (Pa/m), μ is the dynamic viscosity of the fluid (Pa•s), *K* is the intrinsic permeability of the sample (m^2), v_0 is the Darcy velocity (flow rate, *Q*, divided by the cross-sectional area of the sample) (m/s), ρ is the density of the fluid (kg/m^3), and *C* is the form factor of the sample (m^{-1}). Permeability, *K*, and form factor, *C*, are geometric parameters of the foam. *K* is dependent on viscous drag; it is inversely proportional to the contact surface area between the porous material and the fluid. Conversely, *C* is proportional to the projected cross-sectional area of the porous material perpendicular to the direction of fluid flow. In the FHDD equation, these two coefficients represent the resistive forces acting against the flow of fluid through the porous material. At low velocities, viscous loses are

dominant, while at higher velocities inertial loses are dominant as the pressure gradient across the porous material increases to maintain the flow [62].

Block samples were plasma-reticulated with Block Moderate and Block Complete and as-made foam, Control, samples were cut from bulk foam after foam synthesis. Next, all of the samples were cleaned per the protocol detailed in section III.1.2. After lyophilization, the samples were cut to be 20 mm tall using a resistive wire cutter and a biopsy punch was used to cut 15.876 mm diameter cylinders out of the samples. Each sample was gently rolled and slightly compressed to fit into a 30 x 19.05 x 15.875 mm (length x OD x ID) poly(methyl methacrylate) (PMMA) tube. UV cure epoxy (Dymax See-Cure 1202-M-SC, Dymax Corporation, Torrington, CT) was applied to the round surface of each foam sample using a small plastic spatula. Each sample was then placed into the PMMA tube, with one end of the cylinder sample flush with one end of the PMMA tube. Then each side of the cylinder sample was UV cured for 30 sec (OmniCure® S1000, Lumen Dynamics, Canada). The samples were stored in a dry container with desiccant until permeability testing.

Prior to permeability testing, each sample was sonicated for 1 hr to remove air bubbles from the sample, and then the sample was placed within the pressure chamber of the flow loop used to collect the permeability measurements. The permeability measurement system utilized in this thesis was the system presented by Rodriguez et al. (2014). The pressure drop across the foam sample was measured at various flow rates to determine the K and C of the foam. The flow rates measured ranged from 0 to 750 mL/min, Darcy velocities between 0 and 0.065 m/s, for each of the samples. For each

flow rate measured, the flow rate and pressure gradient across the sample were recorded for at least 30 sec. Three types of pressure transducers were used to measure the range of pressures observed: 1) 2,482 Pa differential pressure transducer (model #PX409-10WDWUV, Omega Engineering, Inc., Stamford, CT), 2) 17,240 Pa differential pressure transducer (model #PX409-2.5DWUV, Omega Engineering, Inc., Stamford, CT), and 3) two 206,800 Pa absolute membrane pressure transducers (model #PX42G7-030GV, Omega Engineering, Inc., Stamford, CT). Two digital 206,800 Pa pressure gauges (model #DPGWB-06, Dwyer Instruments, Michigan City, IN) were used to determine the maximum pressure differential of the highest flow rate prior to measurement with the transducers [62]. Measuring the maximum pressure differential of the highest flow rate with the digital pressure gauges determined that the Block Complete samples would be analyzed using the 2,482 and 17,240 Pa differential pressure transducers, and the Block Moderate and as-made foam samples would be analyzed using the two 206,800 Pa differential pressure transducers because the maximum pressure differential of the highest flow rate for these samples could exceed the maximum pressures of the 2,482 and 17,240 Pa differential pressure transducers.

The permeability measurement system, shown in Figure 8, utilized a peristaltic pump (Verderflex®, England, U.K.) with a non-standard six head roller on an isolated cart for reduction of pulse within the system. After the peristaltic pump, 20 ft of large diameter (12.7 x 15.875 mm, ID x OD) flexible silicone tubing was placed upstream of five pulse dampeners. A flow meter probe, attached to a small animal flow meter (model #T206, Transonic Inc., Ithaca, NY) was placed after the five pulse dampeners to quantify

the pulse within the system and for measuring the flow rate. After the five pulse dampeners, there was an additional 5 ft of semi-rigid flexible tubing (12.7 x 19.1 mm, ID x OD) and subsequently 3 ft of rigid tubing (15.875 x 19.05 mm, ID x OD) before the pressure chamber. After the pressure chamber, there was at total of 9 ft of rigid tubing (15.875 x 19.05 mm, ID x OD); 2 ft of tubing with a bend followed by 7 ft of straight tubing. Finally, 3 ft of semi-rigid flexible tubing (12.7 x 19.1 mm, ID x OD) allowed the water to flow out of the system and into a water tank. To minimize the pulse of the system experienced by the sample, the water tank was also isolated on its own cart [62].

After conducting the permeability measurements, a second-order least squares fit was applied to the pressure gradient versus Darcy velocity data to calculate the K and C for each sample, using Equation 11 with water at room temperature as the working fluid.

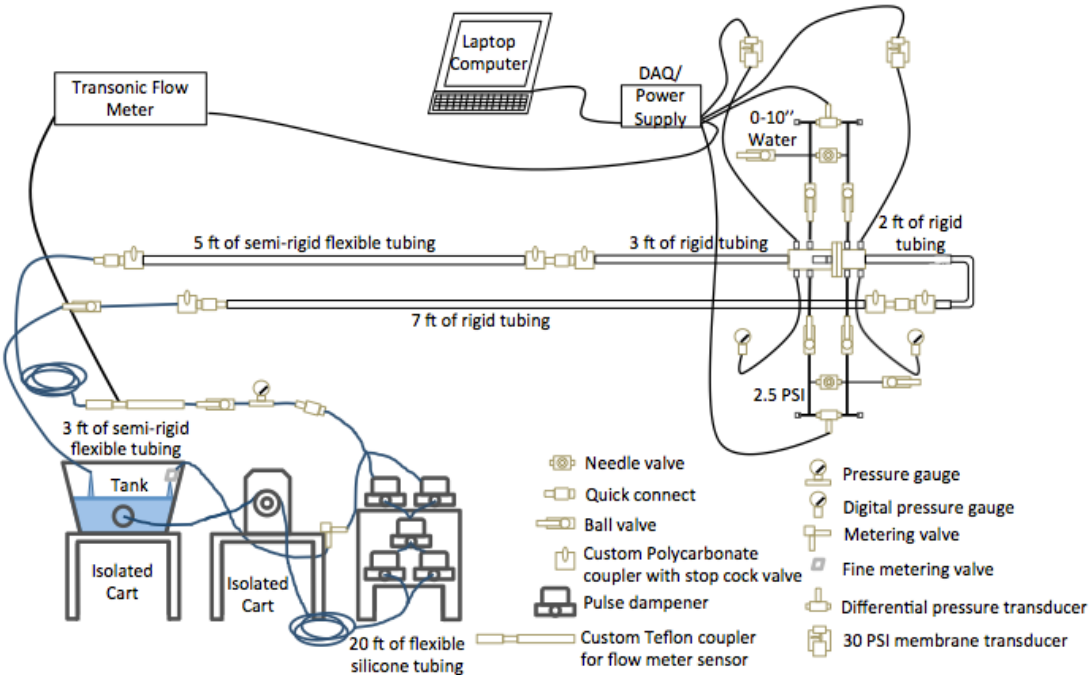

Figure 8: Diagram of permeability measurement system [62].

III.1.4 Volume Expansion in Water

After lyophilization, to prepare samples for V_E studies, a resistive wire cutter and biopsy punch was used to cut 6 x 5 mm (OD x height) cylinder samples. The foam samples were threaded onto a 0.2032 mm diameter nitinol wire (NDC, Fremont, CA), by threading the wire through the center of the sample, along its axial length. The samples were loaded into a pre-heated, 100°C, SC150 Stent Crimper (Machine Solutions, Flagstaff, AZ). The samples equilibrated within the stent crimper for 15 min before being radially compressed to their smallest possible diameter and cooled down to room temperature to fix the compressed diameter [7]. The samples were allowed to rest for at least 24 hrs in a dry box with desiccant before testing. After resting, a digital camera was used to photograph the compressed foam to measure and record the initial sample diameter using ImageJ software. The foam samples were then placed in a 50°C RO water bath for 20 min. While still submerged in the water bath, a digital camera was used to photograph the expanded foam to measure and record the recovered diameter using ImageJ software. Volume expansion was calculated using the following equation,

$$V_E = \left(\frac{D_r}{D_c}\right)^2 \quad (12)$$

where, V_E is volume expansion, D_r is the recovered diameter (mm), and D_c is the compressed diameter (mm) [7]. In addition to measuring V_E of plasma-reticulated block and sheet samples, V_E was measured for as-made block and sheet samples in an effort to observe whether sample geometry had an effect on V_E.

III.1.5 Differential Scanning Calorimetry (DSC)

To evaluate the T_g after water plasticization, the wet T_g, of plasma-reticulated and as-made foam was measured. To measure wet T_g, 3-8 mg of cleaned and lyophilized foam was submerged in RO water at 50°C for 5 min to allow full plasticization. The samples were then removed from the RO water and pressed dry in a Kim Wipe (Kimberly-Clark Professionals, Roswell, GA), weighed, and placed in an aluminum pan sealed with a vented aluminum lid. A Q-200 DSC (TA Instruments, New Castle, DE) was used to cool each sample to -40°C, hold it isothermal for 2 min, then heat it to 80°C at 10°C/min increments. TA instruments software was used to generate the thermogram and obtain the wet T_g using the average inflection point of the thermal transition.

III.2 Results and Discussion

III.2.1 Measuring Apparent Density

The ρ_{app} of plasma-reticulated foam samples before and after plasma treatment, and the percent change in ρ_{app} achieved by each plasma process are reported in Table 6.

Table 6: The apparent density before and after plasma treatment and the change in apparent density achieved by each plasma process.

Plasma Process	Apparent Density Before Plasma Reticulation (g/cm^3)*	Apparent Density After Plasma Reticulation (g/cm^3)*	Percent Change in Apparent Density (%)*
Block Moderate	0.0116 ± 0.0004	0.0097 ± 0.0002	-18.0 ± 2.9
Block Complete		0.0077 ± 0.0003	-33.8 ± 2.2
Sheet Moderate		0.0107 ± 0.0004	-7.3 ± 3.7
Sheet Complete		0.0082 ± 0.0004	-27.6 ± 4.0

*Average ± Standard Deviation, n = 5

Sheet Moderate achieved the lowest P_{ret}, 68.11 ± 3.59%, and the lowest change in ρ_{app} of all the plasma processes. Sheet Complete and Block Complete resulted in comparable P_{ret} but Block Complete caused a greater change in ρ_{app}. Overall, the P_{ret} achieved by the plasma processes corresponded to the change in ρ_{app} achieved by the plasma processes. The moderate reticulation processes volatized some cell membranes, but a significant number of the membranes were ruptured open and left intact, thus preventing the ρ_{app} from decreasing as significantly as in the complete reticulation processes. The plasma processes for complete reticulation resulted in greater ρ_{app} changes because these processes volatized most of the cell membranes, thus achieving extremely low densities.

III.2.2 Permeability Measurements

The average permeability measurements of the pressure gradient, $\frac{\partial P}{\partial x}$, Darcy velocity, v_0, and the FHDD second order fitted curves for Control samples, Block Moderate plasma-reticulated samples, and Block Complete plasma-reticulated samples are shown in Figure 9. The maximum $\frac{\partial P}{\partial x}$ observed for the Control foam samples was two orders of magnitude greater than the maximum $\frac{\partial P}{\partial x}$ observed for the Block Complete plasma-retiuclated samples. This two order of magnitude difference in maximum pressure gradient causes the Block Complete permeability plot in Figure 9 to appear linear. Figure 10 shows only the average permeability measurements of $\frac{\partial P}{\partial x}$ and v_0 for the Block Complete plasma-reticulated samples to more accurately demonstrate the second order polynomial plot.

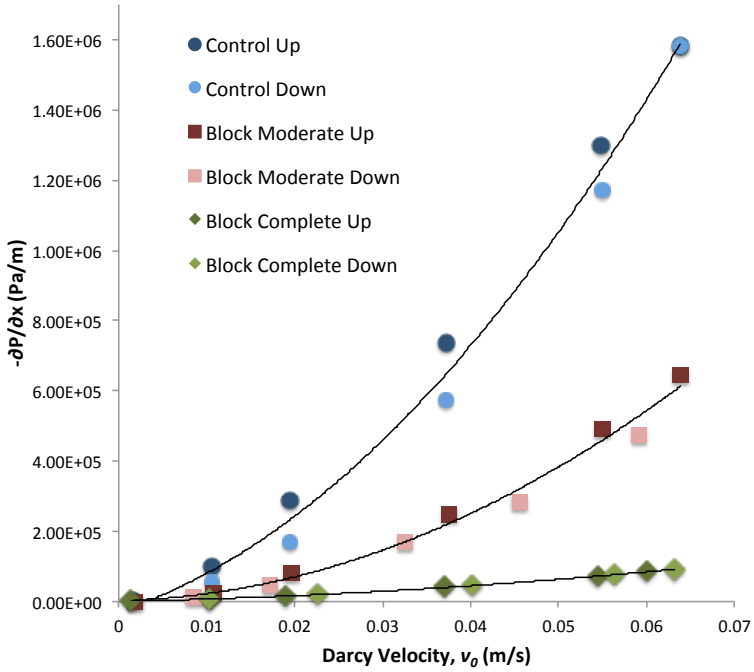

Figure 9: Average pressure gradient versus Darcy velocity measurements and Forchheimer-Hazen-Dupid-Darcy equation second order fitted curves for Control foam samples, Block Moderate, and Block Complete plasma-reticulated samples.

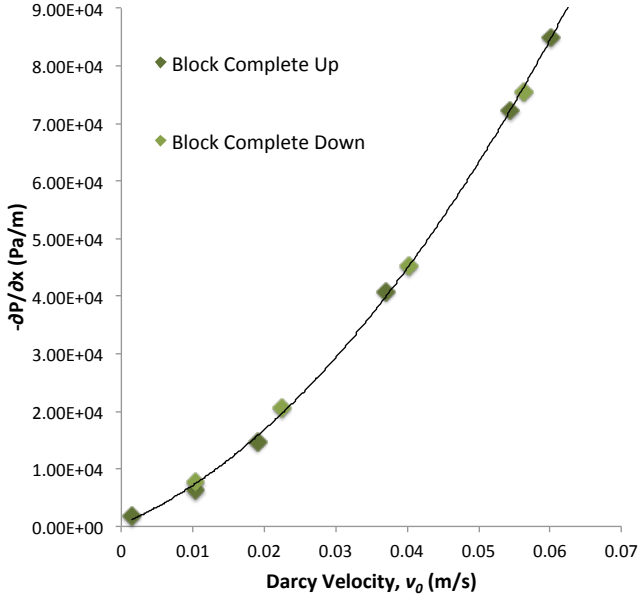

Figure 10: Average pressure gradient versus Darcy velocity measurements and Forchheimer-Hazen-Dupid-Darcy equation second order fitted curve for Block Complete plasma-reticulated samples.

Table 7 presents the *K* and *C* calculated for each of foam samples using the second-order least squares fit applied to the $\frac{\partial P}{\partial x}$ versus v_0 data for each of the samples.

Table 7: Permeability and form factor parameters calculated for as-made samples, Block Moderate, and Block Complete plasma-reticulated samples by applying second-order least squares fit to pressure gradient versus Darcy velocity data.

Plasma Process	Permeability (m^2)*	Form Factor (m^{-1})*
Control	0.16E-09 ± 0.04E-09	2.91E05 ± 0.21E05
Block Moderate	1.44E-09 ± 0.81E-09	1.43E05 ± 0.87E05
Block Complete	2.55E-09 ± 0.57E-09	0.15E05 ± 0.06E05

* Average ± Standard Deviation, n = 5

There was an order of magnitude increase in *K* between the as-made foam and both plasma-reticulated foams. The *C* of the Block Complete plasma-reticulated foam was one order of magnitude less than both the as-made foam and the Block Moderate plasma-reticulated foam.

The Block Moderate plasma-reticulated foam had large standard deviations for both *K* and *C*. These large standard deviations may be attributed to inconsistent reticulation levels achieved by the Block Moderate plasma process or variations in where the Block Moderate cylinder samples were collected from the plasma-reticulated blocks. The results from measuring the volume with complete membrane removal suggest that variations in where the cylinder samples for permeability measurements were collected within Block Moderate plasma-reticulated foam could produce large

variations in the permeability measurements. Conversely, Block Complete plasma reticulated foam was more homogenously reticulated throughout the sample volume, therefore variation in the location of where these cylinder samples were collected introduced less variation in the permeability measurements of Block Complete foam. Overall, the trend observed from the permeability measurements was of increasing reticulation corresponding to increased permeability and decreased form factor.

III.2.3 Volume Expansion in Water

Volume expansion measurements for the foam samples are reported in Table 8. Comparing the as-made block and sheet data, the two reached the same D_c, however the as-made sheet samples had V_E less than the as-made block samples. This may be attributed to a combination of the thin sheet geometry and robustness of the cleaning process. Upon completion of the cleaning protocol in section III.1.2, the sheets appeared to be less robust than the blocks. The number of rinses and rigorous shaking of the samples within the glass jars to clean out all of the Contrad® may have degraded the sheet samples, and resulted in lower V_E. The as-made foam and Block Complete samples crimped down to the lowest D_c, while Sheet Moderate had the greatest D_c. Compared to as-made foam, only Block Complete increased V_E, while Sheet Complete had almost no effect on V_E of the sheet. Both plasma processes for moderate reticulation reduced the V_E of the foam.

Table 8: Crimped diameter, recovered diameter, and volume expansion of as-made foam and of foam plasma-reticulated with one of the four plasma processes evaluated in this thesis.

Plasma Process	Crimped Diameter (mm)*	Recovered Diameter (mm)*	Volume Expansion *
Block Moderate	0.89 ± 0.03	4.26 ± 0.71	23.59 ± 7.73
Block Complete	0.82 ± 0.04	6.27 ± 0.83	58.95 ± 15.73
Block Control	0.83 ± 0.04	4.68 ± 0.91	32.88 ± 12.59
Sheet Moderate	0.95 ± 0.02	2.90 ± 0.24	9.41 ± 1.79
Sheet Complete	0.89 ± 0.05	3.89 ± 0.67	19.44 ± 5.58
Sheet Control	0.83 ± 0.04	3.68 ± 0.59	20.83 ± 7.31

* Average ± Standard Deviation, n = 5

Explanations for the differences between as-made, moderately reticulated, and completely reticulated foam samples' D_c and V_E provided here are only speculation and require further investigation to be verified. It is speculated that the discrepancies may be explained by the presence of residual cell membranes, plasma induced surface modifications, and foam damage during cleaning. As-made foam has a high number of unruptured cell membranes and struts that have not been exposed to the reactive species in the plasma. The unruptured cell membranes may allow for high compression of the foam because they are aligned along the foam axis. During volume expansion the unruptured cell membranes are hypothesized to apply outward forces to expand the foam, while also applying inward forces to prevent the cell struts from fully expanding the foam. In moderately plasma-reticulated foam, the majority of the cell membranes are ruptured open and many have been volatized. The ruptured cell membranes may limit

the compressibility of the foam because they are no longer aligned along the foam axis; instead they increase the amount of material in the radial direction that must be compressed. During volume expansion, it is speculated that the ruptured cell membranes apply weaker outward forces to expand the foam and inward forces to prevent the cell struts from expanding the foam. Thus, the overall effect of moderate reticulation is decreased V_E.

Conversely, in completely plasma-reticulated foam, nearly all of the cell membranes have been completely removed, allowing the foam to be compressed optimally because there is significantly less material to radially compress. However, the increase in D_c observed for the Sheet Complete is inconsistent with this theory. The increase in D_c of the Sheet Complete may be attributed to the combination of the cleaning process and plasma treatment hindering the amount of deformation the Sheet Complete can experience. It is speculated that the high V_E observed for Block Complete foam is attributed to the lack of cell membranes and surface modifications of the foam. While few membranes are present to apply outward forces to contribute to foam expansion, the lack of membranes applying inward forces allows the struts to achieve greater V_E than as-made foam. Furthermore, complete membrane removal allows all of the cell struts to be exposed to the reactive species within the plasma. The reactive species formed by ionization of oxygen might induce the formation of carbon-oxygen double bond, C=O, and OH groups on the strut surface, thus increasing hydrophilicity and allowing the foam to achieve a greater V_E [63, 64]. Exposure of all the struts to the plasma reactive species in the Sheet Complete may explain why it did not experience a

significant decrease in V_E compared to as-made foam. It is hypothesized that a change in surface hydrophobicity of the Sheet Complete may have compensated for the loss of mechanical integrity, allowing it to achieve V_E comparable to as-made foam.

III.2.4 DSC

The wet T_g results for as-made foam and each plasma-reticulated foam sample are shown in Table 9.

Table 9: Wet T_g results of as-made foam and of foam plasma-reticulated with one of the four plasma processes evaluated in this thesis.

Plasma Process	Wet T_g (°C)*
Block Moderate	28.6 ± 0.4
Block Complete	28.5 ± 0.6
Sheet Moderate	27.4 ± 0.5
Sheet Complete	28.5 ± 0.7
Control	27.6 ± 0.4

* Average ± Standard Deviation, n = 5

The wet T_g of plasma-reticulated foam was not significantly greater than the wet T_g of as-made foam. Free electrons and ion bombardment of the polymer surface do not provide enough thermal to allow unbound hydroxyls (OH) and isocynates (NCO) to cross-link [65]. If the unbound OH and NCO groups did cross-link, the wet T_g of the plasma-reticulated foam be greater than the wet T_g of as-made foam. These results indicate that plasma-reticulation does not change the wet T_g of SMP foam.

III.3 Conclusions

Material characterization of plasma-reticulated and as-made foam showed that complete reticulation decreased foam ρ_{app} the most because material was completely removed from the foam, while moderate reticulation processes decreased foam ρ_{app} less significantly because these processes achieved more membrane rupture and less membrane removal. The permeability measurements overall indicate that increased reticulation corresponds to increased K and decreased C because rupture and removal of cell membranes decreases resistance to fluid flow through the foam. However, Block Moderate foam permeability measurements demonstrated high variability in K and C compared to Block Complete plasma-reticulated foam and as-made foam. The increased variability of Block Moderate foam's porous media properties suggests that there was an inhomogeneous reticulation percentage throughout the Block Moderate foam. Thus, variation in where the cylinder samples for permeability testing were collected from the Block Moderate foam blocks resulted in large variations in K and C of Block Moderate foam. V_E of the sheet samples was less than that of as-made foam and plasma-reticulated foam block samples. This may be attributed to the rigorous cleaning process hindering the SME of this sample geometry because the other plasma-reticulated samples exhibited greater V_E and the volume expansion studies were performed at a temperature over 20°C > the wet T_g of these foams. The block samples exhibited decreased and increased V_E for moderately and complete plasma-reticulated foam, respectively, compared to as-made foam. These changes in V_E are speculated to be attributed to the foam structure being dominated by closed, mixed-, or open membranes, and surface modifications of the cell

struts by the plasma reactive species. Plasma reticulation did not have a significant effect on the wet T_g of the foam. This indicates that the foam's specific glass transition temperature will not be changed by plasma reticulation; the same thermal stimuli will actuate as-made and plasma-reticulated SMP foam. These characterization results indicate that the moderate reticulation processes did not achieve a homogenous reticulation percent throughout the foam and these processes must be further optimized for fine control over the *K* and *C* parameters of these foams. The sheet samples exhibited a significant decrease in V_E, which may be a reason to eliminate the geometry as an option for EII prevention.

CHAPTER IV

CONCLUSIONS AND FUTURE WORK

This thesis was aimed at utilizing cold plasma treatment to control reticulation of ultra-low density polyurethane SMP foam for EII prevention and to characterize the effects of plasma reticulation on the material properties of ultra-low density SMP foam. Previous studies by Singhal showed cold plasma treatment to be an effective technique for reticulating ultra-low density polyurethane foam and this thesis expanded upon those studies. Initial plasma process parameters provided by Plasma Technology Systems and information collected from an extensive literature search were utilized to develop the four plasma processes characterized in this thesis.

The four plasma processes evaluated in this thesis met the P_{ret} requirements that were specified for demonstrating that cold plasma treatment could achieve controlled reticulation of ultra-low density SMP foam. Plasma reticulation is a diffusive process by which the reactive species of the plasma first rupture open then volatize cell membranes of the foam at the surface, which allows the reactive species to progressively access membranes deeper within the foam to continue the reticulation process. The microscope images taken from the center of the plasma-reticulated foam block samples in the XY and ZY planes to calculate the sample volume with complete membrane removal supported this concept. Both moderately and completely reticulated samples exhibited an outer region free of membranes, while the presence of ruptured or closed membranes was only observed at the center of the samples. Thus, these results suggest that to

achieve a specific reticulation percentage for a whole foam device, the device may need to be cut out of a large foam block to prevent the surface of the device from being completely reticulated and the center of the device being only moderately reticulated.

All of the reticulation processes decreased the ρ_{app} of the foam but there was not a consistent decrease in ρ_{app} for both of the moderate or complete reticulation processes. However, both complete reticulation processes decreased foam ρ_{app} more than the moderate reticulation processes, which corresponds to the increased amount of material removal accomplished by the complete reticulation processes.

The permeability measurements collected from the plasma-reticulated foam blocks and as-made foam showed that Block Moderate did not achieve homogenous reticulation throughout the foam because the *K* and *C* of Block Moderate had larger variations than both the Block Complete and as-made foam. The large variability in Block Moderate *K* and *C* may have been caused by variations in where the cylinder permeability samples were cut from the Block Moderate blocks. The P_{ret} of Block Moderate foam had the greatest variation of the evaluated plasma-reticulated foam, which supports the conclusion that Block Moderate did not achieve homogenous reticulation of the block samples and this contributed to the large variability in the permeability measurements. Overall, plasma reticulation successfully increased *K* and decreased *C* of ultra-low density polyurethane SMP foam. However, further optimization studies must be conducted to specifically control the *K* and *C* of an ultra-low density SMP foam sample with plasma reticulation.

Complete removal of membranes and surface modifications accomplished by the plasma reactive species are hypothesized to be what allowed the completely reticulated SMP foam block samples to exhibit a significant increase in V_E. Overall, the sheet geometry exhibited V_E less than the foam blocks; this is considered to be a result of the cleaning protocol. The large aspect ratio of sheet length to sheet thickness is believed to be the reason why the cleaning protocol caused the sheets to appear degraded and less robust after cleaning compared to the block samples after cleaning. Considering only the plasma-reticulated block samples and as-made foam, there appears to be a threshold of P_{ret} at which V_E increases or decreases. SMP foam with a reticulated foam structure that is predominately ruptured membranes results in a decrease in V_E. Conversely, SMP foam with a reticulated structure that is predominately closed membranes or only struts with few or no cell membranes results in an increase in V_E.

Plasma reticulation did not affect the wet T_g of ultra-low density SMP foam. Plasma processing did not result in thermal cross-linking of the SMP foam, which would have caused an increase in wet T_g. Thus, the plasma-reticulated foams will still actuate when exposed to body temperature. However, wet T_g of plasma-reticulated foam should continue to be measured in future studies and applications of plasma reticulation to SMP foam because a significant increase in T_g could hinder the ability of the foam to actuate upon exposure to specific thermal stimuli.

The evaluated foam geometries in this thesis were selected because the sheet was anticipated to be the geometry for the SMP foam device utilized for prevention of EII associated with AAA and the block geometry was believed to be a second option that

would allow a single piece of SMP foam to be plasma-reticulated and smaller devices to be cut out of the foam block post plasma reticulation. Results from the volume expansion study suggest that the sheet geometry is not a viable option for the SMP foam device because as-made foam cleaned in the sheet geometry, and both of the plasma-reticulated sheet samples, exhibited V_E less than the block foam. The sheet devices would be able to be compressed and rolled into a small temporary cylinder geometry to fit into a catheter for delivery into the aneurysm sac but the decreased V_E exhibited by these foams would prevent them from recovering enough of their original sheet geometry to fill the aneurysm sac for optimal EII prevention.

The material characteristics of plasma-reticulated foam blocks indicate that it is a viable geometry for plasma reticulating a bulk piece of foam for cutting out smaller devices post plasma reticulation. The plasma process for moderate reticulation was unable to achieve homogenous reticulation throughout the foam volume due to the diffusive characteristic of plasma reticulation. As a result, the moderately reticulated foam produced large variations in the P_{ret} achieved by the plasma process and the foam's K and C. Thus, of the plasma-reticulated foam evaluated in this thesis, only the completely reticulated foam block samples could be utilized for EII prevention because it resulted in complete membrane removal throughout over 98% of the foam volume. Complete membrane removal from nearly the entire volume allowed the foam to experience a significant decrease in ρ_{app}, to attain high and low K and C coefficients, respectively, and to exhibit a significant increase in V_E compared to as-made foam.

Finally, wet T_g of the completely reticulated foam blocks still allows this foam to actuate when exposed to body temperature upon delivery into the aneurysm sac during EVAR.

For future studies, plasma processes should be developed for plasma reticulating other SMP foam geometries in an effort to plasma-reticulate the final device geometry. Achieving moderate plasma-reticulation of foam blocks must further be optimized and evaluated because the plasma process in this thesis failed to achieve homogenous reticulation and produce plasma-reticulated foam with consistent material characteristics. Further optimization studies could aim to improve the results of plasma reticulation by changing the configuration of the sample within the reaction chamber and analyzing other combinations of the plasma process parameters of process gases, gas flow rates, RF power, and process duration.

Overall, this thesis showed that cold plasma treatment is a viable technique for reticulating ultra-low density polyurethane SMP foam because specific reticulation percentages were achieved and plasma reticulation did not significantly hinder the material characteristics of the ultra-low density SMP foam. The specific combination of plasma process parameters, foam geometry, and sample configuration within the reaction chamber is critical to the final reticulation results achieved by a plasma reticulation process. Optimization studies must be conducted in order to identify the specific combination of factors that achieve consistent and homogenous moderate and complete reticulation of different geometries of ultra-low density polyurethane SMP foam. Identifying plasma processes for controlled reticulation of ultra-low density

polyurethane SMP foam will open up new areas of research, expand the applications of SMP foam, and make it an even more advantageous biomaterial.

REFERENCES

1. De Nardo, L., Bertoldi, S., Tanzi, M.C., Haugen, H.J., Fare, S., *Shape Memory Polymer Cellular Solid Design for Medical Applications.* Smart Materials and Structures, 2011. **20**(3): p. 1-12.

2. Sokolowski, W., Metcalfe, A., Hayashi, S., Yahia, L., Raymond, J., *Medical Applications of Shape Memory Polymers.* Biomedical Materials, 2007. **2**: p. S23-S27.

3. Metcalfe, A., Desfaits, A., Salazkin, I., Yahia, L., Sokolowski, W.M., Raymond, J., *Cold Hibernated Elastic Memory Foams for Endovascular Interventions.* Biomaterials, 2003. **24**(3): p. 491-497.

4. Baer, G., Wilson, T.S., Matthews, D.L., Maitland, D.J., *Shape-Memory Behavior of Thermally Stimulated Polyurethane for Medical Applications.* Journal of Applied Polymer Science, 2007. **103**(6): p. 3882-3892.

5. Hearon, K., Singhal, P., Horn, J., Small, W. Olsovsky, C., Maitland, K.C., Wilson, T.S., Maitland, D.J., *Porous Shape Memory Polymers.* Polymer Reviews, 2013. **4**(53): p. 41-75.

6. Ratna, D., Karger-Kocsis, J., *Recent Advances in Shape Memory Polymers and Composites: A Review.* Journal Of Material Science, 2008. **43**: p. 254-269.

7. Singhal, P., Rodriguez, J.N., Small, W., Eagleston, S., Van de Water, J., Maitland, D.J., Wilson, T.S., *Ultra Low Density and Highly Crosslinked Biocompatible Shape Memory Polyurethane Foams.* Journal of Polymer Science, 2012. **50**(10): p. 724-737.

8. Hanson, S.R., Ratner, B.D., *Evaluation of Blood-Material Interactions*, in *Biomaterials Science: An Introduction to Materials in Medicine*, B.D. Ratner, et al., Editors. 2004, Elsevier Academic Press: San Diego. p. 367-79.

9. Piazza, M., Frigatti, P., Scrivere, P., Bonvini, S., Noventa, F., Ricotta, J.J., Grego, F., Antonello, M., *Role of Aneurysm Sac Embolization During*

Endovascular Aneurysm Repair in the Prevention of Type II Endoleak-Related Complications. Journal of Vascular Surgery, 2013. **57**(4): p. 934-941.

10. Weerakkody, Y., D'Souza, D. *Endoleak*. Radiopaedia.[cited 2014 December 4]; Available from: http://radiopaedia.org/articles/endoleak.

11. Anderson, J.M., Rodgriguez, A., Chang, D.T., *Foreign Body Reaction to Biomaterials.* Seminars in Immunology, 2008. **20**(2): p. 86-100.

12. Carreno, M.P., Labarre, D., Jozefowicz, M., Kazatchkine, M.D., *The Ability of Sephadex to Activate Human Complement is Suppressed in Specifically Substituted Functional Sephadex Derivatives.* Molecular Immunology, 1988. **25**(2): p. 165-171.

13. Diggs, T. *Contact Activation of Blood-Plasma Coagulation*. Master's Thesis, 2008, Pennsylvania State University, State College, PA.

14. Kumar, V., Abbas, A.K., Fausto, N., Mitchell, R., *Robbins Basic Pathology*. 8th ed. 2007, Philadelphia, PA: Saunders/Elsevier.

15. Datta, B.N., *Textbook of Pathology*. 2nd ed. 2004, New Delhi, India: Jaypee Brothers Medical Publishers (P) Ltd.

16. Singhal, P. *Ultra Low Density Shape Memory Polymer Foams with Tunable Physiochemical Properties for Treatment of Intracranial Aneurysms*. Ph.D Dissertation, 2013, Texas A&M University, College Station, TX.

17. Zhang, D., Burkes, W.L., Schoener, C.A., Grunlan, M.A., *Porous Inorganic-Organic Shape Memory Polymers.* Polymer (Guildford), 2012. **53**(14): p. 2935-2941.

18. Brooks, M., *Effects of Isophorone Diisocyanate on Hydrophobicity of Shape Memory Polymers for Cerebral Aneurysm Treatments*. 2013, Undergraduate Summer Research Grant Poster Presentations: Texas A&M University, College Station, Texas.

19. Rhee, J.Y., Trocciola, S.M., Dayal, R., Lin, S., Chaer, R., Kumar, N., Mousa, A., Bernheim, J., Christos, P., Prince, M., Marin, M.L., Gordon, R., Badimon, J., Fuster, V., Kent, C.K., Faries, P.L., *Treatment of Type II Endoleaks with a Novel Polyurethane Thrombogenic Foam: Induction of Endoleak Thrombosis and Elimination of Intra-Aneurysmal Pressure in the Canine Model.* Journal of Vascular Surgery, 2005. **42**(2): p. 321-328.

20. Rodriguez, J.N., Clubb, F.J., Wilson, T.S., Miller, M.W., Fossum, T.W., Hartman, J., Tuzun, E., Singhal, P., Maitland, D.J., *In Vivo Response to an Implanted Shape Memory Polyurethane Foam in a Porcine Aneurysm Model.* Journal of Biomedical Materials Research Part A, 2013. **102**(5): p. 1231-1242.

21. Dhandayuthapani, B., Yoshida, Y., Maekawa, T., Kumar, D.S., *Polymeric Scaffolds in Tissue Engineering Application: A Review.* International Journal of Polymer Science, 2011. **2011**: p. 1-19.

22. Cheung, H.Y., Lau, K.T., Lu, T.P., Hui, D., *A Critical Review on Polymer-Based Bio-Engineered Materials for Scaffold Development.* Composites: Part B, 2007. **38**(3): p. 291-300.

23. Lubarsky, M., Ray, C.E., Funaki, B., *Embolization Agents—Which One Should Be Used When? Part 1: Large-Vessel Embolization.* Seminars in Interventional Radiology, 2009. **26**(4): p. 352-357.

24. Lubarsky, M., Ray, C.E., Funaki, B., *Embolization Agents—Which One Should Be Used When? Part 2: Small Vessel Embolization.* Seminars in Interventional Radiology, 2010. **27**(1): p. 99-104.

25. Szafron, J.M., Muschenborn, A.D., Maitland, D.J., *Design and Characterization of an Endovascular Mechanical Thrombectomy Device.* Journal of Medical Devices, 2014. **8**(2).

26. Hollister, S.J., Maddox, R.D., Taboas, J.M., *Optimal Design and Fabrication of Scaffolds to Mimic Tissue Properties and Satisfy Biological Constraints.* Biomaterials, 2002. **23**(20): p. 4095-4103.

27. Zawadzak, E., Bil, M., Ryszkowska, J., Nazhat, S.N., Cho, J., Bretcanu, O., Roether, J.A., Boccaccini, A.R., *Polyurethane Foams Electrophoretically Coated*

with Carbon Nanotubes for Tissue Engineering Scaffolds. Biomedical Materials, 2008. **4**(1): p. 1-9.

28. Pham, Q.P., Sharma, U., Mikos, A.G., *Electrospinning of Polymeric Nanofibers for Tissue Engineering Applications: A Review.* Tissue Engineering, 2006. **12**(5): p. 1197-1211.

29. Guelcher, S.A., *Biodegradable Polyurethane: Synthesis and Applications in Regenerative Medicine.* Tissue Engineering, 2008. **14**(1): p. 3-17.

30. Bertoldi, S., Fare, S., Denegri, M., Rossi, D., Haugen, H.J., Parolini, O., Tanzi, M.C., *Ability of Polyurethane Foams to Support Placenta-Derived Cell Adhesion and Osteogenic Differentiation: Preliminary Results.* Journal of Material Science: Materials in Medicine, 2010. **21**(3): p. 1005-1011.

31. Augustinos, P., Ouriel, K., *Invasive Approaches to Treatment of Venous Thromboembolism.* Circulation, 2004. **110**(9): p. I27-I34.

32. Mackman, N., *New Insights Into the Mechanisms of Venous Thrombosis.* Journal of Clinical Investigation, 2012. **122**(7): p. 2331-2336.

33. Chesnutt, J.K.W., Han, H.C., *Effect of Red Blood Cells on Platelet Activation and Thrombus Formation in Tortuous Arterioles.* Frontiers in Bioengineering and Biotechnology, 2013. **1**(18): p. 1-12.

34. *Abdominal Aortic Aneurysm*. Medline Plus.[cited 2014 May 28]; Available from: http://www.nlm.nih.gov/medlineplus/ency/article/000162.htm.

35. Sorin, I., Senetscu, R., *Polymeric Materials Review on Oxidation, Stabilization and Evaluation Using CL and DSC Methods*. 2009, TE Technical note.

36. Eliason, J.L., Upchurch, G.R., *Endovascular Abdominal Aortic Aneurysm Repair.* Circulation, 2008. **117**: p. 1738-1744.

37. Bolland, J.L., *Kinetics of Olefin Oxidation.* Quarterly Reviews, Chemical Society, 1949. **3**(1): p. 1-21.

38. Greiner, A., Grommes, J., Jacobs, M.J., *The Place of Endovascular Treatment in Abdominal Aortic Aneurysm.* Deutsches Ärzteblatt International 2013. **110**(8): p. 119-125.

39. Guidoin, R., Peirano, M.A., Barone, H.D., Douville, Y., Zhang, Z., Guzman, R., Bertoni, H., Merhi, Y., Marinov, G.R., McGregor, R., Zhang, H., Chappard, D., Dionne, G., Deng, X., *Transrenal Deployment of a Modular Stent Graft to Repair AAAs with Short Necks: Experiments in Dogs.* Artificial Cells Blood Substitutes and Biotechnology, 2008. **36**(4): p. 310-339.

40. White, S.B., Stavropoulos, S.W., *Management of Endoleaks Following Endovasclar Repair.* Seminars in Interventional Radiology, 2009. **26**(1): p. 33-38.

41. Saqib, N.U., Charlton-Ouw, K.M., Azizzadeh, A., *Managing Type II Endoleaks.* Endovascular Today, 2013(February): p. 45-50.

42. Walker, S.R., Macierewicz, J., Hopkinson, B.R., *Endovascular AAA Repair: Prevention of Side Branch Endoleaks With Thrombogenic Sponge.* Cerebrovascular Interventions, 1999. **6**(4): p. 350-353.

43. Olson III R.A., S., P.K. Improved Fine Pore Media and Method of Making Same, PTC/US2003/041108 2003. Provair PLC 2003.

44. Lerouge, S., Wertheimer, M.R., Hahia, L'H., *Plasma Sterilization: A Review of Parameters, Mechanisms and Limitations.* Plasmas and Polymers, 2001. **6**(3): p. 175-188.

45. Mukhopadhyay, S.M., Joshi, P., Datta, S., Macdaniel, J., *Plasma Assisted Surface Coating of Porous Solids.* Applied Surface Science, 2002. **201**: p. 219-226.

46. Sanchis, M.R., Calvo, O., Fenollar, O., Garcia, D., Balart, R., *Surface Modification of a Polyurethane Film by Low Pressure Glow Discharge Oxygen Plasma Treatment.* Journal of Applied Polymer Science, 2007. **105**: p. 1077-1085.

47. Wang, C.X., Liu, Y., Xu, H.L., Ren, Y., Qiu, Y.P., *Influence of Atmospheric Pressure Plasma Treatment Time on Penetration Depth of Surface Modification Into Fabric.* Applied Surface Science, 2008. **254**: p. 2499-2505.

48. Hild, F., Biering, D. Hydrophobic Insulation Material, US20090061200 A1 2007. Tristart Plastics Corporation.2007.

49. De Nardo, L., Alberti, R., Cigada, A., Yahia, L'H., Tanzi, M.C., Fare, S., *Shape Memory Polymer Foams for Cerebral Aneurysm Reparation: Effects of Plasma Sterilization on Physical Properties and Cytocompatibility.* Acta Biomaterialia, 2009. **5**(5): p. 1508-1518.

50. Fu, X., Jenkins, M.J., Sun, G., Bertoti, I., Dong, H., *Characterization of Active Screen Plasma Modified Polyurethane Surfaces.* Surface and Coathings Technology, 2012. **206**(23): p. 799-4807.

51. Wasa, K., Hayakawa, S., *Handbook of Sputter Disposition Technology: Principles, Technology, and Applications*. Materials Science and Process Technology Series. 1992, Westwood, New Jersey: Noyes Publications.

52. Harry, J., *Introduction to Plasma Technology: Science, Engineering, and Applications*. 2010, Weinheim, Germany: Wiley-VCH Verlag & Co. KGaA.

53. Bittencourt, J.A., *Fundamentals of Plasma Physics*. 3rd ed. 2004, Brazil: Springer. p. 678.

54. Keidar, M., Beilis, I.I., *Plasma Engineering: Applications from Aerospace to Bio and Nanotechnology*. 2013, London, UK: Academic Press. p. 442.

55. Moss, S., Jolly, A.M., Tighe, B.J., *Plasma Oxidation of Polymers.* Plasma Chemistry and Plasma Processing, 1986. **6**(4): p. 401-416.

56. *Controlled Chemical Plasma Etching for Advanced Technology Applications*. Nordson MARCH.[cited 2014 May 14]; Available from: http://www.nordson.com/en-us/divisions/march/support/Literature/Documents/techpaper-medicalapplications3.pdf.

57. Ghosh, M.K., Mittal, K.L., ed. *Polyimides: Fundamentals and Applications*. Plastics Engeering. 1996, Marcel Dekker, Inc.: New York, New York. 912.

58. Hartney, M.A., Hess, D.W., Soane, D.S., *Oxygen Plasma Etching for Resist Stripping and Multilayer Lithography.* Journal of Vacuum Science and Technology B, 1989. **7**(1): p. 1-13.

59. Rack, P.D. *Plasma Etching Outline*. University of Wisconsin-Madison College of Engineering.[cited 2014 September 30]; Available from: https://http://www.google.com/url?sa=t&rct=j&q=&esrc=s&source=web&cd=1&cad=rja&uact=8&ved=0CB4QFjAA&url=http%3A%2F%2Fwcam.engr.wisc.edu%2FPublic%2FReference%2FPlasmaEtch%2FEtching.pdf&ei=KPAqVJzCD5G2yATf7YHQCA&usg=AFQjCNFzLwaymhaFHR3lw_9yIjdbHHItFQ.

60. Saher, S., Moon, S., Jun Kim, S., Jin Kim, H., Hyup Kim, Y., *O2 Plasma Treatment for Ionic Polymer Metal Nano Composite (IPMNC) Actuator.* Sensors and Actuators B: Chemical, 2010. **147**: p. 170-179.

61. Singhal, P., Boyle, A., Brooks, M.L., Infanger, S., Letts, S., Small, W., Maitland, D.J., Wilson, T.S., *Controlling the Actuation and Rate of Low-Density Shape-Memory Polymer Foams in Water.* Macromolecular Chemistry and Physics, 2013. **214**(11): p. 1204-1214.

62. Rodriguez, J.N., Millier, M.W., Boyle, A., Horn, J., Yang, C.K., Wilson, T.S., Ortega, J.M., Small, W., Nash, L., Skoog, H., Maitland, D.J., *Reticulation of Low Density Shape Memory Polymer Foam with an In Vivo Demonstration of Vascular Occlusion.* Journal of the Mechanical Behavior of Biomedical Materials, 2014. **40**: p. 102-114.

63. Alves, P., Pinto, S., de Sousa, H.C., Gil, M.H., *Surface Modification of a Thermoplastic Polyurethane by Low-Pressure Plasma Treatment to Improve Hydrophilicity.* Journal of Applied Polymer Science, 2011. **122**(4): p. 2302-2308.

64. Desmet, T., Morent, R., De Geyter, N., Leys, C., Schacht, E., Dubruel, P., *Nonthermal Plasma Technology as a Versatile Strategy for Polymeric Biomaterials Surface Modification: A Review.* Biomacromolecules, 2009. **10**(9): p. 2351-2378.

65. Moles, M.D., Scotchford, C.A., Ritchie, A.C., *Oxidation State of a Polyurethane Membrane after Plasma Etching.* Conference Papers in Science, 2014. **2014**: p. 1-11.

APPENDIX A

PLASMA PROCESS DEVELOPMENT

The four plasma processes evaluated for plasma reticulation in this thesis were selected based on an extensive literature review and a number of experimental processes performed using the AURORA 0350 Plasma Surface Treatment System. The first three plasma process evaluated, shown in Table A-1, were performed on 76.2 x 76.2 x 25.4 mm (L x W x H) block samples utilizing the process parameters provided by Plasma Technology Systems. The foam geometry and coordinate system is shown in Figure A-1.

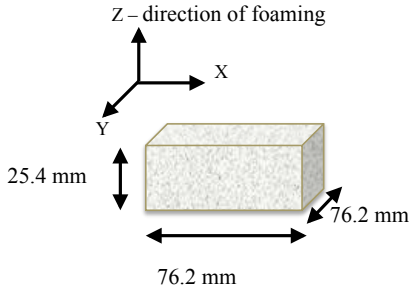

Figure A-1: Foam block geometry of sample evaluated with plasma reticulation Processes 1-3.

Table A-1: Plasma process parameters provided by Plasma Technology Systems (Belmont, CA). These parameters were the first process parameters utilized to plasma reticulate ultra-low density shape memory polymer foam with the block geometry.

Process	Gas Flow Rate O_2 | CF_4 (sccm)	RF Power (W)	Process Duration (min)	Chamber Pressure (mTorr)
Process 1	200 | 200	150	10	210
Process 2	200 | 200	150	15	210
Process 3	100 | 100	150	10	135

For the three initial plasma processes, the foam sample was placed directly on the glass shelf within the reaction chamber, such that the direction of foaming was parallel to the electrode. Process 1 produced inhomogeneous reticulation levels throughout the sample and the majority of the sample volume exhibited no increase in reticulation. A Plasma Technology Systems engineer suggested increasing the process duration and decreasing the gas flow rates to increase reticulation levels and uniformity throughout the sample. The percent reticulation for the samples plasma reticulated with Processes 1-3 was calculated per the protocol described in II.1.5, and the results are shown in Table A-2.

Table A-2: Percent reticulation results in the XY and ZY planes and for the overall foam samples achieved by the first three plasma processes.

Process	Whole Sample Percent Reticulation (%)*	XY Plane Percent Reticulation (%)*	ZY Plane Percent Reticulation (%)*
Process 1	74.9 ± 6.64	79.2 ± 2.4	70.6 ± 6.8
Process 2	76.4 ± 7.0	79.4 ± 6.4	73.4 ± 6.5
Process 3	69.5 ± 7.9	74.8 ± 6.8	64.1 ± 4.7

* Average ± Standard Deviation, n = 1

Calculating the percent reticulation achieved by the first three plasma processes indicated that these process parameters were not capable of achieving complete reticulation. Furthermore, the reticulation achieved by these processes was anisotropic

because there was a significant difference in percent reticulation between the ZY and XY planes ($p < 0.05$).

After evaluating Processes 1-3, the block geometry was changed to 50.8 x 50.8 x 25.4 mm (L x W x H), as shown in Figure 3. In the next plasma process evaluated, Process 4, the RF power was increased to 300 W, while the other process parameters were the same as those of Process 1, as shown in Table A-3. Placing the sample directly on the glass shelf within the reaction chamber resulted in a visible reticulation gradient along the sample height; the sample was highly reticulated at the top and slightly reticulated at the bottom. To inhibit the development of a reticulation gradient along the sample height, the next sample was placed on two 5 mm tall stacks of glass slides, with 6.4 mm of the sample resting on each stack of glass slides, and treated with Process 4. This sample also developed a visible reticulation gradient along the sample height. The next sample was placed on 38.1 mm tall Delrin cylindrical supports, as shown in Figure A-2, to further increase the distance between the glass shelf and the sample. The supports were spaced 38.1 mm apart, with 6.4 mm of the sample resting on each Delrin support. The whole setup was placed at the center of the reaction chamber for plasma reticulation.

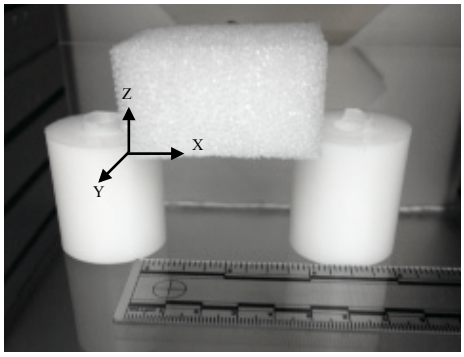

Figure A-2: Placement of block samples on 38.1 mm Delrin cylinder supports for Processes 4-13.

The sample treated on the Delrin supports with Process 4 did not have a visible reticulation gradient from along the sample height, but there was a visible gradient within the sample volume; the inner region of the sample was moderately reticulated while the outer sample region was completely reticulated. From this experiment, it was determined that a number of plasma processes would be tested on samples using the Delrin support configuration. The plasma process parameters for these processes, Processes 4-11, are listed in Table A-3.

Table A-3: Plasma process parameters utilized to plasma reticulate ultra-low density shape memory polymer foam with the block geometry via Processes 4-11.

Process	Gas Flow Rate O_2 | CF_4 (sccm)	RF Power (W)	Process Duration (min)	Chamber Pressure (mTorr)
Process 4	200 | 200	300	10	220
Process 5	50 | 50	300	10	100
Process 6	25 | 25	300	10	75
Process 7	25 | 25	400	10	80
Process 8	50 | 50	500	10	110
Process 9	50 | 50	600	10	115
Process 10	50 | 50	300	50	100
Process 11	50 | 50	300	25	105

In Processes 5 and 6, the flow rates were lowered from 200|200 sccm to 50|50 and 25|25 sccm, respectively, because the sample treated with Process 4 was slightly discolored and had a reticulation gradient throughout the volume. Process 5 resulted in slight discoloration of the sample, while still producing an outer region with complete reticulation. Processes 6 and 7 were aimed at eliminating sample discoloration and the boundary region of complete reticulation by decreasing the flow rates and increasing the RF power. Reducing the flow rates to 25|25 sccm in Processes 6 and 7 successfully eliminated sample discoloration, but the boundary region of complete reticulation continued to develop at both 300 and 400 W. Greater RF powers were tested in Processes 8 and 9 at the flow rates of 50|50 sccm because it was determined that slight sample discoloration would allowable to achieve homogenous reticulation throughout the sample volume. However, Process 8 resulted in discoloration at the top of the sample and a reticulation gradient along the sample height, instead of throughout the sample

volume. Process 9 produced results similar to Process 8, but the sample was highly discolored at the top. Processes 10 and 11 were aimed at pushing the limits of process duration to examine the effect on sample discoloration and homogeneity of reticulation. Increasing the process time to 25 and 50 min, with flow rates of 50|50 sccm at 300 W, resulted in slight discoloration but significant sample degradation. Furthermore, the samples developed a slight reticulation gradient along their height. After observing that homogenous reticulation was not achieved at extreme process durations, it was hypothesized that a reticulation gradient would develop in samples with large volumes, such as those tested here, due to the diffusive characteristic of plasma reticulation. Thus, homogenous reticulation throughout a large sample volume could only be achieved in extreme plasma process conditions, which might compromise the material properties of the SMP foam.

Observing the gradient within plasma-reticulated samples led to the measurement of the boundary layer of complete reticulation within each plasma-reticulated sample. After collecting three SEM images from the center of a slice to calculate the percent reticulation, following the protocol described in II.1.5, four additional SEM images were taken along the slice edges to measure the depth of the region with complete membrane removal. ImageJ was used to measure the length of the completely reticulated region at three locations in each image, providing twelve measures of the fully reticulated region in each plane (ZY and XY), as shown in Figure A-3.

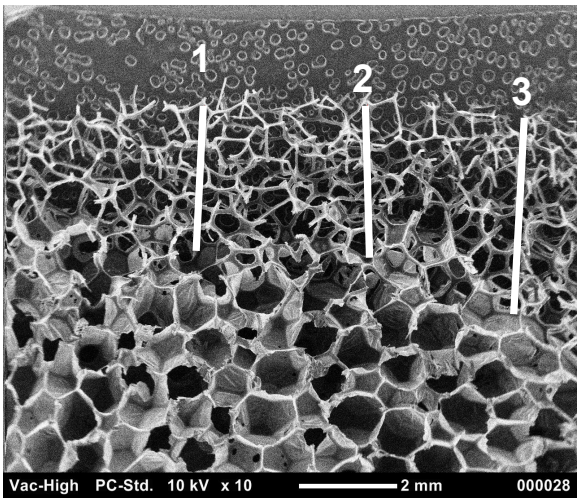

Figure A-3: Image used to measure length of completely reticulated region within plasma-reticulated sample treated with Process 8. The length of Line 1 is 2.96 mm, Line 2 is 3.09 mm, and length of Line 3 is 3.93 mm.

The twelve measures of the depth of the completely reticulated region were averaged to calculate the average depth of complete reticulation in each plane. Finally, all twenty-four measures of complete reticulation depth were averaged to calculate the average depth of complete reticulation for the whole sample.

For Processes 4-9, the percent reticulation and depth of the complete reticulation boundary layer were calculated. For Processes 10 and 11, the high levels of sample degradation caused by these processes negated the need to quantify the percent reticulation and depth of complete reticulation achieved by these processes. The percent reticulation results and depth of the completely reticulated region for Processes 4-9 are shown in Table A-4.

Table A-4: Percent reticulation and depth of complete reticulation boundary layer for ultra-low density shape memory polymer foam block samples treated with Processes 4-9.

Process	Whole Sample Percent Reticulation (%)*	XY Plane Percent Reticulation (%)*	ZY Plane Percent Reticulation (%)*	Depth of Complete Reticulation (mm)*
Process 4	72.4 ± 8.6	70.5 ± 4.2	74.3 ± 12.5	3.2 ± 1.0
Process 5	77.6 ± 7.2	79.9 ± 10.1	75.3 ± 3.5	2.6 ± 0.6
Process 6	71.4 ± 4.1	70.8 ± 5.5	72.2 ± 3.1	2.6 ± 0.6
Process 7	71.7 ± 9.3	80.0 ± 2.0	63.4 ± 2.3	2.5 ± 0.6
Process 8	67.0 ± 5.8	70.8 ± 3.3	63.1 ± 5.2	3.7 ± 0.6
Process 9	66.5 ± 9.3	72.3 ± 3.2	60.8 ± 10.3	4.8 ± 0.8

* Average ± Standard Deviation, n = 1

None of the processes evaluated up to this point had achieved complete reticulation at the center of the sample. This led to an extensive literature review related to plasma etching of polymers, as detailed in I.3.3. The literature review influenced the subsequent plasma processes to be conducted with an O_2/CF_4 molar ratio of 80:20 and a target chamber pressure of 400 mTorr. A calibration study was conducted on the AURORA 0350 Plasma Surface Treatment System to identify which gas flow rates preserved the 80:20 O_2/CF_4 molar ratio and completed the plasma process at 400 mTorr. The calibration study identified the appropriate gas flow rates to be 800|200 sccm of O_2/CF_4. The next two processes evaluated, Processes 12 and 13, incorporated the new gas flow rates and molar ratio, as shown in Table A-5, and were conducted using the Delrin support configuration.

Table A-5: Plasma process parameters utilized to plasma reticulate ultra-low density shape memory polymer foam via Processes 12 and 13.

Process	Gas Flow Rate O_2 | CF_4 (sccm)	RF Power (W)	Process Duration (min)	Chamber Pressure (mTorr)
Process 12	800 | 200	300	10	400
Process 13	800 | 200	300	20	400

Process 12 developed a reticulation gradient along the sample height, with minimal reticulation achieved in the bottom 1 cm of the sample. Process 13 also developed a reticulation gradient along the sample height; with minimal reticulation achieved in the bottom 0.5 cm of the sample and slight degradation at the top. The lack of reticulation at the sample base caused the sample configuration to be investigated with a number of different sample stages.

Process 12 was the plasma process utilized to evaluate the effects of different sample stages. The first new stage, S1, consisted of press fitting two 1 mm diameter aluminum rods into a 25.4 mm tall PMMA block, such that the two rods were 25.4 mm apart. The foam sample was gently pressed onto the aluminum rods. The second stage evaluated, S2, was similar to S1, except one aluminum rod was used to hold the foam. Both stages were placed in the center of the reaction chamber for the plasma process, the foam was oriented such at the foaming direction was parallel to the electrode, and the sample was elevated 127 mm above the glass shelf.

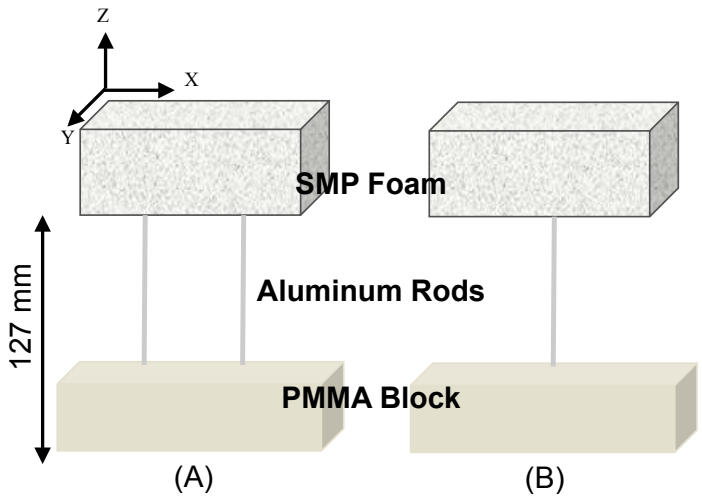

Figure A-4: First two stages evaluated using Process 12 to improve reticulation homogeneity throughout ultra-low density shape memory polymer foam block samples. (A) Stage 1 consisted of two 1 mm diameter aluminum rods press fit into a 25.4 mm tall PMMA block, and the foam sample was gently pressed onto the aluminum rods. Image not drawn to scale. (B) Stage 2 consisted of one 1 mm diameter aluminum rod press fit into a 25.4 mm tall PMMA block, and the foam sample was gently pressed onto the aluminum rod. Both stages were placed in the center of the reaction chamber and elevated the sample 127 mm above the glass shelf.

During plasma treatment of samples with stages S1 and S2, the foam was successfully reticulated but the resulting reticulation caused the foam to slip down the rods. After cutting the samples down the center, along the ZY plane, it was observed that the samples were highly reticulated but complete reticulation did not extend to the sample center. The next stage, S3, consisted of the PMMA block and the two aluminum rods press fit into the PMMA block as in S1. However, to support the foam without piercing it, a 76.2 x 76.2 mm (L x W) mesh polypropylene sheet was epoxied to the aluminum rods, allowing the sample to be elevated 139.7 mm above the glass shelf in the reaction chamber. The stage was placed at the center of the reaction chamber, and the foam sample was placed directly at the center of the mesh polypropylene sheet for

plasma reticulation with the foaming direction parallel to the electrode, as shown in Figure A-4.

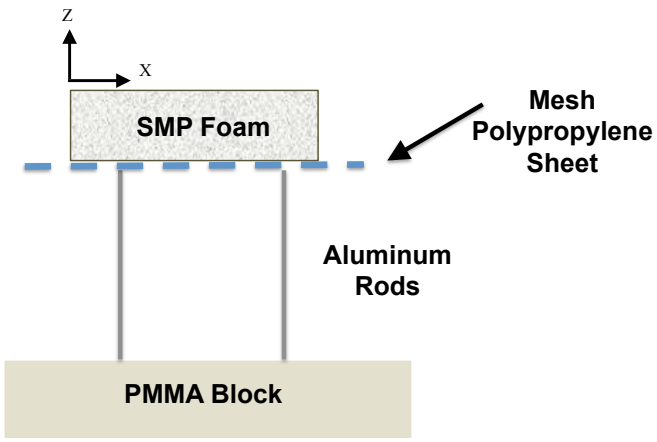

Figure A-5: Third stage, S3, evaluated using Process 12 to improve reticulation homogeneity throughout ultra-low density shape memory polymer foam block samples without piercing foam with sample stage. S3 consisted of two 1 mm diameter aluminum rods press fit into a 25.4 mm tall PMMA block, and a 76.2 x 76.2 mm (L x W) mesh polypropylene sheet epoxied to the tops of the aluminum rods, allowing the sample to be elevated 139.7 mm above the glass shelf in the reaction chamber. After S3 was placed in center of the reaction chamber, the foam sample was gently placed at the center of the mesh polymer sheet for plasma reticulation. Image not drawn to scale.

The aggressive nature of the plasma process employed by Process 12 completely degraded the epoxy attaching the mesh polypropylene sheet to the aluminum rods, and initiated degradation of the mesh polypropylene sheet. Thus S3 was not a viable sample stage. Next, a 50.8 x 50.8 x 25.4 mm (L x W x H) aluminum mesh cage was created, S4, to place the block samples on top of at the center of the reaction chamber, as shown in Figure A-5. This stage elevated the sample 25.4 mm above the glass shelf in the reaction chamber.

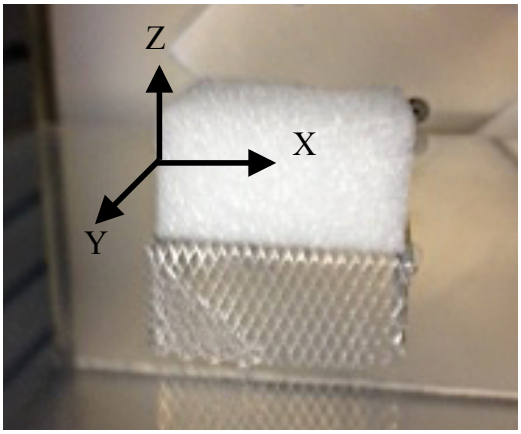

Figure A-6: Fourth stage, S4, evaluated using Process 12 to improve reticulation homogeneity throughout ultra-low density shape memory polymer foam block samples without piercing foam with sample stage. S4 consisted of a 50.8 x 50.8 x 25.4 mm (L x W x H) aluminum mesh cage, allowing the sample to be elevated 25.4 mm above the glass shelf in the reaction chamber. After S4 was placed in center of the reaction chamber, the foam sample was gently placed on the center of the stage for plasma reticulation.

The sample treated on S4 with Process 12 was similar to the sample treated with Process 12 on the Delrin supports; a reticulation gradient was developed along the sample height, with minimal reticulation achieved in the bottom 1 cm of the sample. Based on the results from treating samples with the four different stages described above, and the Delrin supports, it was concluded that the samples needed to be elevated approximately 127 mm above the glass shelf to allow the bottom of the sample to be reticulated and to minimize the development of a reticulation gradient along the sample height. Furthermore, to increase the surface area directly exposed to the electrode, the samples would be oriented with the foaming direction perpendicular to the electrode, allowing the 50.8 x 50.8 mm surfaces of the sample to be parallel to the electrode. The next sample stage, S5, tested with Process 12, was a 50.8 x 50.8 x127 mm (L x W x H)

aluminum stage, as shown in Figure A-6. The stage was placed in the center of the reaction chamber and the foam was placed on the stage with the new orientation.

Figure A-7: Fifth stage, S5, evaluated using Process 12 to improve reticulation homogeneity throughout ultra-low density shape memory polymer foam block sample. S5 consisted of a 50.8 x 50.8 x 127 mm (L x W x H) aluminum mesh stage, allowing the sample to be elevated 127 mm above the glass shelf in the reaction chamber. S5 was utilized while orienting the foam with such that the foaming direction was perpendicular to the electrode.

The sample plasma-reticulated with Process 12 on S5 was homogenously reticulated throughout the sample height, and a reticulation gradient was developed throughout the sample volume. From this test it was concluded that this stage and sample orientation would be utilized for the subsequent processes. The next step was to identify the plasma process parameters that achieved moderate (60-80%) and complete (> 95%) reticulation at the sample center. The final plasma processes, Processes 14-18, evaluated for plasma-reticulation of the foam block samples are listed in Table A-6.

Table A-6: Plasma process parameters utilized to plasma reticulate ultra-low density shape memory polymer foam with the block geometry via Processes 14-18.

Process	Gas Flow Rate O_2 | CF_4 (sccm)	RF Power (W)	Process Duration (min)	Chamber Pressure (mTorr)
Process 14	800 | 200	500	10	400
Process 15	800 | 200	200	12	400
Process 16	800 | 200	300	15	400
Process 17	800 | 200	300	5	400
Process 18	800 | 200	300	8	400

The high RF power of Process 14 caused the sample to become highly discolored, taking on an orange-brown color, and the sample experienced a significant reduction in volume. Decreasing RF power to 200 W and increasing process time to 12 min in Process 15 produced a sample that exhibited no visual increase in reticulation. As a result, the subsequent processes were performed at 300 W and the process duration was varied. Samples plasma-reticulated with Processes 16-18 had slices collected per the protocol in II.1.5 to quantify the percent reticulation achieved by each process and the results are shown in Table A-7.

Table A-7: Percent reticulation results in the XY and ZY planes and for the overall foam samples achieved by the Processes 16-18.

Process	Whole Sample Percent Reticulation (%)*	XY Plane Percent Reticulation (%)*	ZY Plane Percent Reticulation (%)*
Process 16	98.1 ± 1.36	98.7 ± 1.8	97.1 ± 2.7
Process 17	51.8 ± 10.6	53.9 ± 10.4	49.7 ± 11.0
Process 18	70.3 ± 2.7	72.5 ± 9.5	66.9 ± 8.1

* Average ± Standard Deviation, n = 3

Process 18 achieved the required moderate reticulation percentage (60-80%) and Process 16 achieved the required complete reticulation percentage (> 95%), therefore these were the two process selected for full material characterization in this thesis. Process 18 corresponds to Block Moderate and Process 16 corresponds to Block Complete.

The plasma processes developed for the sheet sample geometry maintained the gas flow rates of 800|200 O_2/CF_4, the O_2/CF_4 molar ratio of 80:20, and the chamber pressure of 400 mTorr. The sheet samples had the dimensions 50.8 x 101.6 x 5 mm (L x W x H). The first sample stage evaluated for plasma reticulating the sheet samples, S6, was made of two stainless steel L-brackets screwed into a PMMA base, and a 0.2 mm diameter nitinol wire suspended between the L-brackets. The sheet samples were threaded onto the wire along the 101.6 mm edge, as shown in Figure A-7.

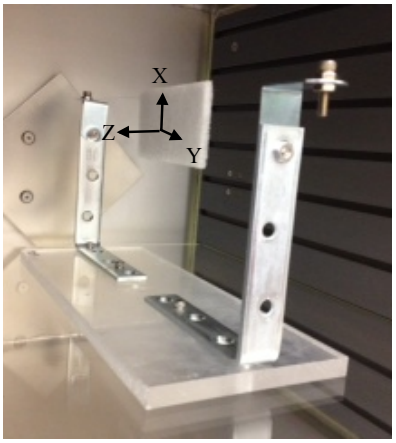

Figure A-8: First sample stage for plasma reticulating ultra-low density shape memory polymer foam sheet samples, S6. The sample stage was made of two stainless steel L-brackets screwed into a PMMA base, and a 0.2 mm diameter nitinol wire suspended between the L-brackets. The sheet samples were threaded onto the wire along the 101.6 mm edge, allowing the sample to be elevated 114.3 mm above the glass shelf. The samples were oriented such that the foaming direction was perpendicular to the electrode.

This sample stage elevated the samples approximately 114.3 mm above glass shelf. The sample, threaded on the nitinol wire, was placed in the reaction chamber such that the foaming direction was perpendicular to the electrode. Processes 19-22 were performed utilizing this sample stage with the foam in this orientation. The plasma process parameters for Processes 19-22 are listed in Table A-8.

Table A-8: Plasma process parameters utilized to plasma reticulate ultra-low density shape memory polymer foam with the sheet geometry via Processes 19-22.

Process	Gas Flow Rate O_2 | CF_4 (sccm)	RF Power (W)	Process Duration (min)	Chamber Pressure (mTorr)
Process 19	800 | 200	150	15	400
Process 20	800 | 200	150	5	400
Process 21	800 | 200	300	2	400
Process 22	800 | 200	300	4	400

The lower RF power of Processes 19 and 20 resulted in the samples plasma-reticulated with these processes to have no significant discoloration and to exhibit visible reticulation throughout the sample. Process 21 resulted in the region around the nitinol wire to become highly discolored and the perimeter of the sample to be completely reticulated, while the center of the sample appeared to have minor reticulation levels. Process 22 caused the region around the nitinol wire to become highly degraded, while the other three sample edges were complete reticulated and the center of the sample was only moderately reticulated. The percent reticulation calculated for Processes 19-22, using the protocol described in II.1.5, are shown in Table A-9.

Table A-9: Percent reticulation results in the XY and ZY planes and for the overall foam samples achieved by the Processes 19-22.

Process	Whole Sample Percent Reticulation (%)*	XY Plane Percent Reticulation (%)*	ZY Plane Percent Reticulation (%)*
Process 19	64.5 ± 9.1	64.7 ± 5.7	64.2 ± 13.2
Process 20	55.8 ± 12.0	58.1 ± 17.9	53.6 ± 5.2
Process 21	73.7 ± 5.6	71.0 ± 7.0	76.4 ± 2.9
Process 22	75.5 ± 4.8	76.9 ± 5.5	74.1 ± 4.6

* Average ± Standard Deviation, n = 1

The significant amount of metal in this sample stage caused the plasma processes to reach temperatures > 30°C, which was greater than the desired operating plasma process temperature (< 30 °C). The next sample stage, S7, was constructed of aluminum mesh; the stage was 152.4 x 76.2 x 127 mm (L x W x H) and had single pieces of the mesh holding the sample upright, such that the 50.8 x 101.6 mm (L x W) surface of the sample was parallel with the electrode within the reaction chamber, as shown in Figure A-8(A). Processes 23 and 24 were performed using this sample stage; the plasma process parameters for these processes are listed in Table A-10.

Table A-10: Plasma process parameters utilized to plasma reticulate ultra-low density shape memory polymer foam with the sheet geometry via Processes 19-27.

Process	Gas Flow Rate O_2 | CF_4 (sccm)	RF Power (W)	Process Duration (min)	Chamber Pressure (mTorr)
Process 23	800 | 200	300	10	400
Process 24	800 | 200	400	5	400
Process 25	800 | 200	300	8	400
Process 26	800 | 200	250	10	400
Process 27	800 | 200	250	8	400

Process 23 achieved a high percent reticulation in the sample, but the foam was degraded, which caused the sample to be bent over the mesh pieces that were holding it upright. Process 24 achieved complete reticulation and degradation along the sample edges, while the center of the sample was not completely reticulated. The next process, Process 25, was performed using a 152.4 x 76.2 x 127 mm (L x W x H) aluminum mesh stage, S8, with one 10 x 10 mm (W x H) piece of aluminum mesh on each side of the sample to hold it upright, as shown in Figure A-8(B). The process parameters for Process 25 are shown in Table A-10. This stage created two regions within the sample with different visible levels of reticulation. In an effort to minimize the creation of zones with different reticulation levels, the next stage evaluated, S9, utilized the 152.4 x 76.2 x 127 mm (L x W x H) aluminum mesh stage with three 10 x 10 mm (W x H) pieces of aluminum mesh on each side of the sample to hold it upright. The design of this stage is shown in Figure A-8(C). Processes 25-27 were evaluated utilizing this stage; the process parameters of these processes are listed in Table A-10.

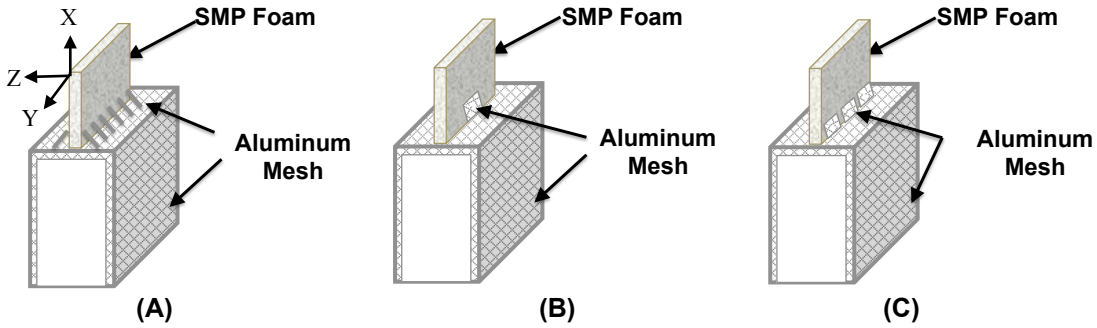

Figure A-9: (A) S7, the second sample stage evaluated to plasma reticulate ultra-low density shape memory polymer foam sheet samples. This sample stage was constructed of mesh aluminum and utilized pieces of the mesh to hold the sample upright. (B) S8, the third sample stage evaluated for plasma reticulating the sheet samples. The sample stage was constructed of mesh aluminum and one 10 x 10 mm (W x H) piece of mesh aluminum on each side of the sample to hold it upright. (C) S9, the fourth sample stage evaluated for plasma reticulating sheet samples. The sample stage was constructed of mesh aluminum and three 10 x 10 mm (L x H) pieces of mesh aluminum on each side of the sample to hold it upright. All three of these sample stages were 152.4 x 76.2 x 127 mm (L x W x H), and elevated the sample 127 mm above the glass shelf within the reaction chamber. All samples were oriented such that the foaming direction was perpendicular to the electrode.

The sample plasma reticulated on S9 with Process 25 experienced a significant decrease in material properties, which caused the sample to bend over the mesh aluminum supports that were holding it upright. Furthermore, inhomogeneous reticulation was observed at the sample's center. Process 26 almost achieved complete reticulation throughout the sample but the sample was completely blown over the mesh supports during the process because the sample had become very fragile.

Observing the sheet samples bending over the mesh aluminum supports and the development of zones with different reticulation levels led to the conclusion that using the mesh aluminum to hold the sheet upright was not an effective stage. Thus, the next sample stage, S10, was made of mesh aluminum, with dimensions: 152.4 x 76.2 x 127 mm (L x W x H), and the samples were placed flat on the top of the stage, such that the

foaming direction was parallel to the electrode in the reaction chamber, as shown in Figure A-9. Processes 27-31 were completed using S10 and the process parameters for these processes are listed in Table A-11.

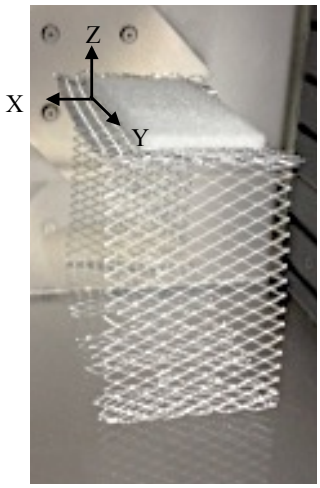

Figure A-10: Fifth sample stage for plasma reticulating ultra-low density shape memory polymer foam sheet samples, S10. The sample stage was made of mesh aluminum with dimensions: 152.4 x 76.2 x 127 mm (L x W x H), and elevated the sample 127 mm above the glass shelf within the reaction chamber. All samples were oriented such that the foaming direction was parallel to the electrode.

Table A-11: Plasma process parameters utilized to plasma reticulate ultra-low density shape memory polymer foam with the sheet geometry via Processes 27-31.

Process	Gas Flow Rate O_2 | CF_4 (sccm)	RF Power (W)	Process Duration (min)	Chamber Pressure (mTorr)
Process 27	800 | 200	250	8	400
Process 28	800 | 200	250	5	400
Process 29	800 | 200	300	5	400
Process 30	800 | 200	300	8	400
Process 31	800 | 200	300	3	400

Process 27 achieved high reticulation throughout the sample, but the reticulation was visually inhomogeneous. The sample appeared to have homogenous reticulation along the sample perimeter, however the center was less reticulated than the perimeter. These observations led to the utilization of this stage and configuration for plasma reticulating the ultra-low density SMP foam sheet samples. The percent reticulations achieved by Processes 27-31 were calculated per the protocol described in II.1.5 and the results are shown in Table A-12.

Table A-12: Percent reticulation results in the XY and ZY planes and for the overall foam samples achieved by the Processes 27-31.

Process	Whole Sample Percent Reticulation (%)*	XY Plane Percent Reticulation (%)*	ZY Plane Percent Reticulation (%)*
Process 27	76.7 ± 9.5	85.0 ± 1.7	68.4 ± 4.3
Process 28	72.5 ± 6.3	71.0 ± 6.6	74.0 ± 6.9
Process 29	97.1 ± 2.3	98.5 ± 1.3	95.6 ± 2.3
Process 30	97.3 ± 1.1	96.8 ± 0.1	97.7 ± 1.6
Process 31	78.4 ± 7.6	85.0 ± 1.3	71.8 ± 3.3

* Average ± Standard Deviation, n = 1

While Processes 27 and 28 satisfied the required moderate reticulation percentage (60-80%), these processes did not produce visible homogenous reticulation levels throughout the samples treated with these processes. Process 31 achieved the required moderate percent reticulation and the sample was visibly homogenously reticulated, thus it was selected for full material characterization in this thesis and corresponds to Sheet Moderate. Processes 29 and 30 achieved the required complete percent reticulation (>

95%). Process 30 achieved the greatest percent reticulation and visibly achieved homogenous reticulation throughout the sample; therefore it was selected for full material characterization in this thesis and corresponds to Sheet Complete.

APPENDIX B

SEM IMAGES FOR QUANTIFYING PERCENT RETICULATION

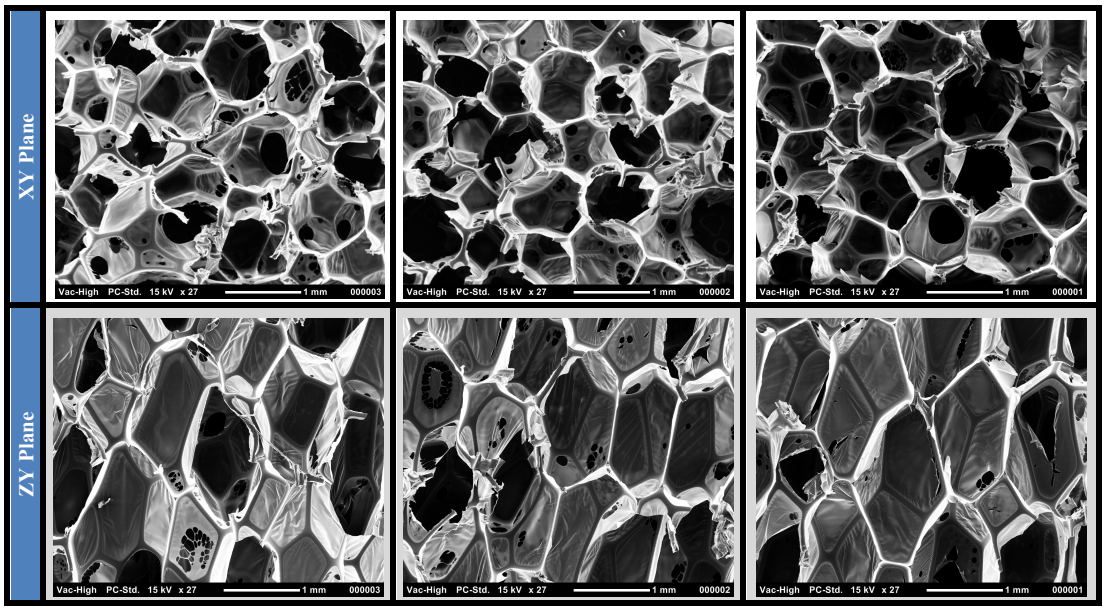

Figure B-1: **SEM images in XY and ZY plan for quantifying percent reticulation of Block Moderate n1.**

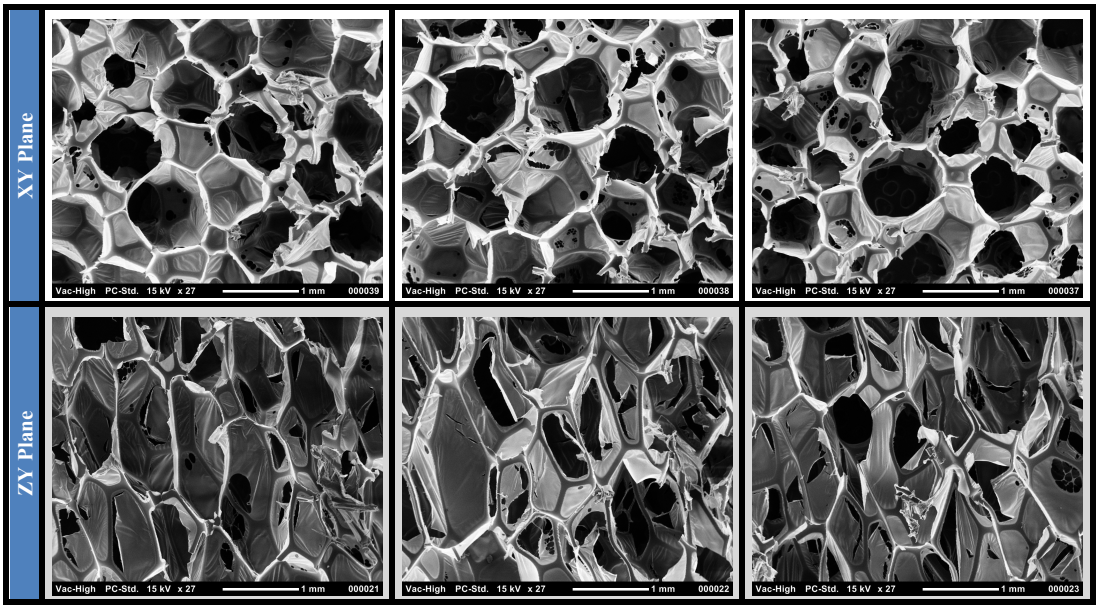

Figure B-2: SEM images in XY and ZY plan for quantifying percent reticulation of Block Moderate n2.

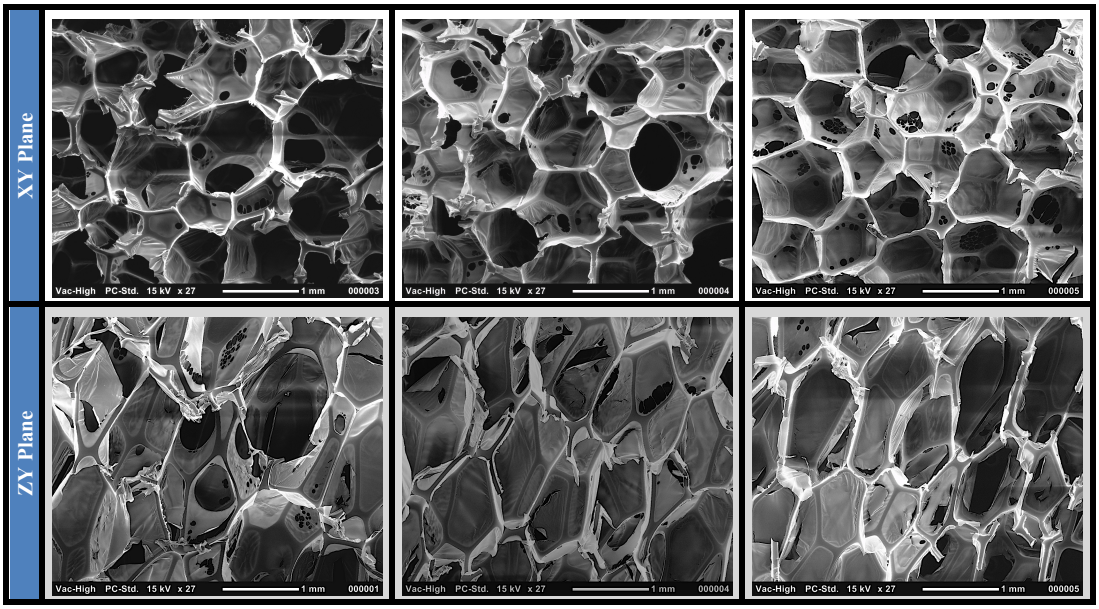

Figure B-3: SEM images in XY and ZY plan for quantifying percent reticulation of Block Moderate n3.

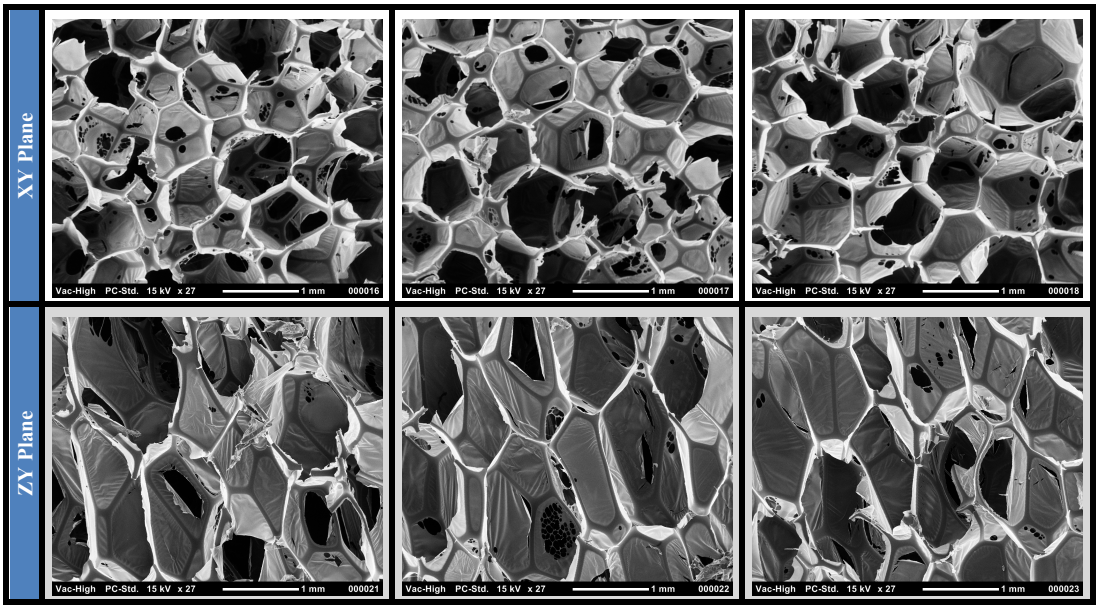

Figure B-4: SEM images in XY and ZY plan for quantifying percent reticulation of Block Moderate n4.

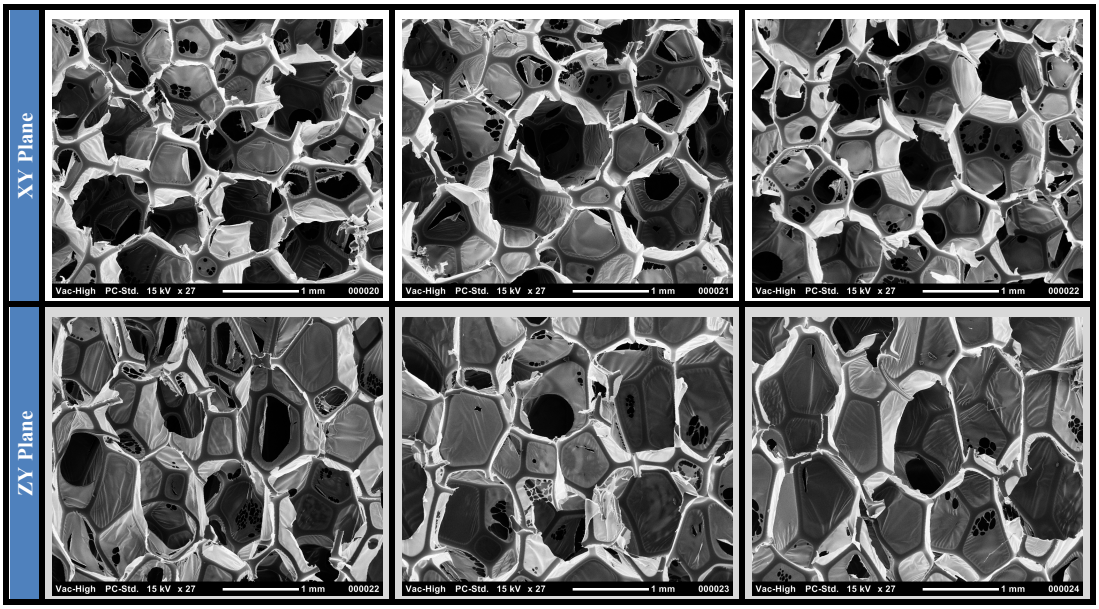

Figure B-5: SEM images in XY and ZY plan for quantifying percent reticulation of Block Moderate n5.

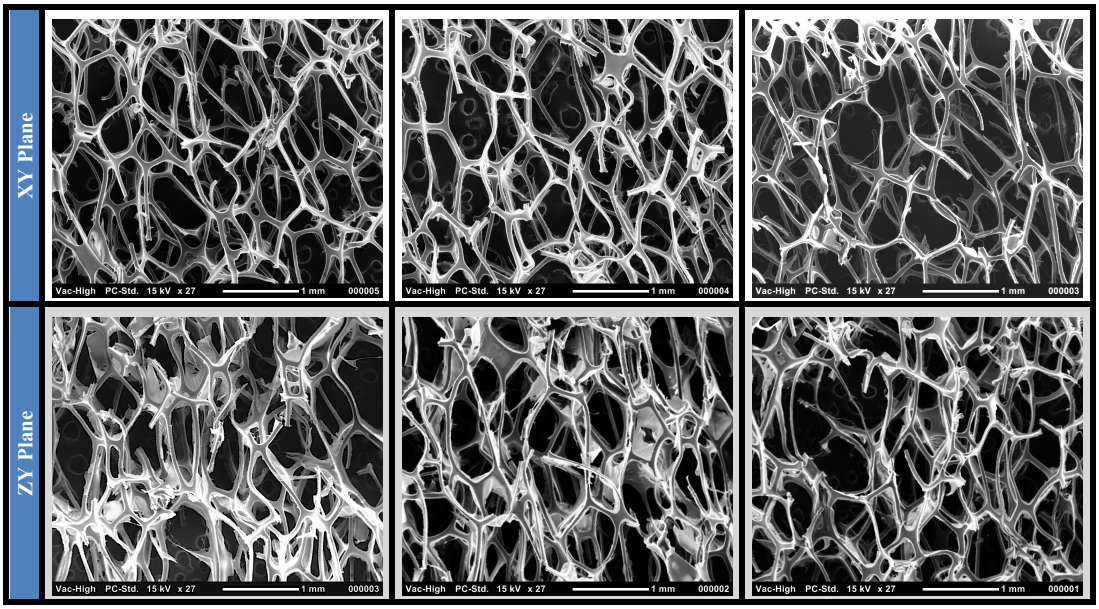

Figure B-6: SEM images in XY and ZY plan for quantifying percent reticulation of Block Complete n1.

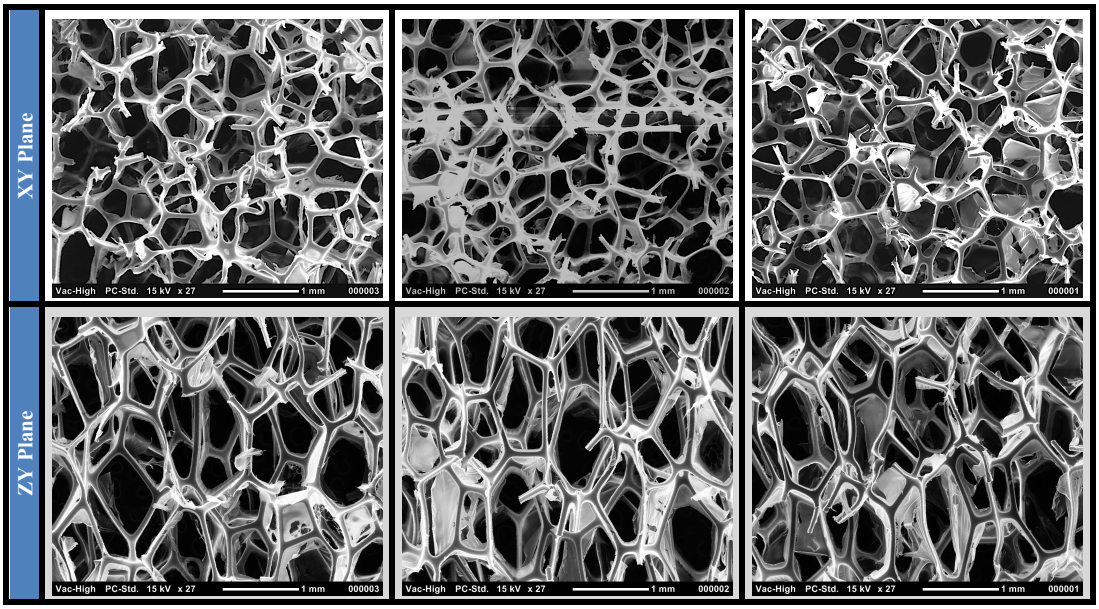

Figure B-7: SEM images in XY and ZY plan for quantifying percent reticulation of Block Complete n2.

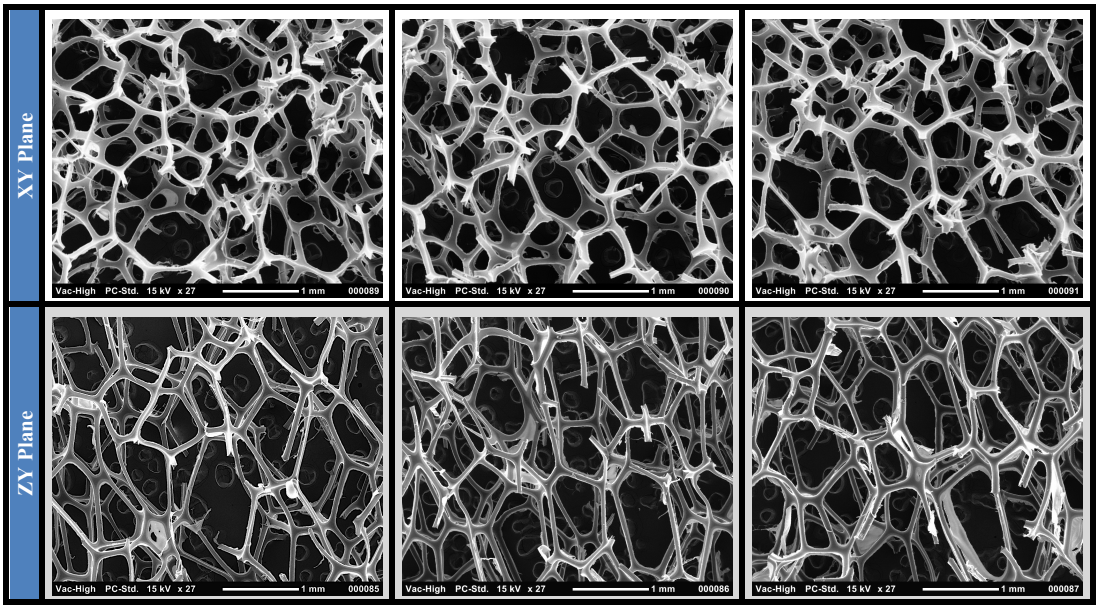

Figure B-8: SEM images in XY and ZY plan for quantifying percent reticulation of Block Complete n3.

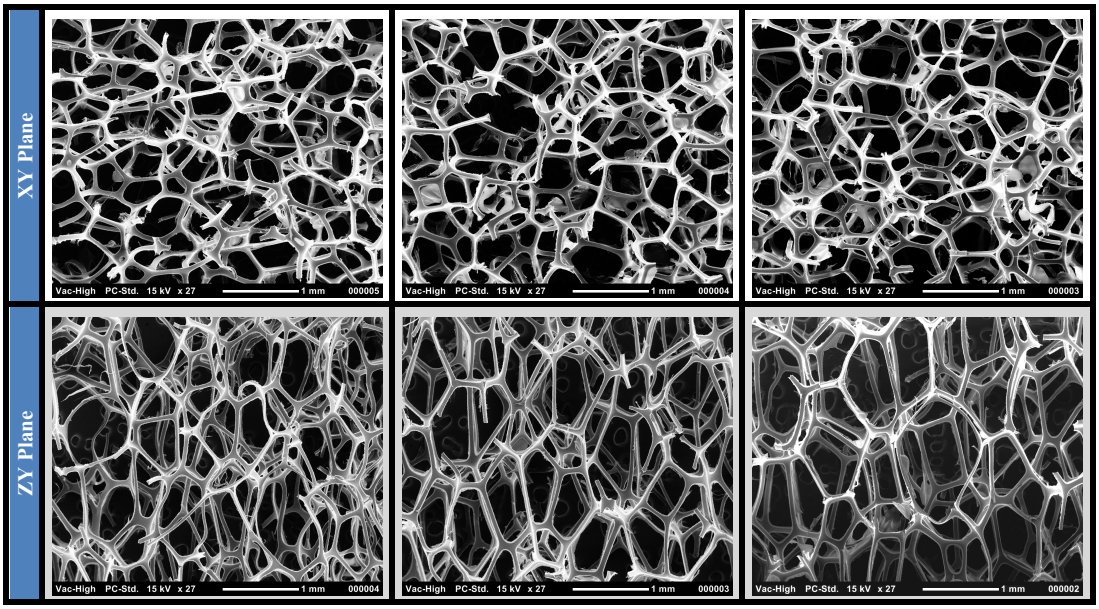

Figure B-9: SEM images in XY and ZY plan for quantifying percent reticulation of Block Complete n4.

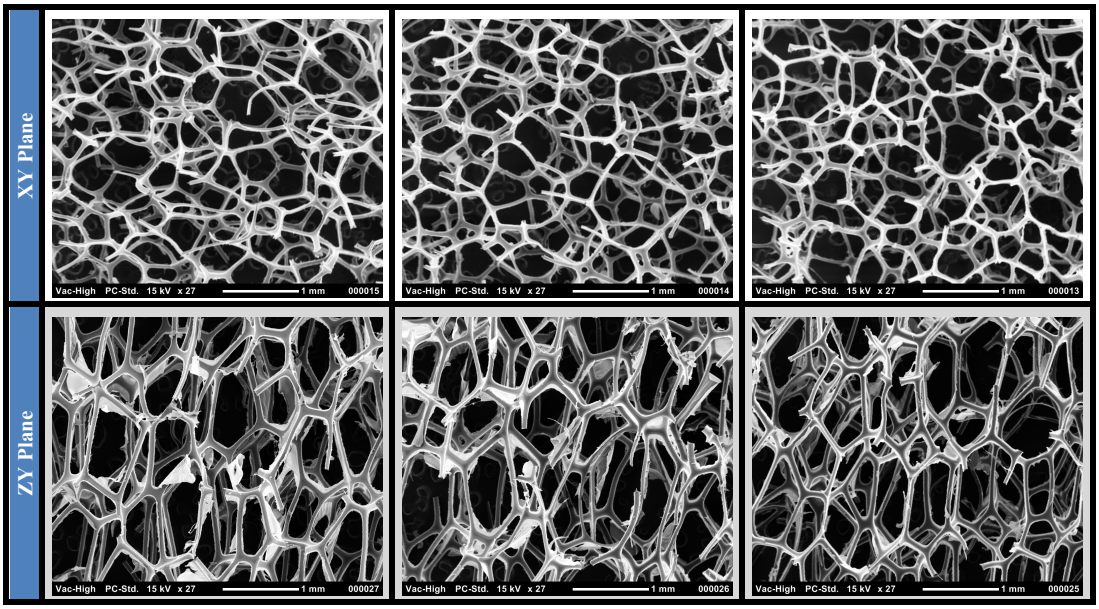

Figure B-10: SEM images in XY and ZY plan for quantifying percent reticulation of Block Complete n5.

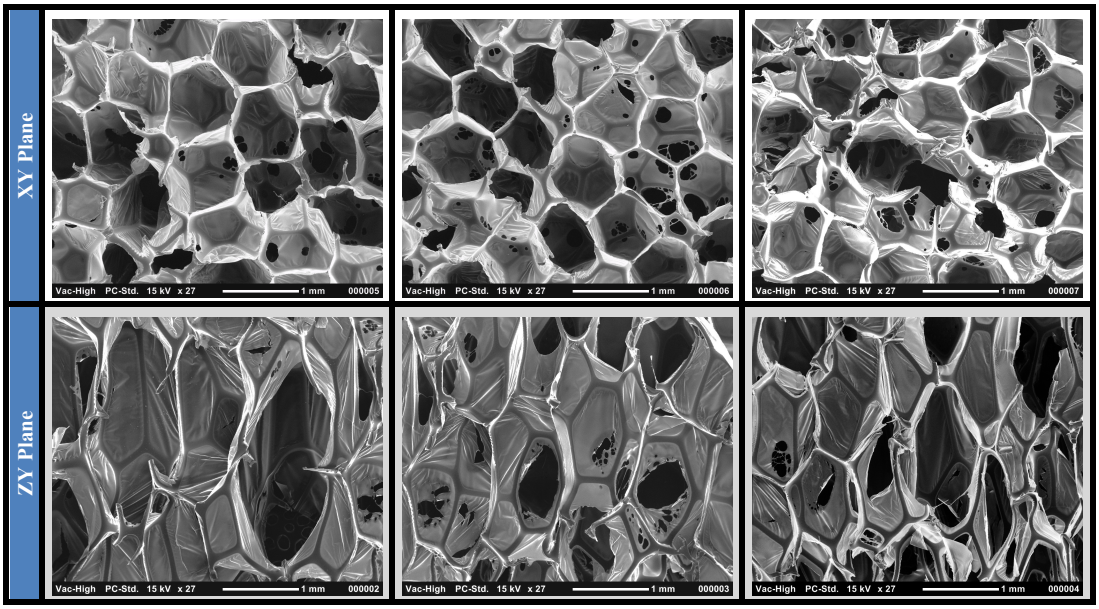

Figure B-11: SEM images in XY and ZY plan for quantifying percent reticulation of Sheet Moderate n1.

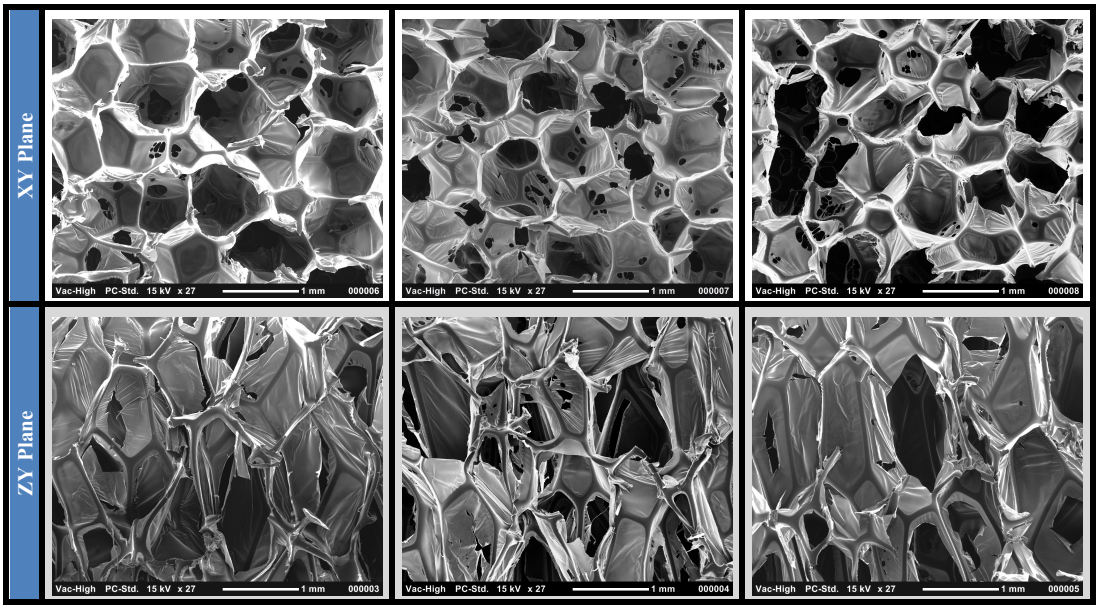

Figure B-12: SEM images in XY and ZY plan for quantifying percent reticulation of Sheet Moderate n2.

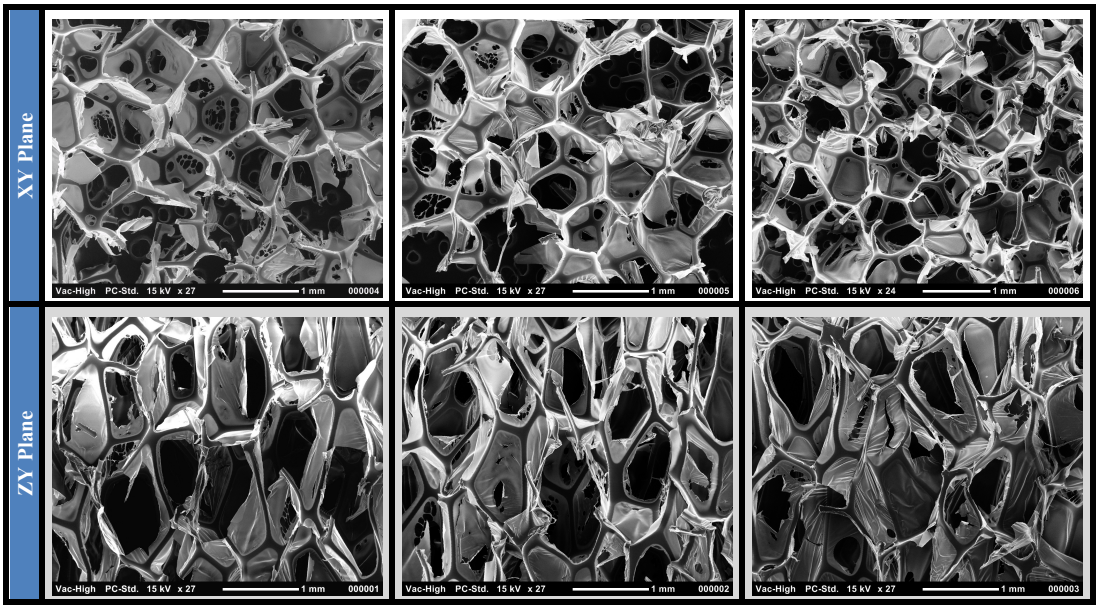

Figure B-13: SEM images in XY and ZY plan for quantifying percent reticulation of Sheet Moderate n3.

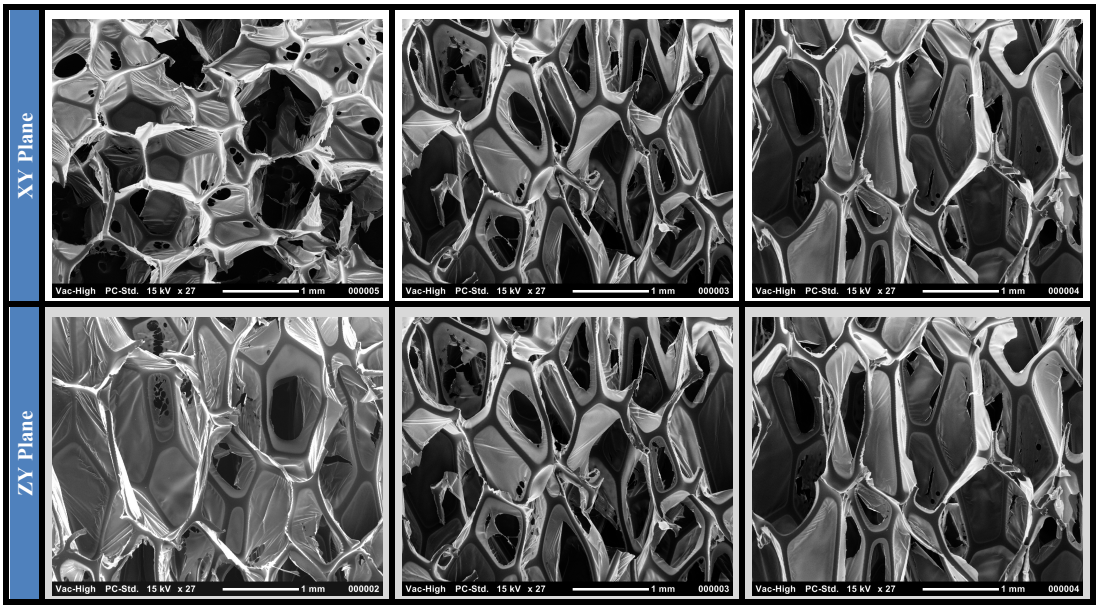

Figure B-14: SEM images in XY and ZY plan for quantifying percent reticulation of Sheet Moderate n4.

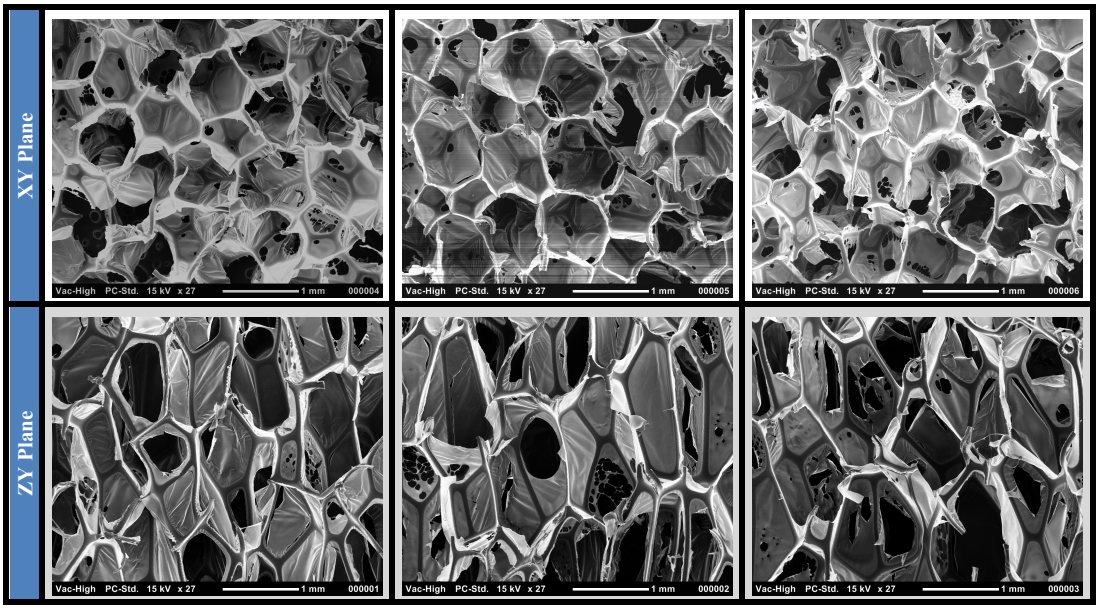

Figure B-15: SEM images in XY and ZY plan for quantifying percent reticulation of Sheet Moderate n5.

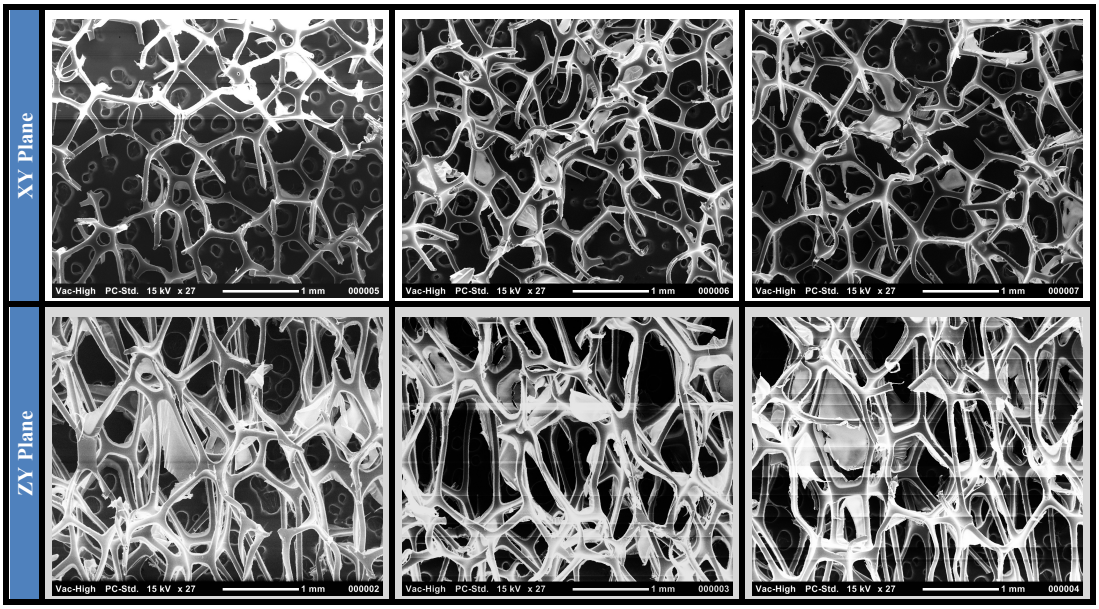

Figure B-16: SEM images in XY and ZY plan for quantifying percent reticulation of Sheet Complete n1.

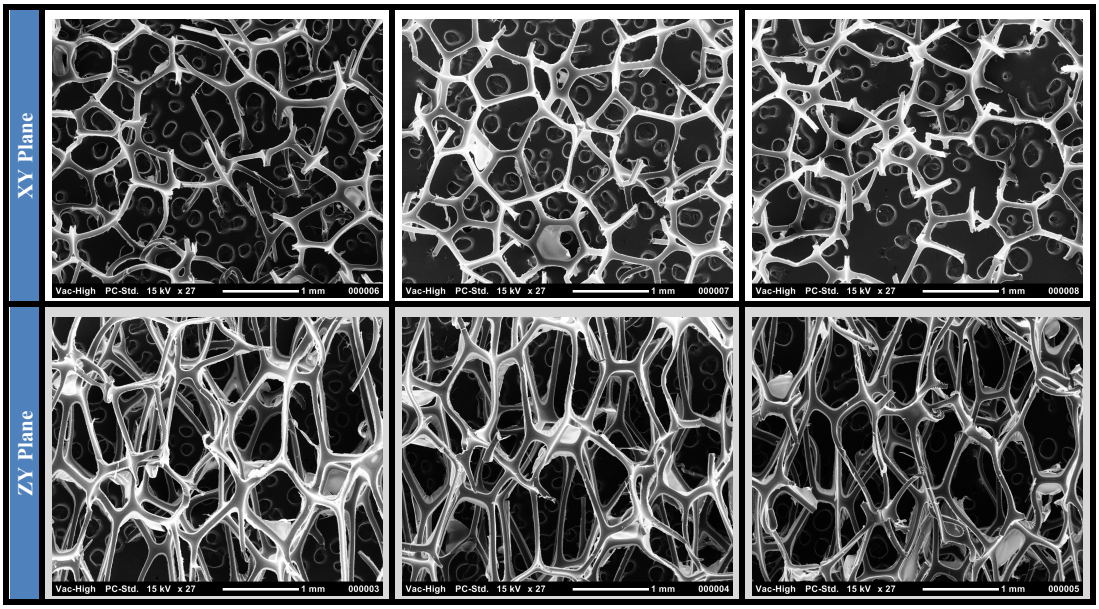

Figure B-17: SEM images in XY and ZY plan for quantifying percent reticulation of Sheet Complete n2.

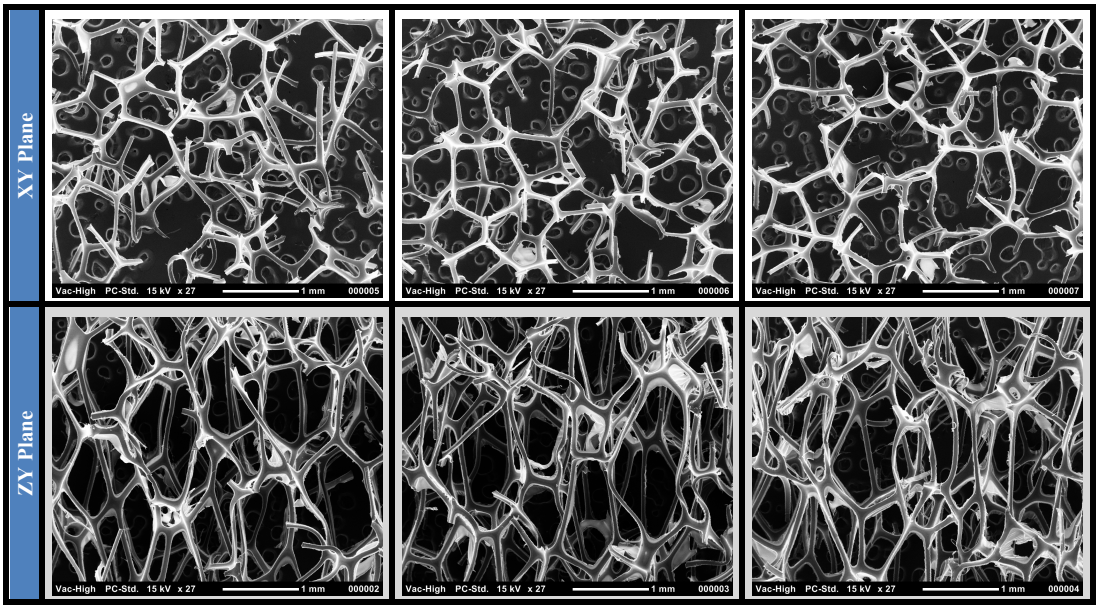

Figure B-18: SEM images in XY and ZY plan for quantifying percent reticulation of Sheet Complete n3.

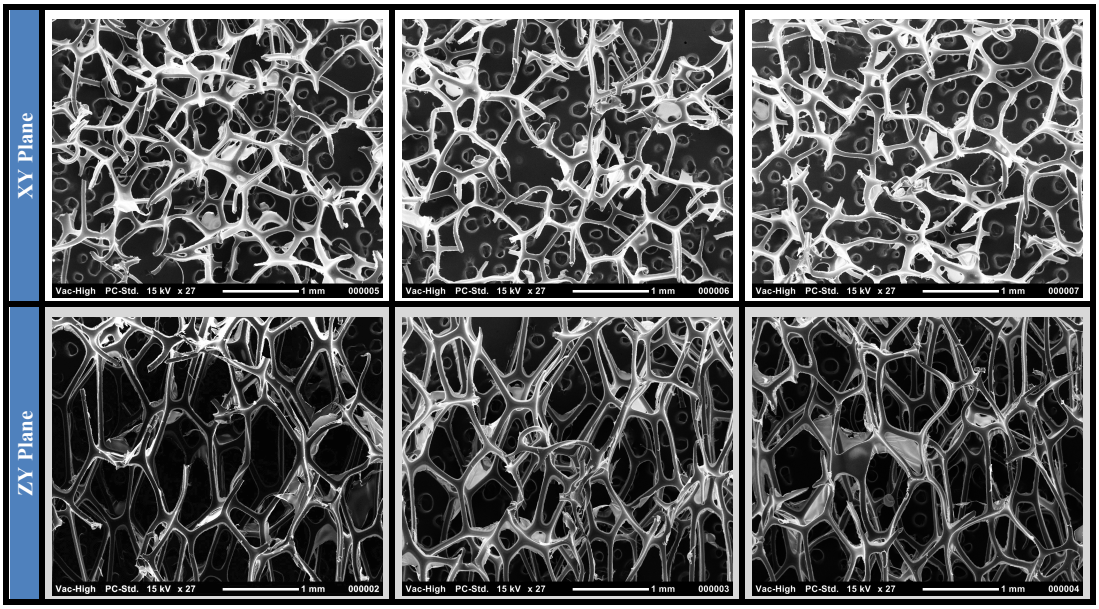

Figure B-19: SEM images in XY and ZY plan for quantifying percent reticulation of Sheet Complete n4.

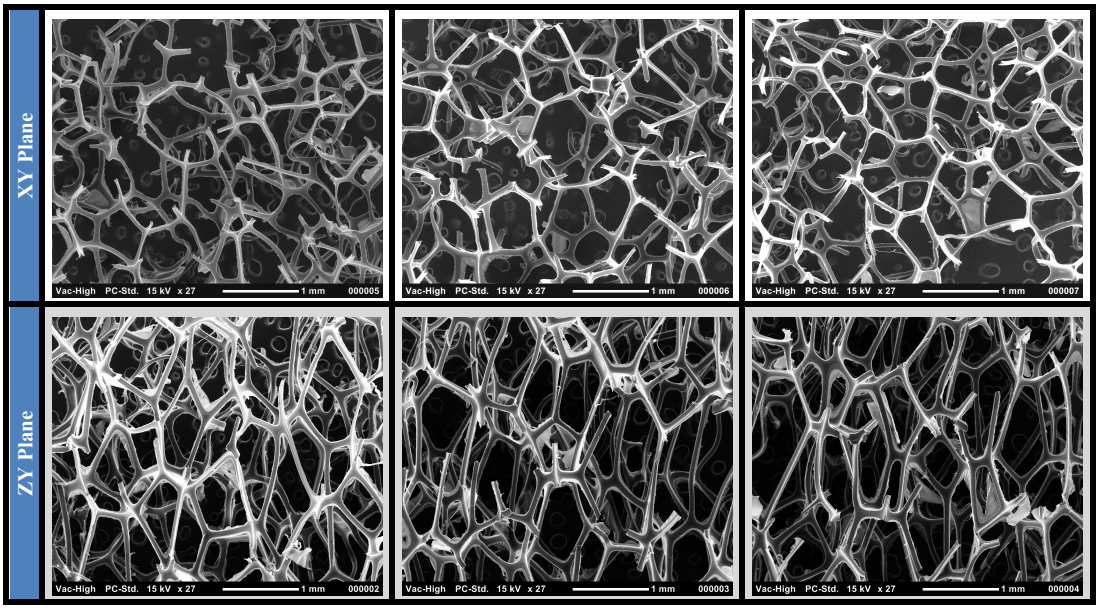

Figure B-20: SEM images in XY and ZY plan for quantifying percent reticulation of Sheet Complete n5.

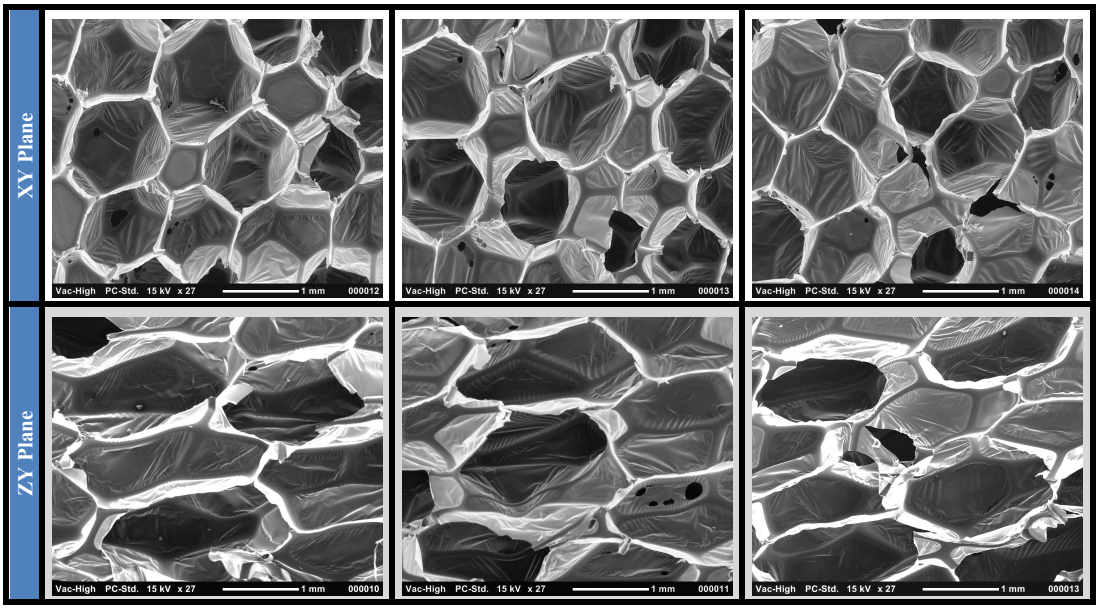

Figure B-21: SEM images in XY and ZY plan for quantifying percent reticulation of Control n1.

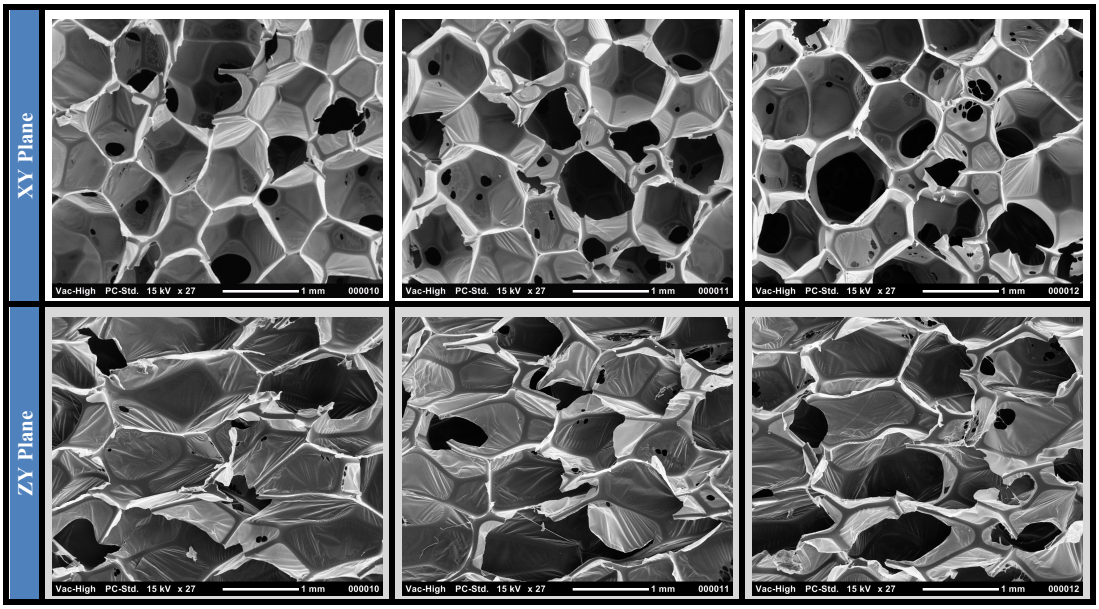

Figure B-22: SEM images in XY and ZY plan for quantifying percent reticulation of Control n2.

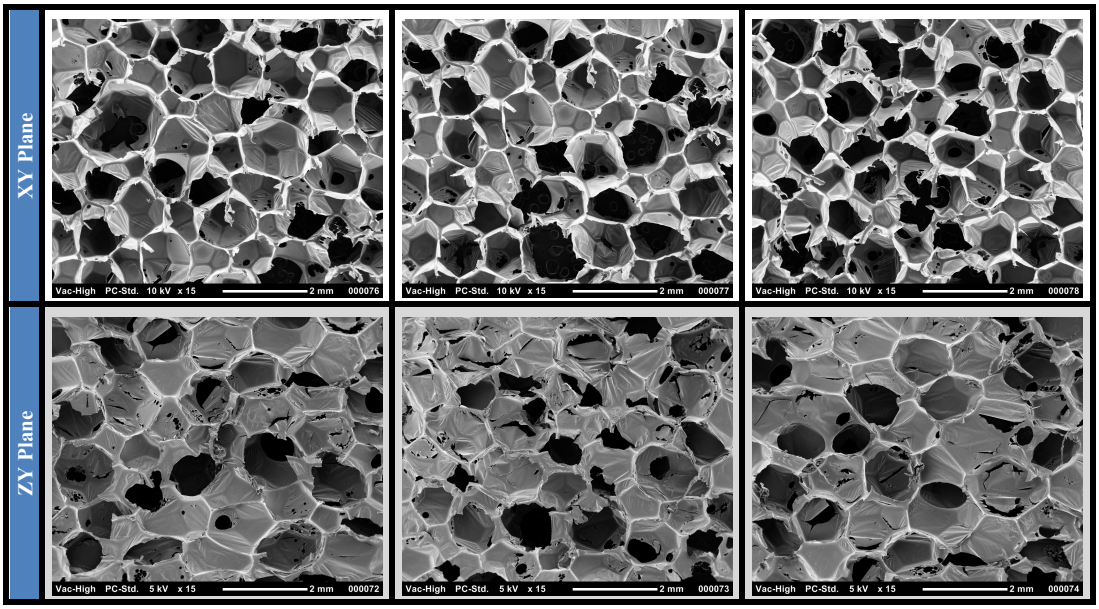

Figure B-23: SEM images in XY and ZY plan for quantifying percent reticulation of Control n3.

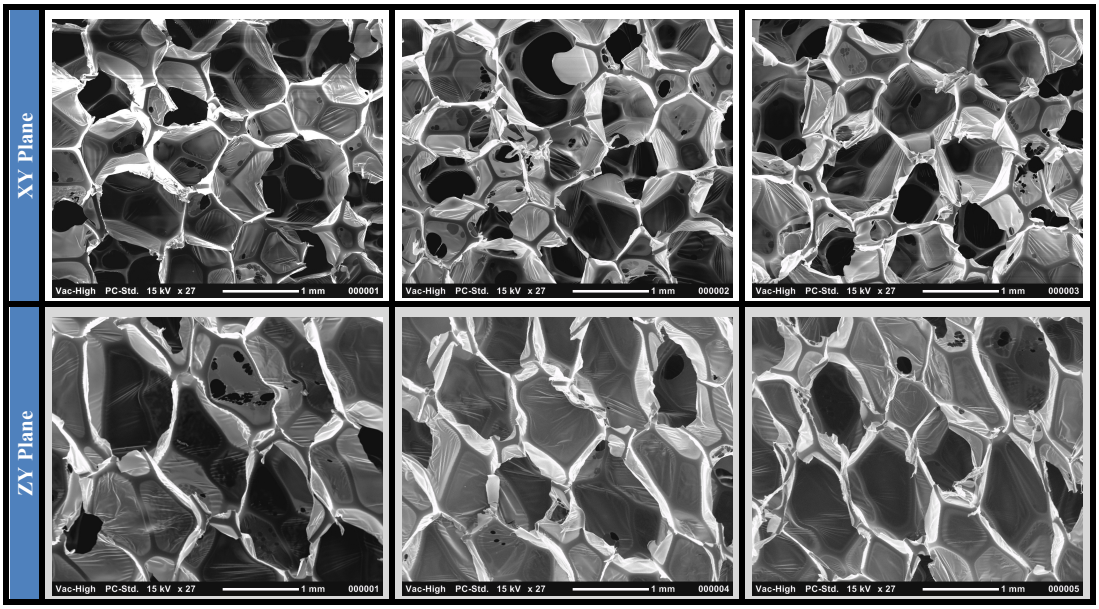

Figure B-24: SEM images in XY and ZY plan for quantifying percent reticulation of Control n4.

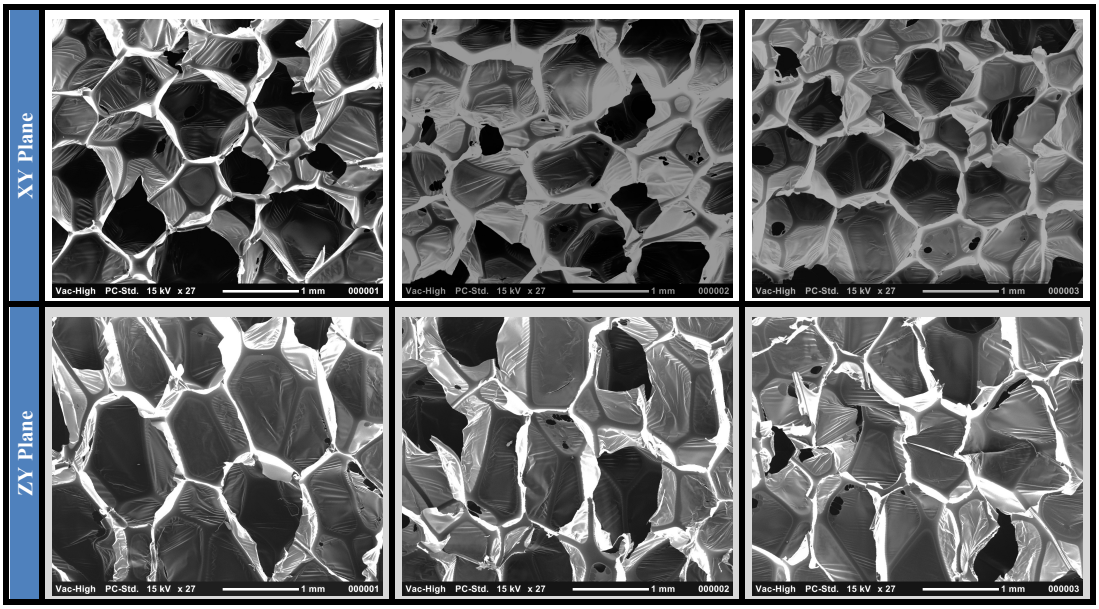

Figure B-25: SEM images in XY and ZY plan for quantifying percent reticulation of Control n5.

APPENDIX C

MACRO-IMAGES FOR MEASURING PERCENT VOLUME WITH COMPLETE MEMBRANE REMOVAL

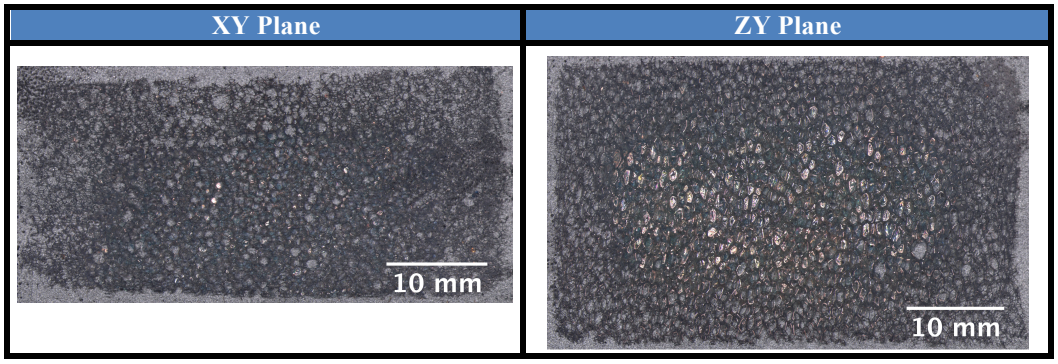

Figure C-1: Macro-images of the slices taken in the XY and ZY planes for measuring percent volume with complete membrane removal within Block Moderate n1.

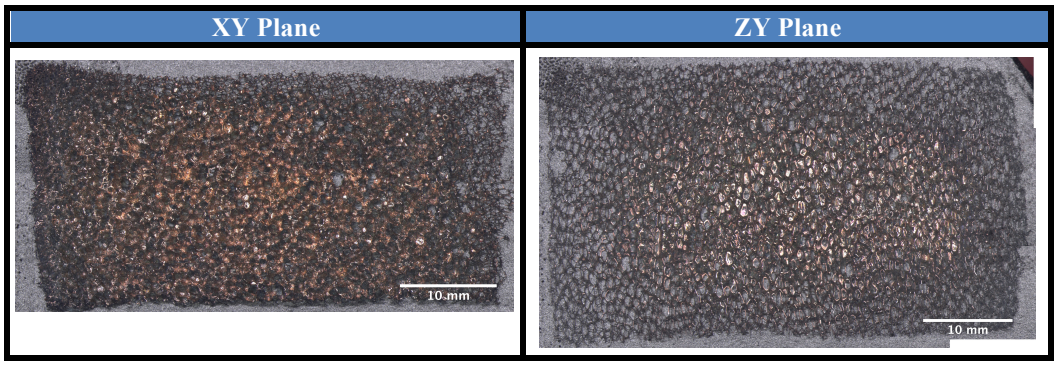

Figure C-2: Macro-images of the slices taken in the XY and ZY planes for measuring percent volume with complete membrane removal within Block Moderate n2.

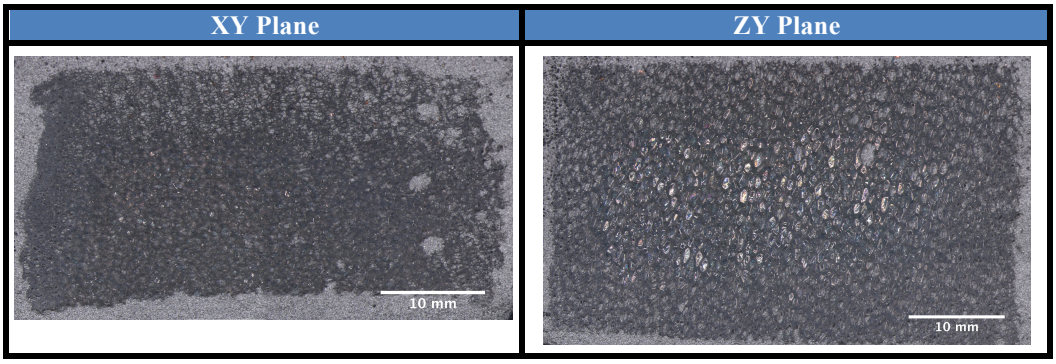

Figure C-3: Macro-images of the slices taken in the XY and ZY planes for measuring percent volume with complete membrane removal within Block Moderate n3.

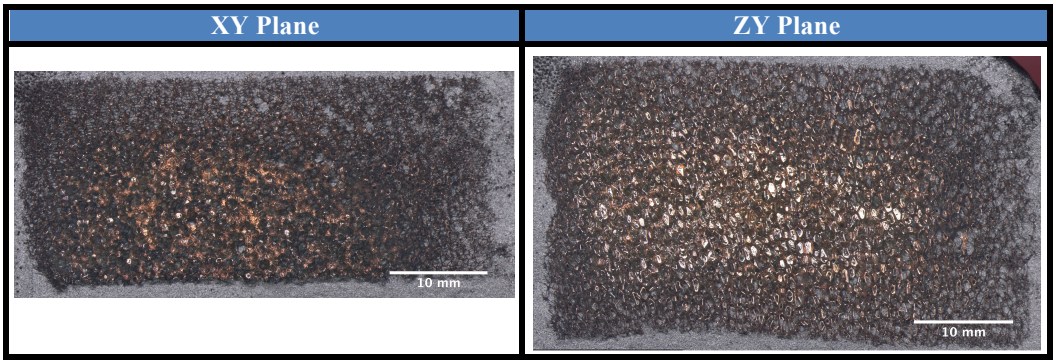

Figure C-4: Macro-images of the slices taken in the XY and ZY planes for measuring percent volume with complete membrane removal within Block Moderate n4.

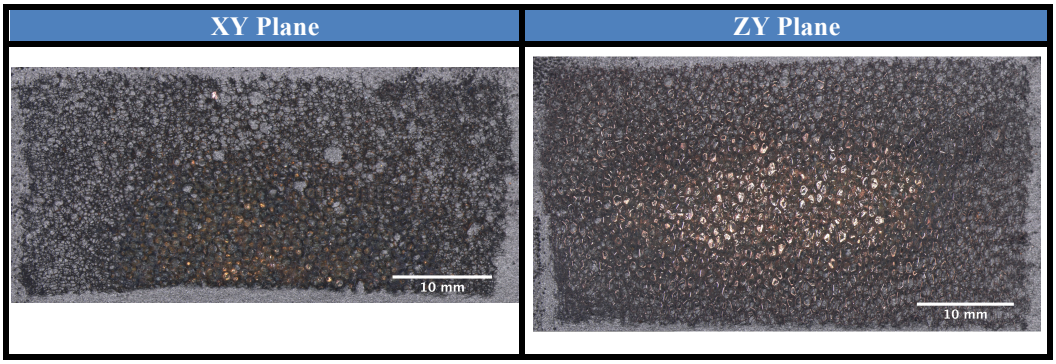

Figure C-5: Macro-images of the slices taken in the XY and ZY planes for measuring percent volume with complete membrane removal within Block Moderate n5.

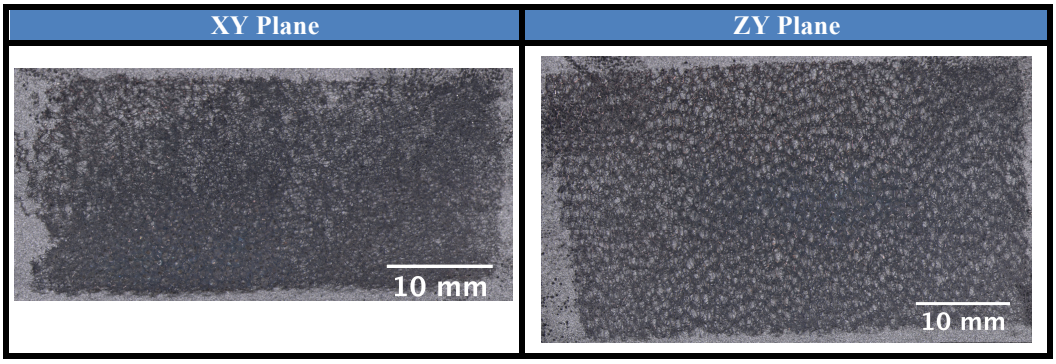

Figure C-6: Macro-images of the slices taken in the XY and ZY planes for measuring percent volume with complete membrane removal within Block Complete n1.

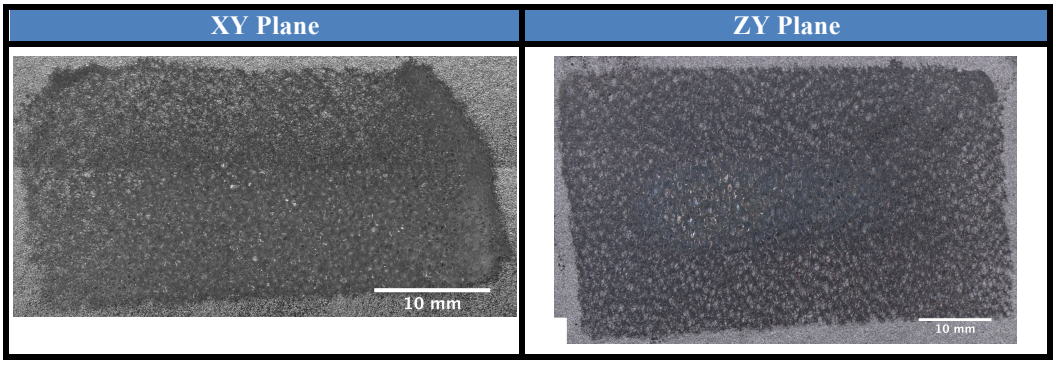

Figure C-7: Macro-images of the slices taken in the XY and ZY planes for measuring percent volume with complete membrane removal within Block Complete n2.

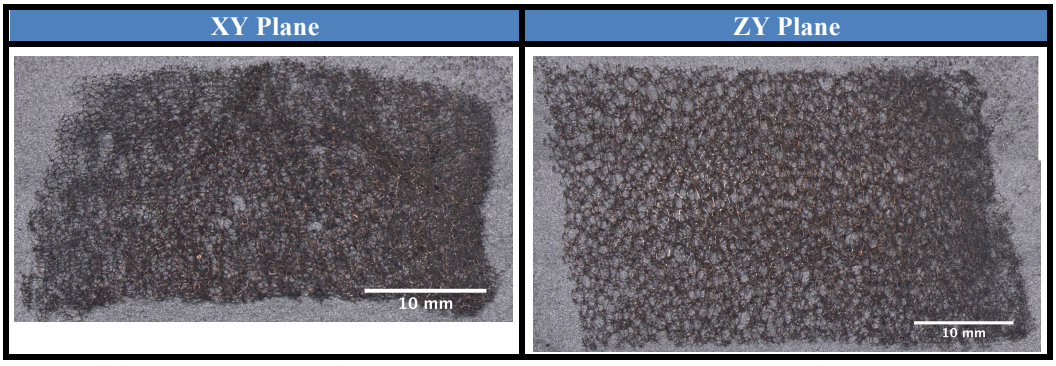

Figure C-8: Macro-images of the slices taken in the XY and ZY planes for measuring percent volume with complete membrane removal within Block Complete n3.

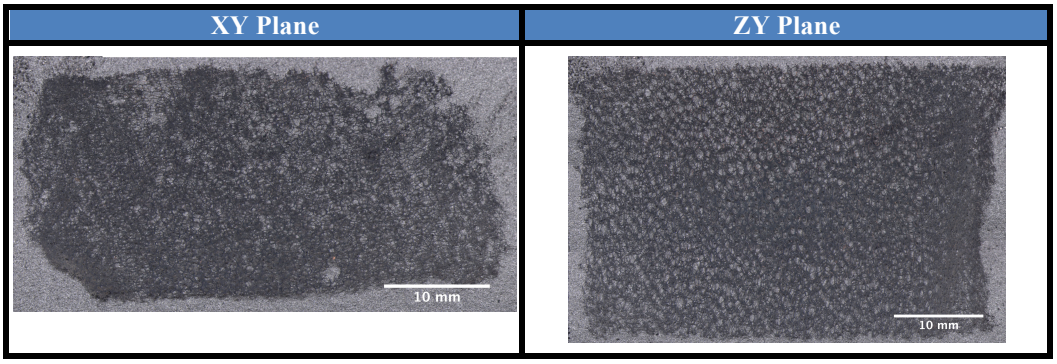

Figure C-9: Macro-images of the slices taken in the XY and ZY planes for measuring percent volume with complete membrane removal within Block Complete n4.

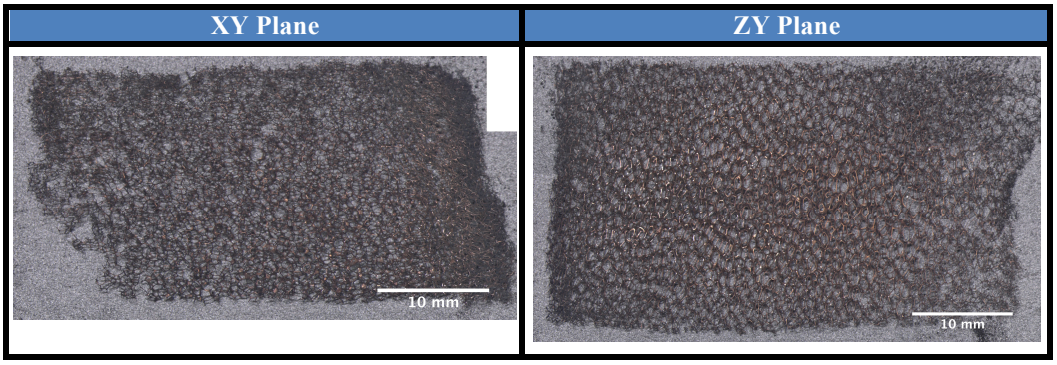

Figure C-10: Macro-images of the slices taken in the XY and ZY planes for measuring percent volume with complete membrane removal within Block Complete n5.